

T U B E R G A K A D E M I E F R E I B E R G

**Numerical Investigation of
Air-Side Heat Transfer and Pressure Drop
in Circular Finned-Tube Heat Exchangers**

Von der Fakultät für Maschinenbau, Verfahrens- und Energietechnik
der Technischen Universität Bergakademie Freiberg, Germany

genehmigte

Dissertation

vorgelegt von

Mi Sandar Mon

Numerical Investigation of Air-Side Heat Transfer and Pressure Drop in Circular Finned-Tube Heat Exchangers

Von der Fakultät für Maschinenbau, Verfahrens- und Energietechnik
der Technischen Universität Bergakademie Freiberg, Germany

genehmigte

DISSERTATION

zur Erlangung des akademischen Grades

Doktor-Ingenieur

Dr.-Ing.

vorgelegt

von **Mi Sandar Mon (M.E)**

geboren am 20.06.1967 in Yangon, Myanmar

Gutachter: Prof. Dr.-Ing. habil. Ulrich Groß, Freiberg
Prof. Dr. rer.nat. habil. Frank Obermeier, Freiberg
Prof. Dr.- Ing. habil. Günter Wozniak, Chemnitz

Tag der Verleihung: 10.02.2003

Acknowledgement

I would like to acknowledge the following people for their guidance and support during my doctoral study and writing of this dissertation at the Institute of "Wärmetechnik und Thermodynamik", Technische Universität Bergakademie Freiberg, Germany.

First and foremost, I would like to express my gratitude to Prof. Dr.-Ing. habil. U. Groß, who accepted to supervise this dissertation. His teaching, patience, and encouragement throughout my doctoral study were invaluable.

I am very grateful to Prof. Dr. rer. nat. habil. F. Obermeier, who accepted to be a member of my dissertation committee. His constructive comments and suggestions were inestimable to the completion of this dissertation.

I would like also to thank Prof. Dr.-Ing. habil. G. Wozniak, who also accepted to be a member of my dissertation committee and is highly appreciated.

Many thanks should be ascribed to Dr-Ing. I. Riehl and Dr-Ing. S. Kaminski with whom I had many useful discussions.

I also appreciate the help of Mr. T. Polet, who assists for the problems concerned with the computers and thanks also go to Mr. M. Brislin who gratefully giving me many important comments on English writing.

Furthermore, I would like to thank all colleagues of the institute for contributing to such an inspiring and pleasant atmosphere.

I would like also to acknowledge the German Government and DAAD for their benevolence in providing a full scholarship grant for my doctoral study.

Last, but not least, I would like to thank my husband Aung Myat Thu for his understanding and support, as well as my parents, families and friends' encouragement.

Freiberg, May 2003.

Mi Sandar Mon

Abstract

Numerical Investigation of Air-Side Heat Transfer and Pressure Drop in Circular Finned-Tube Heat Exchangers

The present numerical study has been carried out to investigate the temperature and velocity profiles in banks with circular finned-tubes in cross flow. The purpose of this investigation is to develop satisfactory correlations and concurrently providing complements to the local convective characteristics. The coolant passes through the tubes, which are maintained at a constant temperature and the dry air is used as the convective heat transfer medium. To demonstrate the influence of the geometric parameters, numerical investigations are carried out for different finning geometries and number of rows. In addition, attempts are made to validate which tube configuration is more constructive.

A large computational effort is involved for the memory access of the computers and computing time for the simulation of the complex geometries associated with the dense grids. The available computational fluid dynamics software package FLUENT is applied to determine the related problems. Renormalization group theory (RNG) based $k - \varepsilon$ turbulence model is allowed to predict the unsteady three-dimensional flow and the conjugate heat transfer characteristics.

The numerical flow visualization results reveal the important aspects of the local heat transfer and flow features of the circular finned-tube bundles. These include boundary layer developments between the fins, the formation of the horseshoe vortex system, the local variations of the velocity and temperature on the fin geometries and within the bundles. The boundary layers developments and horseshoe vortices between the adjacent fins and tube surface are found to be dependent substantially on the fin spacing and Reynolds number. The local temperature distributions over the fin surface vary both circumferentially and radially, and there is no significant difference over the fin surface and in the middle of the fin for both tube arrays.

To determine the optimum dimension of the geometries, comparisons are prepared in terms of the bundle performance parameter. These data indicate that for the benefit of pumping power, the in-line array has a better performance than the staggered arrangement at low Reynolds number. However, the margin between the in-line and staggered arrays becomes narrower when the Reynolds number is increased.

The average heat transfer and pressure drop results for both tube configurations are presented. All proposed correlations, based on the numerical and relevant experimental data, are recommended for a wide range of Reynolds numbers (based on the air velocity through the minimum free flow area and the tube outside diameter) from 5×10^3 to 7×10^4 . The heat transfer and pressure drop results agree well with several existing experimental correlations. The present numerical investigations suggest a good estimate of the Nusselt number and Euler number for circular finned-tube heat exchangers.

Kurzfassung

Numerische Untersuchungen des luftseitigen Wärmeübergangs und Druckabfalls in Rippenrohrbündeln

Die vorliegenden numerischen Untersuchungen wurden durchgeführt, um die luftseitigen Temperatur- und Geschwindigkeitsprofile in Bündeln von Kreisrippenrohren zu untersuchen. Zweck dieser Untersuchungen ist die Entwicklung von Korrelationen sowie zusätzlich eine Beschreibung des örtlichen Verhaltens der Konvektion. Das Kühlmittel fließt durch die Rohre, deren Temperatur damit konstant gehalten wird. Um den Einfluß auf die geometrischen Parameter zu demonstrieren, wurden numerische Betrachtungen für unterschiedliche Rippengeometrien und eine unterschiedliche Anzahl von Reihen vorgenommen. Außerdem wurde überprüft, welche Rohrkonfiguration bessere konstruktive Eigenschaften aufweist.

Ein großer rechentechnischer Aufwand ist in Bezug auf Arbeitsspeicher und Rechenzeit erforderlich, da die Simulation der komplexen Geometrien durch ein dichtes Netz geprägt ist. In einigen Fällen (nahe der Wand) mußte ein dichteres Netz gebildet werden, um die Berechnungen dennoch durchführen zu können. Das verfügbare (Computational Fluid Dynamics) CFD-Softwarepaket FLUENT wird zur Lösung dieser Fragestellungen verwendet. Ein $k-\varepsilon$ -Turbulenzmodell auf Basis der Renormalization Group Theory (RNG) wird für die Berechnung der instationären dreidimensionalen Strömung und ihrer entsprechenden Wärmeübertragungscharakteristika genutzt.

Die Visualisierung der numerischen Untersuchungen der Strömung verdeutlichen die bedeutenden Aspekte der lokalen Wärmeübertragung und der Strömungseigenschaften. Dies umfaßt die Grenzschichtbildung zwischen den Rohren, die Entstehung von Hufeisenwirbelsystemen, die lokalen Abweichungen der Geschwindigkeit und der Temperatur abhängig von der Rohrgeometrie und der geometrischen Struktur der Bündel. Die Grenzschichtbildung und Hufeisenwirbel zwischen den angrenzenden Rippen und der Oberfläche der Rohre haben sich als sehr stark abhängig vom Rippenabstand und der Reynoldszahl erwiesen. Die örtliche Temperaturverteilung über die Rippenoberfläche variiert sowohl an der Peripherie als auch radial, und es gibt keinen signifikanten Unterschied zwischen der Rippenoberfläche und der Mitte der Rippe für fluchtenden und versetzten Anordnung des Rohrbündels.

Zur Bestimmung optimaler geometrischer Parameter, werden Vergleiche in Bezug auf die Leistungsparameter der Bündel durchgeführt. Diese Daten zeigen, daß bei niedrigen Reynoldszahlen, die fluchtende Anordnung leistungsfähiger ist als die versetzte ist insbesondere wenn man die Pumpleistung betrachtet. Jedoch wird die Abweichung zwischen der fluchtenden und der versetzten Anordnung geringer, wenn die Reynoldszahl ansteigt.

Die Daten für die mittlere Wärmeübertragung und den Druckverlust werden für beide Rohrkonfigurationen präsentiert. Alle vorgeschlagenen Korrelationen, welche auf numerischen und relevanten experimentellen Daten basieren, werden für einen großen Bereich der Reynoldszahlen (auf Basis der Strömungsgeschwindigkeit der Luft durch den minimalen freien Strömungsquerschnitt und den Außendurchmesser des Rohres) von 5×10^3 bis 7×10^4 empfohlen. Die Ergebnisse für die Wärmeübertragung und den Druckabfall sind mit verschiedenen existierenden experimentellen Korrelationen sehr gut vergleichbar. Die vorliegenden numerischen Simulationen erlauben eine gute Abschätzung der Nusselt- und der Eulerzahl für Wärmeübertrager mit Kreisrippenrohren.

Table of Contents

Nomenclature	x
1 Introduction	1
2 Literature Review	3
2.1 Heat Transfer and Flow Characteristics in a Circular Finned-Tube Heat Exchanger	3
2.2 Local Heat Transfer Behaviour of Circular Finned-Tubes	5
2.3 Analysis of Geometric and Flow Parameters	9
2.3.1 Effect of Fin Height	9
2.3.2 Effect of Fin Spacing	10
2.3.3 Effect of Fin Thickness	12
2.3.4 Effect of Tube Outside Diameter	12
2.3.5 Effect of Tube Spacing	13
2.3.6 Effect of Row	15
2.3.7 Effect of Tube Arrangement	16
2.3.8 Effect of Air Velocity	17
2.4 Average Heat Transfer Correlations	18
2.5 Pressure Drop Correlations	20
2.6 Concluding Remarks	21
3 Objectives	23
4 Numerical Consideration	25
4.1 Governing Equations and CFD models	25
4.1.1 The RNG k - ε model	29

4.2	Numerical Simulation	30
4.2.1	Introduction	30
4.2.2	Computational Domains	31
4.2.3	Grid Generation	34
4.2.4	Choosing the Physical Properties	36
4.2.5	Boundary Conditions	36
4.2.6	Control Parameters	38
4.2.7	Computing Time	38
4.2.8	Algorithm	39
5	Results and Discussion	41
5.1	Evaluation of Nusselt and Euler Numbers	41
5.2	Local Heat Transfer and Flow Results	44
5.2.1	Local Flow Behaviour	44
5.2.2	Local Temperature Distribution	51
5.2.3	Velocity and Temperature distribution near the fin surface plane and on the mid-plane between the fins	59
5.3	Results of Geometric Parameters Effects	66
5.3.1	Results of Fin Height Effect	66
5.3.2	Results of Fin Spacing Effect	71
5.3.2	Results of Fin Thickness Effect	75
5.3.4	Results of Tube Outside Diameter Effect	78
5.3.5	Results of Tube Spacing Effect	81
5.3.6	Results of Row Effect	86
5.3.7	Results of Tube Arrangement Effect	94
6	Correlations and Data Comparison	97
6.1	Heat Transfer Correlations	97
6.1.1	Staggered Tube Arrangement	98

6.1.2 In-line Tube Arrangement	101
6.2 Pressure Drop Correlations	102
6.3 Data Comparison	105
6.3.1 Comparison of Heat Transfer Results for Staggered Arrangement	105
6.3.2 Comparison of Heat Transfer Results for the In-line Arrangement	109
6.3.3 Comparison of Pressured Drop Results.....	111
7 Conclusions	114
References	118
List of Figures	126
List of Tables	130
Appendix	131
A Physical Properties of Air and Aluminium	132
B Further Figures	133
C Dimensions of Finned-Tube Heat Exchangers	141
D The Heat Transfer and Pressure Drop Correlations	143
E Numerical Results	150

Nomenclature

A	m^2	total heat transfer area
A'	m^2/m	heat transfer area of unit length finned tube
A_f	m^2	surface area of fin
A_{ff}	m^2/m	minimum free flow area of finned tube per unit length
A_t	m^2	outside surface area of tube except fins
c_p	$J/(kg\ K)$	specific heat
$C_{1\varepsilon}, C_{2\varepsilon}, C_{\mu}$	-	turbulence model constants
d	m	tube outside diameter
d_{eq}	m	equivalent diameter
d_h	m	hydraulic diameter
d_f	m	fin diameter
E	J	total energy
Eu	-	Euler number, $Eu = \Delta p / \rho U_{max}^2$
Eu_m	-	Euler number, $Eu_m = \Delta p / \rho U_m^2$
f	-	friction factor
F	-	parameter defined by Equation (6.3)
G	kg/sm^2	mass velocity based on minimum free flow area
\dot{H}	W	flow rate of enthalpy
h	$W/(m^2K)$	heat transfer coefficient
\tilde{h}	J/kg	specific enthalpy
h_f	m	fin height
k	$W/(mK)$	thermal conductivity
\tilde{k}	m^2/s^2	turbulent kinetic energy
K	-	performance parameter
L_c	m	characteristic length
LMTD	K	logarithmic mean temperature difference
m	m^{-1}	a fin effectiveness parameter

\dot{m}	kg/s	mass flow rate
N_f	fins/m	number of fins per unit length
n	-	number of tube rows in direction of flow
n	-	exponent
Nu	-	Nusselt number, $Nu = hd/k_a$
P	W	power input
p	P _a	pressure
Pr	-	Prandtl number, $Pr = C_p \mu / k_a$
\dot{Q}	W	heat flow rate
Re	-	Reynolds number, $Re = U_{max} d / \nu$
$Re_{d, eq}$	-	Reynolds number, $Re_{d, eq} = U_{max} d_{eq} / \nu$
Re_{dh}	-	Reynolds number, $Re_{dh} = U_{max} d_h / \nu$
Re_α	-	Reynolds number, $Re_\alpha = U_{in} s_f / \nu$
s	m	fin spacing
S	s ⁻¹	the modulus of the mean rate-of-strain tensor
S_{ij}	s ⁻¹	the mean strain rate
S_d	m	diagonal tube pitch
S_f	m	fin pitch
S_l	m	longitudinal tube pitch
S_t	m	transverse tube pitch
St	-	Stanton number
T	K	temperature
T_{out}	K	outlet temperature
T_{ref}	K	reference temperature
Δt	sec	time step
U	m/s	velocity component in x – direction
U_m	m/s	mean velocity in the finned tube bundle
U_{max}	m/s	velocity of air at minimum cross section
\dot{V}	m ³ /s	volume flow rate
$V1, V2, V3$	-	vortices
x, y, z	m	Cartesian coordinates

Greek Letters:

α_p	-	inverse Prandtl number
δ	m	fin thickness
δ_b	m	boundary layer thickness
ε	m^2/s^3	turbulent energy dissipation rate
η	-	fin efficiency
μ	$\text{kg}/(\text{ms})$	viscosity
ν	m^2/s	kinematic viscosity
θ	-	angle around the tube, measured from the front stagnation point
ρ	kg/m^3	density
τ_p	m	distance to the wall from the adjacent node
ψ	-	factor defined by Equation (5.10)

Subscripts:

<i>a</i>	air
<i>corr</i>	correlation
<i>eff</i>	effective
<i>exp</i>	experiments
<i>f</i>	fin
<i>in</i>	inlet
<i>m</i>	mean
<i>max</i>	maximum
<i>nume</i>	numerical
<i>out</i>	outlet
<i>ref</i>	reference
<i>s</i>	solid
<i>t</i>	tube, turbulent
<i>w</i>	wall

1 INTRODUCTION

One of the important processes in engineering is the heat exchange between flowing fluids, and many types of heat exchangers are employed in various types of installations, as power plants, petrol-chemical plants, building heating, ventilating, air-conditioning and refrigeration (HVAC/R) systems. As far as construction design is concerned, (1) the tubular or shell and tube type and, (2) the extended surface or finned-tube type heat exchangers are widely in use. Finned-tube heat exchangers are used for the processes in which a liquid or gas is required to be either cooled or heated. Generally, a liquid flows within the tubes while gas is directed across the finned-tubes. Because of the poor thermal conductivity and thus the heat transfer coefficient of the gases, it is necessary to apply the extended surfaces on the gas side to enhance the heat transfer without losing its compactness. In addition, the problems concerned with pressure loss in flow medium must not be overlooked. Typical cross-flow circular finned-tube geometry is illustrated in Figure 1.1.

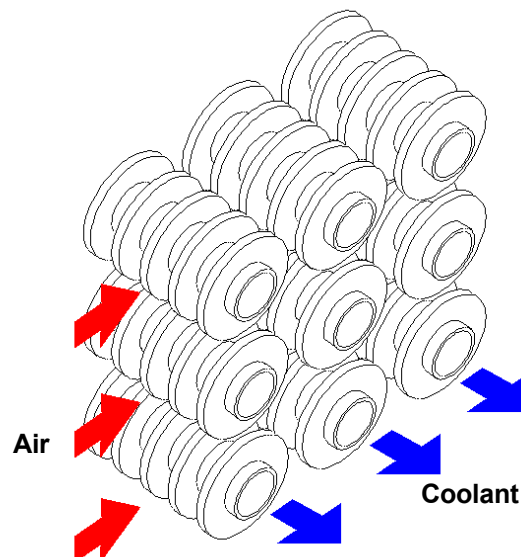


Figure 1.1 *Cross-flow circular finned-tube heat exchanger.*

There are technical constraints when using the fins in actual applications and the proper selection of the effective fin geometric parameters, such as the height of fin and the space between the neighbouring fins, will greatly enhance the performance of a heat exchanger. Moreover, the flow patterns for the in-line and staggered tube arrays are complicated and will have to be dealt in the air-cooled heat exchanger design. Thus, further investigations on the air-side heat transfer enhancement are of broad interest to design more compact and efficient heat exchangers.

The circular finned-tube bundles are commonly used in the industries. In order to improve the air-side heat transfer performance of these bundles, such as to increase the fin efficiency and compactness as well as to reduce the pressure losses, much empirical work has been done diligently [72]. Investigations are carried out mainly for the staggered arrangement under the cross flow conditions and numerous correlations have developed. However, experimental investigations that include a complete coverage of principle factors are relatively rare. Besides, Xi and Torikoshi [79] noted, "...experimental studies cannot adequately reveal the flow and thermal characteristics in finned-tube heat exchangers." In addition, the heat transfer in a finned-tube heat exchanger is a conjugate problem [10]. Conjugate heat transfer means computing more than one mode of the heat transfer simultaneously and it can be established efficiently by the way of numerical means. For a finned-tube heat exchanger, when the convection effect is intended to calculate for the fluid through the bundle, the conduction in the fins has to be considered as well. To provide the better understanding of the most important mechanisms of heat transfer in flow passing finned-tube exchangers; numerical simulations may be therefore helpful tool. Especially, one should examine detailed flow structures and temperature distributions by means of the numerical simulation incorporating the computational fluid dynamics (CFD) technique.

The review of relevant literature for the circular finned-tube bundles will be stated in the next chapter follow by the numerical considerations and simulations procedure. Consecutively, the numerical results are described and examined in the chapter 5, and also the proposed correlations and data comparisons are presented in the chapter 6 before the conclusive results are finalized.

2 Literature Review

Adding the fins in a heat exchanger is a very common procedure to enhance the overall heat transfer coefficient. A large number of experimental works has been performed for this enhancement of air-side heat transfer; however, the flow profiles and the related heat transfer characteristics in the complex geometries are still needed to be verified.

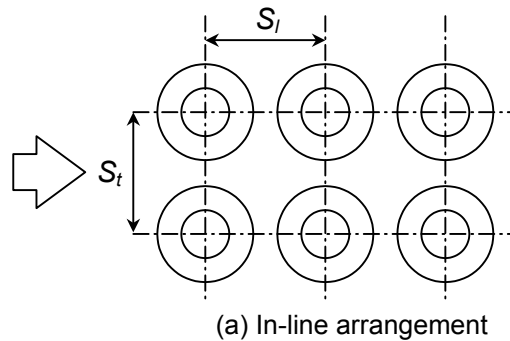
2.1 Heat Transfer and Flow Characteristics in a Circular Finned-Tube Heat Exchanger

The fundamental aim in the thermal design of a heat exchanger is to determine the surface area required to transfer heat at the given fluid temperatures and flow rates. According to Brauer [7], “the total surface area of the finned-tube bundle and the heat transfer coefficient h were closely linked and governed by the layout and the form of fins and tubes.” Therefore, it is important to ensure that an enlargement of the fin surface area must be implemented without causing the decrease in heat transfer coefficient.

It is evident that the fin surface area can be augmented by increasing the fin height h_f and/or the number of fins per meter. Under this circumstance, it is required to set up the maximum possible value of the fin height since the magnitude of the temperature gradient along the radial direction decreases with the fin height. By the nature of temperature distributions on the fin, the temperature difference between the ambient air and the fin will also decrease due to the continuous convection losses from the fin surface. There has also been significant interest in the role of the number of fins per meter. Narrower fin spacing will produce low heat transfer coefficients and this trend depends on the boundary layer development, which arises in accordance with the velocity and turbulence of the flow in the inter fin space. In addition, the problems concerned with bundle configurations of Figure 2.1 and the bundle depth effect must not be overlooked.

There are seven geometric and five flow variables that affect the heat transfer coefficient and friction factor for a plain fin [73]. Without consideration of the tube layout and fin shape, the geometry variables are:

1. Fin height (h_f)
2. Fin spacing (s)
3. Fin thickness (δ)
4. Tube outside diameter (d)
5. Transverse tube pitch (S_t)
6. Longitudinal tube pitch (S_l)
7. Number of rows (n)



In addition, the flow variables are:

1. Air velocity (U)
2. Density (ρ)
3. Viscosity (μ)
4. Thermal conductivity (k)
5. Specific heat (c_p)

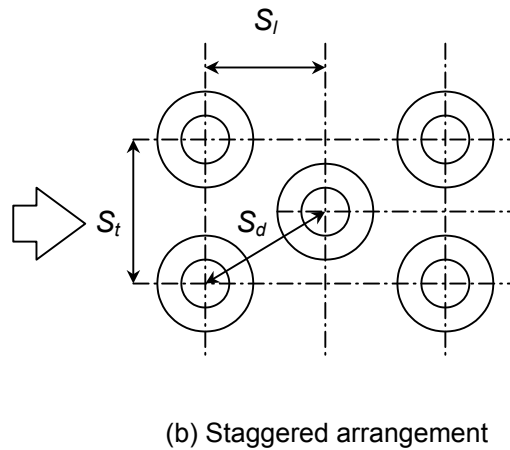


Figure 2.1 Arrangements of tubes in bundles.

Typically, the flow mode should be treated as a temperature dependent problem because the flow variables directly depend on the temperature of air. Furthermore, the heat transfer from a bundle (especially in the first row) depends on the conditions of turbulence intensity occurred at the bundle inlet [83]. That is why flow conditions and geometric parameters are necessary to be considered for a perfect design since such principal factors control the heat transfer and pressure drop.

When describing the Reynolds number, a similar form will not be found since variety of characteristic dimensions was used. The basic form is $\frac{L_c G}{\nu}$, where L_c is the characteristic length and G is usually defined as air velocity through the minimum free flow area [73]. Normally the nature of the flow in a system can be determined according to its Reynolds number. For example, when Reynolds number (based on the average flow velocity and hydraulic diameter of the duct) is lower than 2000, the flow in the duct can be considered to be laminar. However, the most questionable point is the

type of flow, which exists in a circular finned-tube bank. Zhukauskas [81] solely stated that a critical value is $Re \cong 10^5$ for circular finned-tube bundle; however, yet apparently further verifications on this statement were not sought to date. Jacobi and Shah [22] discussed that the air flow was likely to exhibit all of possible flow features (e.g., steady or unsteady, laminar or turbulent) in a single heat exchanger. They suggested that there were still limitations to the air-side heat transfer performance and a clear understanding of airflow in the complex passages of heat exchangers was needed so that surface design can be optimised efficiently.

In designing a heat exchanger, the interactions between the local heat transfer and flow structure around a circular finned cylinder in cross flow is noteworthy. The physics of flow are depending on upstream flow condition, the flow along the tube wall until the separation point and the tube wake condition [62]. The structures of secondary flow are complicated as the flow is a three-dimensional one. As described in the introduction, it is still difficult and complicated to predict and visualize the flow and related heat transfer between the geometrically complex bundles by means of the experimental investigation. As a result, numerical investigation is being widely used in recent years to analyse the flow and temperature fields. By using numerical simulation, one can model physical fluid phenomena that can be easily simulated and one is able to investigate the fluid and thermal systems more cost effective and faster than by experiments. Though, a substantial amount of numerical works on plate finned-tube bundles has been published, only one research work related to the main interest of current study (circular finned-tubes) was found in Jang et al. [25].

Since little progress has been made by the numerical approach to examine the heat transfer and pressure drop characteristics for circular finned-tube bundles, researchers have to rely on the experimental results. Therefore, the relevant experimental literature on the local heat transfer behaviour of circular finned-tubes will be reviewed at first.

2.2 Local Heat Transfer Behaviour of Circular Finned-Tubes

The need for heat exchanger designers to associate the demands of enhanced heat transfer for a given configuration requires clear understanding of the local heat transfer behaviour. In the literature, several of experimental methods can be found for detection and measurement of the local heat transfer and for visualization the physics of flow. It includes:

1. Point heating model (e.g., Lymer [42], Zhukauskas [81], and Zhukauskas et al. [82]),
2. Total heating model (e.g., Jones and Russell [27], Legkiy et al. [41], and Neal and Hitchcock [45]),
3. Naphthalene sublimation technique (e.g., Goldstein and Karni [16], Goldstein et al. [17], Hu and Jacobi [21], Kearney and Jacobi [32], Sparrow and Chastain [60], Sung et al. [63], Wong [78]), and
4. Particle Image Velocimetry (PIV) method (e.g., Watel et al. [70, 71]).

To compare between the alternative heating methods, Stasiulevičius and Skrinska [62] approached an approximate analytical method for a laminar boundary layer of a smooth tube in cross flow. By this comparison, it is seen that the point heating method provides an unrealistic boundary condition and overestimates the local heat transfer coefficients. Besides, Hu and Jacobi [21], and Kearney and Jacobi [32] suggested that the point heating method could lead to serious errors. Unlike the total heating method, the thermal boundary layer will not be developed at the fin tips where both (velocity and thermal) boundary layers should have to develop. Instead, thermal boundary layer only will develop when the airflow reach to the heated area. According to [62], depending on the heating models, the heat transfer distribution patterns over the fin will be dissimilar.

Neal and Hitchcock [45] carried out a comprehensive study on the local heat transfer and airflow occurring within a circular finned-tube bank in staggered tube arrangement. Three different tube spacings were examined and instrumented tubes were installed in row two and six. They found that the heat transfer upstream the fin is considerably higher, and the heat transfer coefficient decreases at the base of the tube as the boundary layer increases. However, Hu and Jacobi [21] pointed out that the use of thermocouples and few sensors might be inadequate for resolving details of the flow and the heat transfer interaction. By comparing the results of Lymer [42] and Neal and Hitchcock [45], it is noteworthy that due to the complex flow pattern the local heat transfer coefficients will vary both circumferentially and radially over the complex geometry of finned-tubes [62].

Legkiy et al. [41] investigated the local heat transfer on the surface of a single tube with circular fins cooled by transverse airflow. However, Hu and Jacobi [21]

discussed that the spatial resolution was insufficient and the results are very limited because of using a single tube. Another investigation on a single circular fin by mass transfer method was performed by Sparrow and Chastain [60]. They measured the variations of the angle of attack by a thin film of a naphthalene sensor. The authors concluded that the overall heat transfer performance of a circular fin was not significantly affected by small angles of attack. However, the measurement of the heat transfer coefficient at only one side may yield erroneous results.

The naphthalene sublimation is the most common implementation of the mass transfer method to measure the local heat transfer coefficients. Hu and Jacobi [21] conducted the detailed investigation to the flow conditions and local heat transfer behaviour on a single row of a circular finned-tube heat exchanger. They established the fin efficiency differences opposing to Gardner's solution [13]. Gardner assumed that the heat transfer coefficient was maintained constant on the fin surface. To the contrary, Hu and Jacobi [21] calculated the fin efficiency by the assumption of a non-constant convective heat transfer coefficient. Their conclusion pointed out that there is a great difference between their calculation and Gardner's solution while the thermal conductivity of fin was low. However, the results of [21] were somewhat limited as it was used only one row and Kearney and Jacobi [32] stated that incorrect choice of the Lewis number lead to a considerable error. Kearney and Jacobi rectified those results by securing the correct Lewis number and also recommended that the fin efficiency of circular fins was less important to the heat transfer coefficient distribution. Kearney and Jacobi obtained such results for circular finned-tubes in staggered and in-line two-row bundles.

Recently Watel et al. [70,71] studied the influence of the fin spacing on the convective heat transfer from a rotating circular finned-tube in transverse airflow. The fin cooling was monitored by aid of the infrared thermography and the flow field in the mid-plane between two fins was obtained by Particle Image Velocimetry (PIV) device. Their results were compared and validated with Schmidt [56], Legkiy et al. [41], and Sparrow and Samie [59]. However, they tested only for a single tube and it did not realize the effect of neighbouring tubes. Here, it is necessary to emphasize that the tube bundle effect should be taken into account in all investigations because Zhukauskas et al. [82] showed that the heat transfer coefficients over the circumference were more uniformly distributed on a tube in the bundle rather than on a single tube.

One of the influence factors controlling the local heat transfer behaviour from a finned-tube bundle is the flow condition within. Since the geometry controlled the flow, the more complex flow in the bundles is expected for the intended circular finned-tubes. To have the more understanding on the local heat transfer distribution over a fin surface, detailed knowledge of such a complex flow will be helpful. To describe the flow patterns, many researchers (Brauer [7], Goldstein and Karni [16], Goldstein et al. [17], Hu and Jacobi [21], Lymer [42], Neal, and Hitchcock [45], Sung et al. [63]) used different ways. A comprehensive review on the flow distribution on a single tube and tube bundles was given by Brauer [7]. According to his achievement, the dead (inactive) area of the fins was about 40 % for circular finned-tube banks. Neal and Hitchcock [45] presented the flow visualization result of general flow pattern over a second row of the staggered arrangement tube bundle, which is shown in Figure 2.2.

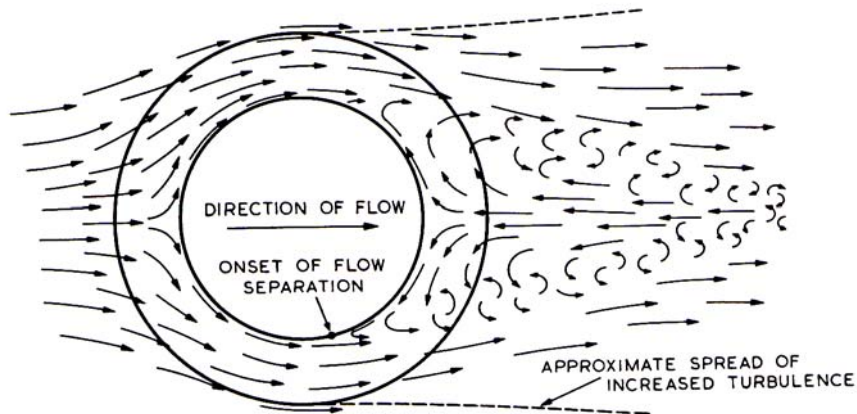


Figure 2.2 Schematic of general flow pattern over a second row of the staggered arrangement tube bundle [45].

Neal and Hitchcock observed that the separation point of second row occurred shortly after ($\theta = 90^\circ$, if measured from the stagnation point.) and at ($\theta > 90^\circ$) for the sixth row. Sparrow and Chastain [60] found the flow separation on the tube at ($\theta = 90^\circ$) and this is similar to the reports by Zhukauskas [81] and Watel et al. [71]. It is useful to note that the flow separation on the tube depends on the Reynolds number and geometrical parameters.

Horseshoe vortices are counter rotating vortices that usually swept around the tube and occur due to adverse pressure gradient near the fin-tube junction. Two horseshoe vortices in the upstream near fin-tube junction were also illustrated by Sparrow and Chastain [60]. Here, the flow was detected by painting on the fin surface

with a mixture of lampblack powder and oil. Depending on the angle of attack, the leading edge flow separation and the reattachment of the flow separated may be apparent in the upstream region of the fin. They noted that the recirculation of the flow and the reattachment zones would be impossible without leading edge separation. Hu and Jacobi [21] also found that when $Re_{dh} \geq 9000$, there will be of the phenomenon of the leading edge separation and reattachment. By using naphthalene sublimation technique, the existence of counter rotating vortices near the corner junction of a cylinder in cross flow was shown by Goldstein and Karni [16], Goldstein et al. [17] and Sung et al. [63].

2.3 Analysis of Geometric and Flow Parameters

The distribution of the heat transfer coefficient over a finned-tube is depending primarily on the flow conditions and the finning geometry. Moreover, there are significant factors controlling the heat transfer and pressure drop from a finned-tube bundle and the interaction between such factors creates further complicated designing problems.

2.3.1 Effect of Fin Height

Enhancement the heat transfer and reduction of the pressure drop from finned-tubes may necessitate considering the many parameters and first of all, the fin height effect of the circular finned-tube. Antuf'ev and Gusev [2], Konstantinidis et al. [33], Mirkovic [43], and Yudin et al. [80] observed that an increase of the fin height of the staggered tube arrangement provides the decrease of heat transfer coefficient and the increase of pressure drop. Brauer [6] probed both in-line and staggered arrays and validated the same trend for pressure drop as others observed. However, different heat transfer results were revealed since Brauer neglected the fin efficiency effect in the experiments. It is imperative to note that the nature of flow over the tube bundle with an increase of fin height comes close to the flow characteristic found along the channel (Zhukauskas [80]).

Brauer and Zhukauskas documented that because of the thicker boundary layer developing at the fin base, the heat transfer at the fin tip was higher than at its base. Zukauskas et al. [82], and Hu and Jacobi [21] reported that the highest value of the average heat transfer coefficients along the fin height, are found to be near ($\theta = \pm 90^\circ$)

where the narrowest flow passage in the bundle exists. It can be explained that due to the constriction in the flow passage, the flow velocity reaches maximum and causes a high local heat transfer. At $(\theta = 0^\circ)$ and $(\theta = 180^\circ)$ the relative heat transfer coefficient, i.e. the ratio of local heat transfer coefficient to the averaged heat transfer coefficient over a fin height, attained its maximum at the fin tip. At $(\theta = 90^\circ)$, the relative maximum heat transfer occurred in the middle of the fin height. Therefore, it is useful to note that the nature of the local heat transfer distribution over the fin height was changed according to the angle of fin surface.

According to Hu and Jacobi [21], the mass transfer is also increased near the fin base $(\theta = \pm 30^\circ)$ due to the vortex at low Reynolds number. For higher Reynolds numbers, about $Re > 9000$, higher mass transfer rates near the fin tip are observed for $(\theta = \pm 170^\circ)$. However, it was studied only a single row of circular finned-tubes.

Kearney [31] described that the effects of bundle arrangement and the fin height on the local and average heat transfer performance are coupled. A low finned-tube $(\frac{d_f}{d} = 2)$ may perform better in the staggered arrangement while high finned-tubes $(\frac{d_f}{d} = 4)$ are not giving a substantial effect to the bundle arrangement. Kearney showed that the inactive region covered less of the total fin area for the in-line arrangement as $\frac{d_f}{d}$ increases. It has to be understood that the heat transfer coefficient will decrease and the pressure drop will increase when the fin height increases.

2.3.2 Effect of Fin Spacing

Upon observation of a variety of finned-tube bundles a selection of the correct spacing between fins is need to emphasize. Experimental results of Antuf'ev and Gusev [2], Brauer [5, 6], Rabas et al. [47], Rabas and Taborek [48], and Yudin et al. [80], show that the heat transfer coefficient near the fin base of closer fin spacing is smaller than the greater fin spacing due to the thicker boundary layer. Generally, the smaller gap fin spacing creates the thicker boundary layers. The stagnation zone formation at the root of the fin and the tube surface is swept by a non turbulent flow and it is excluded from taking part in active heat transfer. Thus, the allowable extent of reducing the fin spacing will depend on the velocity and turbulence of the flow in the

inter fin spaces [2]. Zhukauskas [81] found that the heat transfer coefficient increases when the spacing is raised to 6 mm (the mean distance between the fins = 4.5 mm) and a further increase of the fin spacing does not necessarily change it for the Reynolds range of 4.8×10^4 to 7.6×10^5 . It is reasonable to expect that the influence of the effect of the fin spacing on the heat transfer decreases with higher Reynolds number. However, Rabas et al. [47] gave an important consideration that the thermal performance is almost independent of the Reynolds number for the larger fin density (0.98 fins/mm). They observed that the fin density has much stronger impact on the performance for the larger diameter of tube ($d = 31.75$ mm). They examined for the low fins, which is less than 6.35 mm at the range of $1000 \leq Re \leq 25000$.

For a case of less spacing, a larger pressure drop and worse fouling condition are expected to occur on the air-side. The increasing of the fin density from 275.6 fins per meter to 342.5 fins per meter, affected the pressure drop whereas no effect upon the air-side heat transfer coefficient is found by Jameson [23]. Ward and Young [69] made the same conclusion that the pressure drop decreases when the fin spacing increases from 201.97 to 407.87 fins per meter.

Kyuntys et al. [34] studied the effect of fin height to fin spacing relation $\left(\frac{h_f}{s}\right)$ for the staggered tube arrangement. When $\frac{h_f}{s} \leq 1.9$, the heat transfer coefficient does not depend on the relative depth of the inter fin space, and when $\frac{h_f}{s} > 1.9$, the Nusselt number decreased in proportion to $\left(\frac{h_f}{s}\right)^{-0.7}$. They recommended that this phenomenon was valid from $Re = 5 \times 10^3$ to 5×10^4 and $\frac{h_f}{s} = 1$ to 3.5. However, Briggs and Young [8] and Stasiulevičius and Skrinška [62] found different conditions at $\left(\frac{h_f}{s}\right)^{-0.2}$ and $\left(\frac{h_f}{s}\right)^{-0.14}$ respectively. Therefore, no uniform effect of $\frac{h_f}{s}$ on the heat transfer coefficient is expected, though showing a same trend as increasing $\frac{h_f}{s}$ will cause the decrease the heat transfer coefficient.

Recently, Watel et al. [70, 71] expressed the effect of the dimensionless ratio of fin spacing to the tube diameter as $Nu = c Re^m$. The exponent “m” decreases from 0.73

to 0.59 with increases of $\frac{S}{d}$ from 0.034 to 0.103. When $\frac{S}{d}$ is greater than 0.241, the exponent remains to 0.55. The effect of the geometrical parameter $\frac{S}{d}$ on the heat transfer coefficient is more significant for low Reynolds numbers. By their results at $Re > 10^4$, there is no significant increase of the Nu number when $\frac{S}{d}$ is varied from 0.069 to 0.103. According to the boundary layer theory, the comparative difference of the Nusselt number with the spacing must decrease when the Reynolds number increases. Air velocity and flow patterns also play a critical role when examining the fin spacing effect. Fin spacing led to the occurrence of boundary layer, which determines the outcomes of the heat transfer and pressure drop.

2.3.3 Effect of Fin Thickness

A few researchers performed the observation to the effect of fin thickness. Ward and Young [69] found that the Nusselt number increased with the fin thickness. However, Briggs and Young [8] obtained the opposite results showing that the heat transfer coefficient is less dependent upon the fin thickness and will be decreased as the fin thickness is increased. Three different values of the fin thickness 0.457 mm, 1.06 mm and 2.02 mm of helically finned-tubes were examined and the heat transfer coefficient of the largest value of fin thickness was approximately 8% less than that of the thinness one. By means of the analytical approach, Stasiulevičius and Skrinska [62] showed fin thickness effect is unproductive on the convective heat transfer.

2.3.4 Effect of Tube Outside Diameter

The average heat transfer coefficient depends mainly on the outside diameter of the tube [69]. The flow will change when the tube diameter is varied. The velocity at the narrowest cross section is raised to a certain extent with increasing the tube diameter and the recirculation zone behind the tube is also increased. Jameson [23], Mirkovic [43] and Torikoshi et al. [65] showed that the pressure drop increases with the tube diameter. Jameson [23] tested three different tube diameters, (15.875 mm, 19.05 mm and 25.4 mm) of staggered helically finned-tubes. Mirkovic [43] investigated the heat transfer and pressure drop in an eight-row deep staggered tube bundle for the two tube diameters 38.1mm and 50.8 mm with constant transverse and longitudinal tube

itches. Note that the tube diameter only was changed while other parameters such as the fin height and fin spacing were kept constant in their investigation. When the tube diameter increases, the wake region behind the tube will increase and the air-side pressure drop will rise. Mirkovic [43] also found that the Nusselt number increases for the larger tube diameter. However, Torikoshi et al. [65] observed no significant variation of the average heat transfer coefficient. Torikoshi et al. investigated numerically the tube diameter effect on heat transfer and flow behaviour for a two-row staggered arrangement of plate finned-tubes. In contrast to the circular finned-tubes, the plate fin surface is decreased when the tube diameter increases. It is apparent that the tube diameter effect may be largely ignored for the cases where the diameter is changed only slightly.

2.3.5 Effect of Tube Spacing

Apart from the tube diameter effect, the turbulence intensity inside the bundle depends on the tube spacing and the air velocity. Hence, the pressure drop in the tube bundle will vary according to these parameters. When changing the transverse tube pitch, there are no significant changes on heat transfer performance; however, a remarkable effect on the air-side pressure drop was noted by Briggs and Young [8], Jameson [23], and Stasiulevičius and Skrinska [62]. Nevertheless, Mirkovic [43], Neal and Hitchcock [45], and Nir [46] indicated the consequence of the transverse tube pitch to the heat transfer. For the staggered arrangement, the heat transfer is higher for the closer transverse pitch (Neal and Hitchcock [45], Nir [46], and Sparrow and Samie [59]). Apparently, the velocity at the narrowest cross-section will become higher when decreasing the transverse tube pitch and this effect will lead to the higher heat transfer coefficient and pressure drop. Jameson [23], and Robinson and Briggs [50] showed that when increasing the transverse pitch, the pressure drop is found to decrease. The different conclusion is given by Mirkovic [43] with observation of the fact that both Nusselt and Euler numbers are increasing owing to the larger transverse tube pitch. In addition, he claimed that an enlargement of longitudinal tube pitch for the staggered arrangement decreases the Nu and Eu numbers. The similar result for the longitudinal pitch effect to the heat transfer performance was recorded by Neal and Hitchcock [45], and Rabas et al. [47], and the pressure drop effect was confirmed to Jameson [23].

For the in-line arrangement, Sparrow and Samie [59] observed that the pressure drop increases with the longitudinal pitch. It is possible that the tubes will act

as a single tube if the longitudinal pitch is too wide. Moreover, Rabas et al. [47] discovered that the longitudinal pitch effect depends on the fin density of the low finned-tube bundle. The heat transfer performance is identical for $S_l = 37.12$ mm and 50.80 mm with 0.4 fins per mm. However, for the fin density of 0.98 fins per mm, the heat transfer performance lowered for a larger S_l applied.

For the aspect of equilateral tube arrangements, Briggs and Young [8] investigated the test for two different tube spacings and found almost identical heat transfer performance in both cases. The pressure drop increases when the tube spacing is changed from 111.0 mm to 27.4 mm.

When evaluating the tube spacing effects, some researchers explored the relationships between the tube spacing and other geometric parameters. The relation between the tube spacing and the fin diameter was investigated by Sparrow and Samie [59], and Stasiulevičius and Skrinska [62]. According to [59], decreasing the ratio of transverse tube spacing to fin diameter ($\frac{S_t}{d_f}$) from 1.52 to 1.07, the Nu number is increased by about 35 %. For the two- row in-line array, the Nu number increased at $Re_\alpha = 8 \times 10^3$ as the longitudinal pitch to fin diameter ratio ($\frac{S_l}{d_f}$) is increased. At higher Reynolds numbers ($Re_\alpha = 3.2 \times 10^4$), the Nu number is relatively insensitive to the longitudinal pitch. For the two-row staggered array, the Nusselt number at first increased with increasing S_l , attained a maximum value at $\frac{S_l}{d_f} = 2.05$ and then, decreased as encountered for the larger pitches over the entire Reynolds number range from 7.5×10^3 to 3.2×10^4 .

Stasiulevičius and Skrinska [62] tested seven-row tube bundles and the heat transfer coefficient increased slightly (about 3 %) with an increase in $\frac{S_t}{d}$ (2.67 to 4.13) whereas a reduction in $\frac{S_l}{d}$ (2.14 to 1.46) gives the substantial rise (about 20 %). This result indicates that the longitudinal changes make more progress on the heat transfer performance than the transverse ones. The tube spacing effect is directly concerned with the fin diameter, the fin density, and the Reynolds number.

2.3.6 Effect of Row

The heat transfer from a finned-tube bundle is mainly based on the flow patterns. The flow over a single finned-tube is rather different from the cross flow over the bundle. Zhukauskas et al. [82] observed that a tube within a bundle has a higher heat transfer rate at the leading edge of the fin than a single tube has with the same Reynolds number. It is because of the turbulizing effect of the upstream rows. Brauer [6] showed complex flow visualizations of the different flow patterns of a single finned-tube, one row finned-tube, and two-row finned-tube banks. It is noted that the flow condition around the first and the second rows are different [45].

To determine the minimum number of tube rows, the performance of rows inside the bundle and the relation between such rows were examined by Kuntysh et al. [34], Kuntysh and Stenin [37], Lapin and Schurig [38], Mirkovic [43], Neal and Hitchcock [45], Sparrow and Samie [59] and Ward and Young [69]. It is agreed that the heat transfer coefficient for a first row of the staggered arrangement is about 30 % smaller than the deeper rows. Neal and Hitchcock determined that the heat transfer coefficient of the sixth row is remarkably higher than that of the second row.

For the staggered arrangement, the main flow passes through the tube and its fin surface nearly in the same way for all the rows. The influence of row effect upon heat transfer for the staggered array is less than for the in-line array and for row numbers $n \geq 2$; the heat transfer and the friction factor remain unchanged (Brauer [6], Briggs and Young [8], and Gianolio and Cuti [14]). Kuntysh and Stenin [37] drew the same conclusion by observing that the value of the heat transfer coefficient becomes constant in the second row of the four-row tube bundle. Weierman et al. [76] observed also that the friction factor is independent of the number of rows for the staggered arrangement. Antuf'ev and Gusev [2], and Kuntysh et al. [36] found that the heat transfers coefficient became constant after the third row while Ward and Young [69] discovered that the coefficient is not stabilized until the third and fourth row. In addition, Mirkovic [43], and Neal and Hitchcock [45] observed that the coefficient increases until the fifth or sixth row. As stated above, there are various findings on the flow stability of the finned-tube bundle associated with the different circumstances.

Rabas and Taborek [48], and Yudin et al. [80] developed the row correction factors. It has been assumed [31] that Yudin et al.'s shallow bundle correction factor for staggered and in-line tube banks are reasonable to apply on other correlations. Yudin

et al. investigations were performed within $10^3 \leq Re \leq 2 \times 10^4$ to prove that the average heat transfer performance of a bundle increases with a decreasing number of rows for the in-line arrangement whereas it decreases for a staggered tube bank. Alternatively, Rabas and Taborek [48] studied on the rows effect of low finned-tube bundles and presented a shallow bundle correction factor. It means that the factor increased with the number of rows for low fin density (0.393 fins/mm) but decreased for high fin density (0.984 fins/mm). For a high fin density tube bank in a staggered array, some performance characteristics similar to those of the in-line bank are noted. It is appeared that the heat transfer performances of shallow in-line tube banks always decreased with row number regardless of the fin density.

Like in case of the staggered arrangement, the experimental results were also different on the row effects of the in-line tube bundles that seem to play a more sensitive role than for the staggered bank. The second row heat transfer of the in-line arrangement is found to be lower than the first row (Brauer [6], and Kuntysch and Stenin [37]). Contrary to their reports, Kearney [31], and Sparrow and Samie [59] showed the Nu number of second row is about 35 % greater than that of the first row. The heat transfer coefficient became constant in the second row of the in-line bank as observed by Antuf'ev and Gusev [2], and Kuntysch and Stenin [37]. However, Weierman [75] found that the friction factor is stable in the third row and there are significant changes for one- and two-row banks. Brauer [6] reported that both heat transfer and pressure drop are independent of the number of rows for four or more row deep in-line banks.

All studies verified that the heat transfer coefficient around the fin, and from row-to-row vary in accordance with the bundle depth. It is useful to note that only limited results with a single tube and very few rows are found, and further studies applying four and more tube row bundles should follow. On the other hand, some studies have done to resolve this situation by developing the row correction factors.

2.3.7 Effect of Tube Arrangement

The degree of heat transfer augmentation depends on many other factors encompassing the tube layout, the turbulence intensity, the fin shape and thermal conductivity. It is important to note that selecting the suitable arrangement favours in acquiring better heat transfer rate. A few research on in-line tubes have been pursued by Brauer [6], Hashizume [20], Kuntysch and Stenin [37], Rabas and Huber [49] and

Weierman et al. [76], as widely accepted the notion of that the staggered arrangement has more advantages in terms of thermal behaviours than the in-line arrangement. For staggered tube bundles, a small recirculation zone only appeared behind the tubes since its own structure made blockages whereas in the in-line arrangement both upstream and downstream sites are within the recirculation zone. Consequently, the in-line banks have had the insufficient mixing and lower heat transfer coefficients. In addition, the extent of the advantages of staggered banks depends at least on the effect of fin height, and for high fins (15 mm) Brauer [7] showed that the difference is 100 %. In contrast, Kearney and Jacobi [32] suggested that the high finned in-line bundle performance is found to be comparable to the staggered arrangement. Rabas and Huber [49] show a trend that the thermal performance of shallow in-line banks approaches that of the staggered banks as the Reynolds number increases. On the other hand, Kuntysh et al. [37] claimed that an arrangement lies between the in-line and staggered arrays have the better rate of heat transfer.

2.3.8 Effect of Air Velocity

One of the influential factors governing the heat transfer performance in finned-tubes is the boundary layer development, whose shape is varying according to air velocity. When the air velocity increases, the formation of horseshoe vortices will increase and the boundary layer thickness will decrease. It is generally accepted that the fluid velocity in the recirculation zone is lower than in the main stream and the heat transfer coefficient therein is reduced.

The selection of flow velocity is important to determine the Reynolds number for bodies in cross flow. Remember that there is no unanimous agreement on the characteristic dimension used to define the Reynolds number. The investigators enable to employ the inlet velocity, mean velocity, and the velocity in the minimum cross section area as reference velocity. According to the available literature, the reference velocity is mostly defined as last one. Moreover, the complete design of heat exchangers involves the method of drafting air. There will be a different performance of heat transfer and pressure drop of the finned-tube bundle depending on the flow conditions at the bundle inlet (Gianolio and Cuti [14], and Stasiulevičius and Skrinska [62]).

2.4 Average Heat Transfer Correlations

The information about existing correlations of the average heat transfer on circular finned-tube bundles are reviewed here as a second part of the literature review on the circular finned-tube bundles. As previously mentioned, heat transfer from a circular finned-tube in a bundle is a function of related geometrical parameters and the flow variables involved. In order to demonstrate these principal factors, a large number of heat transfer correlations mostly based on the author's own data were deduced. Analysis of the experimental results shows that there will be different results that depend on the method of the determination of heat transfer coefficients. Generally, there are two possible ways to obtain the heat transfer from a tube: the local simulation technique [80, 81 and 83] (only one test tube is heated) and the complete thermal simulation method (all test tubes heated).

Webb [72] and Nir [46] presented excellent surveys for published data and correlations of overall heat transfer and pressure drop correlations on circular finned-tube bundles. The available correlations are incorporated in the Appendix D. Webb [72] reported that recommendation of a single correlation and direct comparison to the different correlations was a difficult task. However, Webb recommends the heat transfer correlation of Briggs and Young [8]. Their investigation was based on a previous investigation of Ward and Young [69] where seven different staggered finned-tube bundles were tested and the average Nusselt number for the six-row bundle was correlated. Later they proceeded their work by extending the database with nine additional banks of tubes. Briggs and Young's correlation is widely accepted and used because of their investigation based on the widest range of parameters. It is reported that the tube spacing effect is not found in their correlation.

Nir [46] then provided a quantitative comparison of some experimental data with the Briggs and Young correlation. According to Nir, the available heat transfer data of tube banks with the plain fin covered the range of $\pm 20\%$ of Briggs and Young [8] correlation. Nir also gave a set of heat transfer and pressure drop correlations based on his own data and 16 published sources. This correlation corresponds within 10% of the most of available test data. However, Nir described for both segmental and plane fin characteristics in an equation. It is expected that due to the different fin geometries, the respective boundary layer development may be dissimilar.

According to available data, most of the investigations were performed in the Reynolds number range of 10^3 to 3×10^4 and the investigation based on the widest range ($2 \times 10^4 \leq Re \leq 1.3 \times 10^6$) was given by Zhukauskas et al. [82]. They provided an extensive reference database for heat transfer and pressure drop of finned-tube bundles in cross flow. Their work covers 21 different seven-row finned-tube bundles. The heat transfer correlations were obtained from their own data and the experimental data for the bundles scatter over the range of ± 14 %. Note that the effect of bundle configuration and the fin parameters are expressed in these correlations except for the fin thickness effect. The term for bundle depth effect is missing; however, it is reasonable to accept the fact that their investigations are based on the depth of seven-row. Unfortunately, they used some dummy tubes (unheated tubes) in their tests and Nir [46] suggested that this method may lead to errors.

In pursuit of the optimisation of low finned-tube bundles, Rabas and Taborek [48] surveyed the relevant literature of the heat transfer and pressure drop performances. Rabas et al. [47] developed heat transfer and friction factor correlations for low fins and small fin spacing based on 30 different staggered tube bundles. However, it is limited for the bundles to the fin height of under 6.35 mm.

Yudin et al. [80], Weierman [74], and Gianolio and Guti [14] studied on the effect of bundle depth. Gianolio and Guti [14] modified the Briggs and Young [8], and Schmidt [56] correlations by adding an extra term to account for the bundle depth effect, which was left out in it. They run the test for 17 finned-tube banks of the equilateral triangular pitch by varying the number of rows ranging from one to six. Based on their own data, air-side heat transfer coefficient equations for forced draft were provided.

Alternatively, the effects of bundle arrangement, S_t and S_r are not stated in both the Schmidt [56] and the VDI-Wärmeatlas [68] correlations. Their correlations are prepared for the ratio of the total heat transfer surface area to the exposed base tube area. Schmidt provided correlations for both arrangements and VDI-Wärmeatlas presented the average heat transfer correlations for a one to three-row banks and four or more row banks respectively.

Another set of correlations for the in-line, mixed in-line-staggered and the staggered tube bundles were provided by Kuntysh and Stenin [37]. They studied the average heat transfer coefficient on an averaged four-row tube bundle basis and on a

per row basis respectively. However, no consideration was given to fin efficiency effect in their study and they did not express anything for the fin parameters and the bundle effect in the correlations.

2.5 Pressure Drop Correlations

The basic design feature of a heat exchanger is aimed to synchronize heat transfer rate and pressure drop in the system. A minimum pumping power to overcome the effect of fluid friction and to move the fluid through the heat exchanger is essential in designing the compact heat exchanger. For this reason, a number of correlations on pressure drop of circular finned-tube bundles have been verified and showed that the pressure drop depends on the number of rows except for the result of Gianolio and Guti [14]. Jameson [23], Kuntysh et al. [35], Nir [46], Robinson and Briggs [50], Stasiulevičius and Skrinska [62], and Ward and Young [69] that are based on their own data, though Gianolio and Guti [14], Gunter and Shaw [18], Haaf [19], and Rabas and Eckels [47] used wide ranges of data.

Jameson [23] tested the staggered bundles of one to eight rows and varied, $\frac{S_t}{d}$ from 1.9 to 3.6 and $\frac{S_l}{d}$ from 1.1 to 2.5. However, it should be noted that there is no effect of the fin parameters in this relation.

Another pressure drop correlation for the staggered arrangement was given by Ward and Young [69]. This correlation covered for the range of $10^3 < Re < 3 \times 10^4$ and all influence parameters were related. However, Haaf [19] compared this result with other experimental data (Brauer [6], Briggs and Young [8], Kays and London [30] and Weyrauch [77]) and suggested that the heat transfer coefficient of the prediction of [69] can vary by as much as 100%. Haaf developed a new pressure drop correlation for both in-line and staggered arrays in terms of the equivalent diameter and mean velocity in the bundle based on the equation from Ward and Young.

Webb [72] cited his recommendation to Robinson and Briggs [50]'s pressure drop correlation for a staggered tube layout. This correlation was empirically based on 15 equilateral triangular arrangements and two isosceles triangular arrangements. This correlation is found to be valid for four and more tube rows and the standard deviation of this correlation is 10.7 %. However, this equation is questionable for larger $\frac{S}{h_f}$

values, which included a small range of fin geometry variables $\frac{s}{h_f}$ were covered. Moreover, Nir [46] construed that [50] equation's accuracy is insufficient when comparing with his own and other available data. A valid research on the pressure drop works was done by Nir and then correlated by embracing the important factors like the ratio of heat transfer area of a row of tubes to free flow area. It is noted that this correlation was marginalized to within 10% of the data of several authors. However, these correlations are applicable for staggered arrangement only.

Without considering for the in-line arrangement, Stasiulevičius and Skrinska [62] gave pressure drop correlations in terms of Eu number for two different Reynolds number ranges. It is found that the effect of fin parameters apart from the fin thickness and the transverse and longitudinal pitches are reflected in these correlations. It should, however, be stressed that the fin thickness effect is found to be negligible for convective heat transfer but warranted to resolve the problem of pressure drop.

For low fin bundles, Rabas et al. [47] presented the more accurate correlation based on their own and other published data. The correlation is valid for staggered bundles; however, it was not suitable for a high finned-tube bundle.

Gianolio and Guti [14] also gave pressure drop correlations for staggered arrangement under the forced and induced draft modes based on 17 tube banks having one to six rows. It is surprising to find that the number of rows effect is not significantly affect on the pressure drop for forced draft mode. Apparently, the effects of the fin parameter and the longitudinal tube pitch effect have generally overlooked.

2.6 Concluding Remarks

A considerable amount of related data on the local and average heat transfer and the pressure drop were established and qualitative judgements on circular finned-tube configurations are rendered. Despite of these earlier developments, this review indicated that further concentration on the existing problems in designing of optimum fin geometry and tube arrangements are still necessary. Some conclusion points are,

- Considerably more information on numerical simulation has been published for plate fins than circular fin tubes.

- The heat transfer coefficient and flow distribution over a tube in the bundle is different to a single tube.
- Temperature distributions over the fin surface and the flow structures between fins are of complex pattern. When the need arises to measure such effects accurately, it is an experimentally difficult task to do without disturbing the heat transfer behaviour on a fin surface. Therefore, more precise data on the local behaviour are necessary.
- Moreover, clearer effects on the visualization are required and numerical simulations are essential for such complex flow patterns.
- Different results came out of the relevant information regarding the tube spacing adjustments and number of rows.
- Controlling the parameters and the interaction rendered more intricate problems and hence, all dominant geometric parameters should be considered to resolve in the problem.
- All correlations reviewed in the previous section were based on data for a depth of four and more rows at Re from 10^3 to 1.3×10^6 . Majority of the studies were carried out for the staggered arrangement and comparatively very few investigations for the in-line arrangement were found. Moreover, most of the previous correlations are failed to account for all geometric variables involved.
- Since most correlations were based on their own data, authors gave different formula for the heat transfer and pressure drop correlations. In addition, the characteristic dimension to define Reynolds number was dissimilar. Thus, it is fairly anticipated that to compare directly to experimental correlations is found to be difficult.
- Finally, all related works for the circular finned-tubes have been correlated experimental ones and respective correlations have not been verified yet under numerical simulations. Therefore, additional numerical data are needed in order to establish improved correlations.

3 Objectives

The objective of the present study is to provide more complete understanding of the distributions of local and average heat transfer and pressure drop behaviour of circular finned-tube heat exchangers. Since heat transfer coefficients are much lower in air than in liquid flows or two-phase fluids, this study will help to solve the problems associated with the designing of air-side heat transfer enhancement by means of circular finned-tubes.

This numerical investigation was carried out for the range of Reynolds numbers (based on air velocity through the minimum free flow area and tube outside diameter) from 5×10^3 to 7×10^4 . A finite volume numerical scheme is used to predict the conjugate heat transfer and fluid flow characteristics with the aid of the computational fluid dynamics (CFD) commercial code, FLUENT. The governing equations for the energy and momentum conservation were solved numerically with the assumption of three-dimensional unsteady flow. An improved model, the RNG (Renormalization group) based k - ε turbulence model was applied in this investigation.

As described in the section 2.6, the available relevant literature is quite limited with respect to the experiments and it is still difficult to predict the physics of the flow patterns within the circular finned-tube banks. Also, the flow structure will depend on the different geometries, and accurate information on this dimensional local transport phenomenon is required. Therefore, the velocity and temperature distributions over the fin surface and within the bundle were studied numerically. Regarding to this, the flow behaviour of the developing boundary layer, the horseshoe vortex system, the flow separation, and the tube wake region in the circular finned-tube banks will be visualized. Consequently, the influence of the geometric parameters on heat transfer and pressure drop are studied and their results are discussed. Hence, the following geometric parameters were considered in this investigation:

1. Fin Height
2. Fin Spacing
3. Fin Thickness
4. Tube Diameter
5. Tube Spacing (Transverse and Longitudinal)
6. Tube Arrangement (Staggered and In-line) and
7. Number of Rows Effect

The major aim of the present study is to attain reliable correlations. Therefore, the results are evaluated by comparison with available experimental data and then, the average heat transfer and pressure drop data are correlated from two to six rows for staggered tube banks and three to five rows for in-line tube banks in the forms of Nusselt number Nu and Euler number Eu , respectively.

Rather than detailed investigation of numerical and modelling aspects, to pay more attention to verify the heat transfer and pressure drop behaviour of circular finned-tubes by employing the numerical means is the focus of the present work.

4 Numerical Consideration

Due to the advances in computational hardware and available numerical methods, CFD is a powerful tool for the prediction of the fluid motion in various situations, thus, enabling a proper design. CFD is a sophisticated way to analyse not only for fluid flow behaviour but also the processes of heat and mass transfer.

4.1 Governing Equations and CFD Models

The flow and temperature field in the model geometry is determined by the continuity equation, the complete unsteady Navier-Stokes and the energy equation for incompressible fluid with temperature-dependent properties. These three-dimensional equations, to be solved by numerical calculations in the Cartesian coordinates, are as follows:

$$\text{Continuity equation: } \frac{\partial \rho}{\partial t} + \frac{\partial}{\partial x_i} (\rho u_i) = 0 \quad (4.1)$$

$$\text{Momentum equation: } \frac{\partial}{\partial t} (\rho u_i) + \frac{\partial}{\partial x_j} (\rho u_i u_j) = -\frac{\partial p}{\partial x_i} + \frac{\partial \tau_{ij}}{\partial x_j} \quad (4.2)$$

$$\text{Where } \tau_{ij} = \mu \left(\frac{\partial u_i}{\partial x_j} + \frac{\partial u_j}{\partial x_i} \right) - \frac{2}{3} \mu \frac{\partial u_k}{\partial x_k} \delta_{ij} \quad (4.3)$$

$$\text{Energy equation: } \frac{\partial}{\partial t} (\rho E) + \frac{\partial}{\partial x_i} (u_i (\rho E + p)) = \frac{\partial}{\partial x_i} \left(k \frac{\partial T}{\partial x_i} \right) \quad (4.4)$$

Where E is the total energy and k is the thermal conductivity.

In the relevant numerical investigations of plate fin arrangements by [4], [10], [24], [28], [44], [58], [64], [65] and [66], the flow was assumed to be laminar since the Reynolds number is less than 2000 and thus, no discussion has been done for turbulent modelling which has to be considered in the proposed circular finned-tube geometry.

Generally, the Navier-Stokes equations describe the motion of the turbulent flow. However, it is too costly and time-consuming to solve these equations for complex flow problems [26]. Alternatively, two methods have been suggested in the past: (i) Large Eddy Simulation (LES) where the large energy containing eddies are simulated directly while the small eddies are accounted for by averaging. The separation of large and small eddies requires following, (ii) Reynolds averaging (RANS) where all eddies are accounted for by Reynolds stresses obtained by averaging the Navier-Stokes equations (time averaging for statistically steady flows, ensemble averaging for unsteady flows).

The Reynolds-averaged Navier-Stokes equations represent transport equations for the mean flow quantities. The solution variables in the instantaneous exact Navier-Stokes equations are decomposed into the mean (time averaged) and fluctuating components: $u_i = \bar{u}_i + u'_i$, $p = \bar{p} + p'$, $T = \bar{T} + T'$. The Reynolds-averaged Navier-Stokes equations for incompressible flow are sufficiently well approximated by,

$$\frac{\partial \bar{p}}{\partial t} + \frac{\partial}{\partial x_j} (\bar{\rho} \bar{u}_j) = 0 \quad (4.5)$$

$$\frac{\partial}{\partial t} (\bar{\rho} \bar{u}_i) + \frac{\partial}{\partial x_j} (\bar{\rho} \bar{u}_i \bar{u}_j) = - \frac{\partial \bar{p}}{\partial x_i} + \frac{\partial}{\partial x_j} \left[\mu \left(\frac{\partial \bar{u}_i}{\partial x_j} + \frac{\partial \bar{u}_j}{\partial x_i} - \frac{2}{3} \delta_{ij} \frac{\partial \bar{u}_l}{\partial x_l} \right) \right] + \frac{\partial}{\partial x_j} \left(- \bar{\rho} \overline{u'_i u'_j} \right) \quad (4.6)$$

where \bar{u}_i is the i^{th} component of the mean velocity, $\bar{\rho}$ is the density and \bar{p} is the static pressure.

To model appropriately the Reynolds stress term of the Equation (4.6), one of the common methods is applying the Boussinesq hypothesis, which is used in the well-known $k-\varepsilon$ models. The eddy viscosity model (Boussinesq hypothesis) provides the following expression for the Reynolds stress:

$$-\overline{\rho u'_i u'_j} = \mu_t \left(\frac{\partial \bar{u}_i}{\partial x_j} + \frac{\partial \bar{u}_j}{\partial x_i} \right) - \frac{2}{3} \left(\rho k + \mu_t \frac{\partial u_i}{\partial x_i} \right) \delta_{ij} \quad (4.7)$$

where μ_t is the turbulent viscosity. Usually, the molecular viscosity and the turbulent viscosity are combined to an effective viscosity

$$\mu_{eff} = \mu + \mu_t \quad (4.8)$$

In the following, all averaged flow quantities “ \bar{a} ” are replaced by “ a ” for the purpose of convenience:

$$\frac{\partial}{\partial t} (\rho E) + \frac{\partial}{\partial x_i} (u_i (\rho E + p)) = \frac{\partial}{\partial x_i} \left(k_{eff} \frac{\partial T}{\partial x_i} \right) \quad (4.9)$$

where E is the total energy and the effective conductivity, $k_{eff} = k + k_t$ and k_t is the turbulent thermal conductivity. The influence of gravitational force of the airflow and radiation heat transfer effects have been neglected.

The following energy transport equation used within solid region (fins):

$$\frac{\partial}{\partial t} \rho \tilde{h} = \frac{\partial}{\partial x_i} \left(k_s \frac{\partial T}{\partial x_i} \right) \quad (4.10)$$

where ρ = density, k = conductivity, T = temperature, and \tilde{h} = sensible enthalpy, $\int_{T_{ref}}^T c_p dT$.

The Reynolds-averaged approach uses models such as Spalart-Allmaras (one equation model), standard k - ε and its variants. The RNG model is based on the form of the standard k - ε model and derived from the instantaneous Navier-Stokes equations, using a mathematical technique called Renormalization Group (RNG) method. Contrary to the RNG model, the standard k - ε is supported by benchmark data and valid only for fully turbulent flow. Moreover, Tutar and Holdo [67] reported that standard k - ε model does not well evaluate near wall condition at higher Reynolds number and failed to predict the wake behind a tube while the RNG model performed well for predicting for vortex shedding. It was noted by Lee and Chen [40] that the RNG theory provides

low Reynolds number effects also, so that it enables to predict the laminar-like behaviour. Though, the evaluation of such partly turbulent characteristics may be effective subject to appropriate treatment of near wall region [11].

Moreover, the accuracy of the RNG model was enhanced by adding the term that accounts for rapidly strained flow and effects of swirling flow ([11], [40]). The RNG model proved that it has more substantial improvements than the standard model, and offers more accurate and reliable results for the various flow types. Comparing to the standard $k-\varepsilon$ model, the RNG model will occupy 10 to 15 % more CPU time due to extra terms and functions in the governing equations [11].

Even though no single and universal model for the turbulent flow in complex geometry exists, there is another alternative method, which can be employed to transform the Navier-Stokes equations. LES is a model wherein the equations are filtered spatially. To compute the flow eddies, the LES provides a time-dependent simulation by using a set of the filtered equations rather than time averaging. Turbulent flow is characterized by eddies with a wide range of length and time scale. By filtering, only small eddies apparently smaller than the filtered size become accessible to move. It suggested that small eddies are more universal, random, homogeneous and isotropic, which simplifies to develop the appropriate model. In LES, such small eddies have to be modelled by a sub grid scale model.

It is necessary to understand that the choice of the turbulence model depends also on the available computer resource. Contrast to RANS, the LES that may be necessary to use extremely fine grids and the time required for typical calculations, will have taken somebody too long to reach for an acceptable solution. Instead FLUENT generally recommends the Reynolds-averaged approach for the conventional turbulence models and stressed that the application of LES for industrial fluid simulations is in its infancy and typical applications to date have been for simple geometries. In addition, the use of wall functions with LES is an approximation that requires further validation [11]. On the other hand, under the current computation power circumstances, the LES is an optional approach for a complex geometry problem such as supposed circular finned-tube heat exchanger and thus, the conventional turbulence model employing the Reynolds-averaged approach was utilized in order to predict the heat and momentum transfer on the circular finned-tube bundle. In this study, the two-equation RNG model was adopted to solve the turbulence kinetic energy and its dissipation rate.

4.1.1 The RNG k - ε Model

The RNG k - ε model [FLUENT] employs the Boussinesq concepts (Equations 4.7 and 4.8) and adopts the following relations for turbulence closure:

$$\mu_t = \rho C_\mu \frac{\tilde{k}^2}{\varepsilon} \quad (4.11)$$

$$\rho \frac{D\tilde{k}}{Dt} = \frac{\partial}{\partial x_j} \left[\alpha_p \mu_{\text{eff}} \frac{\partial \tilde{k}}{\partial x_j} \right] + \mu_t S^2 - \rho \varepsilon \quad (4.12)$$

$$\rho \frac{D\varepsilon}{Dt} = \frac{\partial}{\partial x_j} \left[\alpha_p \mu_{\text{eff}} \frac{\partial \varepsilon}{\partial x_j} \right] + C_{1\varepsilon} \frac{\varepsilon}{\tilde{k}} \mu_t S^2 - C_{2\varepsilon} \rho \frac{\varepsilon^2}{\tilde{k}} - R \quad (4.13)$$

where $C_\mu = 0.0845$, \tilde{k} is the turbulent kinetic energy, ε is referred to the dissipation rate of \tilde{k} and α_p is the inverse Prandtl number for turbulent transport as computed via the following equation.

$$\left| \frac{\alpha_p - 1.3929}{-0.3929} \right|^{0.6321} \left| \frac{\alpha_p + 2.3929}{3.3929} \right|^{0.3679} = \frac{\mu}{\mu_{\text{eff}}} \quad (4.14)$$

The rate of strain term R is given by

$$R = \frac{C_\mu \rho \eta^3 \left(1 - \frac{\eta}{\eta_0} \right) \varepsilon^2}{1 + \beta \eta^3} \frac{1}{\tilde{k}} \quad (4.15)$$

where $\eta = \frac{S\tilde{k}}{\varepsilon}$, $\eta_0 = 4.38$, $\beta = 0.012$ and $S^2 = 2S_{ij}S_{ij}$ is the modules of the rate of strain tensor expressed as $S_{ij} = \frac{1}{2} \left(\frac{\partial u_i}{\partial x_j} + \frac{\partial u_j}{\partial x_i} \right)$. The RNG theory gives values of the constant $C_{1\varepsilon} = 1.42$ and $C_{2\varepsilon} = 1.68$.

4.2 Numerical Simulation

A difficulty for application of the numerical methods in circular finned-tube exchangers is the fact that one is faced with a complex geometry of the flow configuration. Furthermore, several geometric parameters directly effecting on the enhancement of heat transfer.

4.2.1 Introduction

Advances in physical models, numerical analysis and computational power enable simulation of the heat transfer characteristics in three-dimensional circumstances. A three dimensional approximation of a turbulent flow is chosen to explore since the three-dimensional approach is considerably greater than two-dimensional [4] and moreover, a turbulent flow is fundamentally three-dimensional. Owing to extremely long computation times, detailed studies on the circular finned-tube exchanger in three-dimensional flow are very uncommon [25]. Hence, the simulation of the three-dimensional flow field under complex geometrical conditions is seemingly intricate and challenging task.

The available computational fluid dynamics software package FLUENT [11] is used to determine the related problems. FLUENT uses a finite volume method and requires from the user to supply the grid system, physical properties and the boundary conditions. When planning to simulate a problem, basic computation model considerations such as boundary conditions, the size of computational domain, grid topology, two dimensions or three-dimension model, are necessary. For example, appropriate choice of the grid type can save the set up time and computational expense. Moreover, a careful consideration for the selection of physical models and determination of the solution procedure will produce more efficient results. Dependent on the problem, the geometry can be created and meshed with a careful consideration on the size of the computational domain, and shape, density and smoothness of cells. Once a grid has been fed into FLUENT, check the grids and execute the solution after setting models, boundary conditions, and material properties. FLUENT provides the function for post processing the results and if necessary refined the grids is available and solve again as the above procedure.

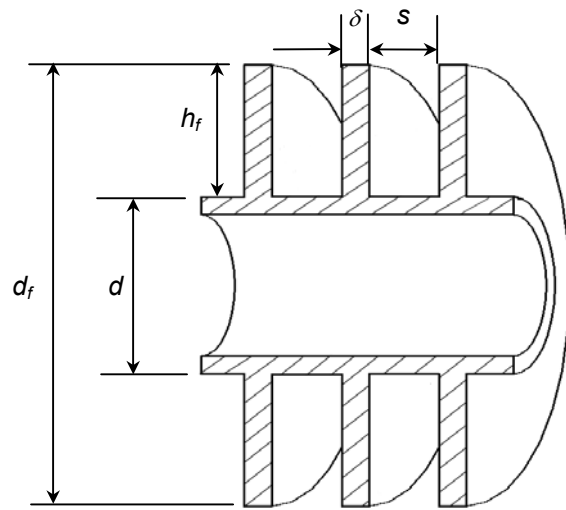


Figure 4.1 Cross-section of a circular fin tube.

As described in the objective, the purpose of this study is to investigate numerically the effects of geometric parameters on the flow, the heat transfer characteristics, and pressure loss coefficients of circular finned-tube heat exchangers. A detailed circular finned-tube scheme is presented in Figure 4.1. The dimensional nomenclature relevant to Figure 4.1 are the tube outside diameter d , fin diameter d_f , fin thickness δ , fin spacing s , and fin height h_f . Numerical calculations were performed for 18 bundles of the staggered arrangement and 11 bundles of the in-line arrangement, which are summarized in Table 4.1. All bundles depths were considered with four rows except for the bundle s6 and i4 where numerical investigations were performed with two to six rows and three to five rows, respectively. All the simulations were carried out for the following ranges: $5 \times 10^3 \leq Re \leq 7 \times 10^4$, $3 \text{ mm} \leq h_f \leq 12 \text{ mm}$, $0.7 \text{ mm} \leq s \leq 4 \text{ mm}$, $0.3 \text{ mm} \leq \delta \leq 0.6 \text{ mm}$, $13.9 \text{ mm} \leq d \leq 28 \text{ mm}$.

4.2.2 Computational Domains

A schematic view of the proposed in-line and staggered tube bundles are shown in Figure 4.2(a) and (b). The numerical simulations were based on a single fin pitch (e.g., [24], [25], [29], [30], [64], and [65]). Computational domains to be considered in this study are displayed by dotted lines with symmetry conditions (e.g., [4], [25], [29], [30]). In Figure 4.2(c) symmetry lines passing through on the mid-plane between two fins and centres of the fin thickness (e.g., [4], [9], [29], [44], [57], [64], and [65]). X and Y direction are the stream wise and the cross - stream respectively with S_x and S_y as the respective tube pitches.

For Staggered Arrangement

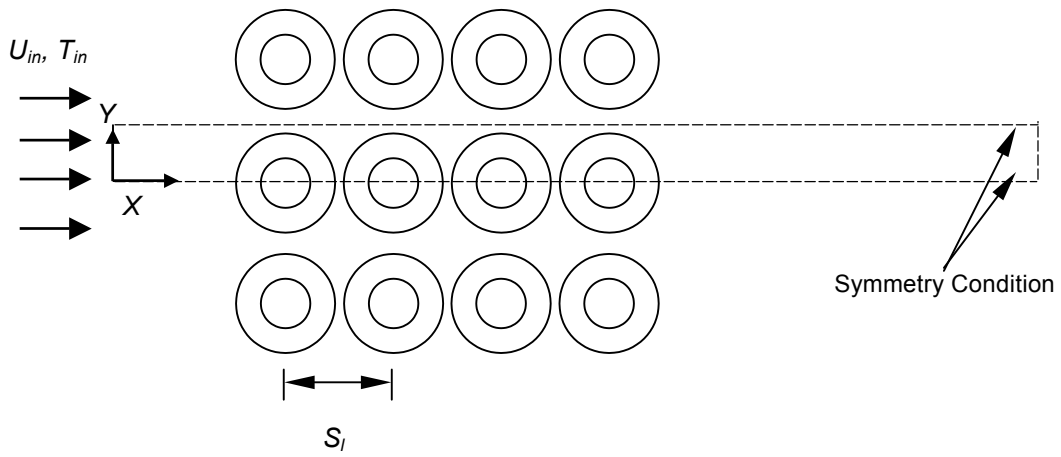
	s1	s2	s3	s4	s5	s6	s7	s8	s9	s10	s11	s12	s13	s14
Tube outside diameter, d	24	24	24	24	24	24	24	24	24	24	13.59	28	24	24
Fin diameter, d_f	30	34	38	44	48	34	34	44	34	34	23.59	38	34	34
Fin height, h_f	3	5	7	10	12	5	5	10	5	5	5	5	5	5
Fin thickness, δ	0.5	0.5	0.5	0.5	0.5	0.5	0.5	0.5	0.3	0.6	0.5	0.5	0.5	0.5
Fin spacing, s	2	2	2	2	2	1,6	4	0,7	2	2	2	2	2	2
Fin pitch, s_f	2.5	2.5	2.5	2.5	2.5	2.1	4.5	1.2	2.3	2.6	2.5	2.5	2.5	2.5
Transverse tube pitch, s_t	36	40.8	45.6	52.8	57.6	40.8	40.8	52.8	40.8	40.8	28.308	45.6	48.4	64.8
Longitudinal tube pitch, s_l	31.177	35.33	39.49	45.73	49.88	35.33	35.33	45.73	35.33	35.33	24.52	39.49	41.92	56.12
Number of row, n	4	4	4	4	4	2 to 6	4	4	4	4	4	4	4	4

For In-line Arrangement

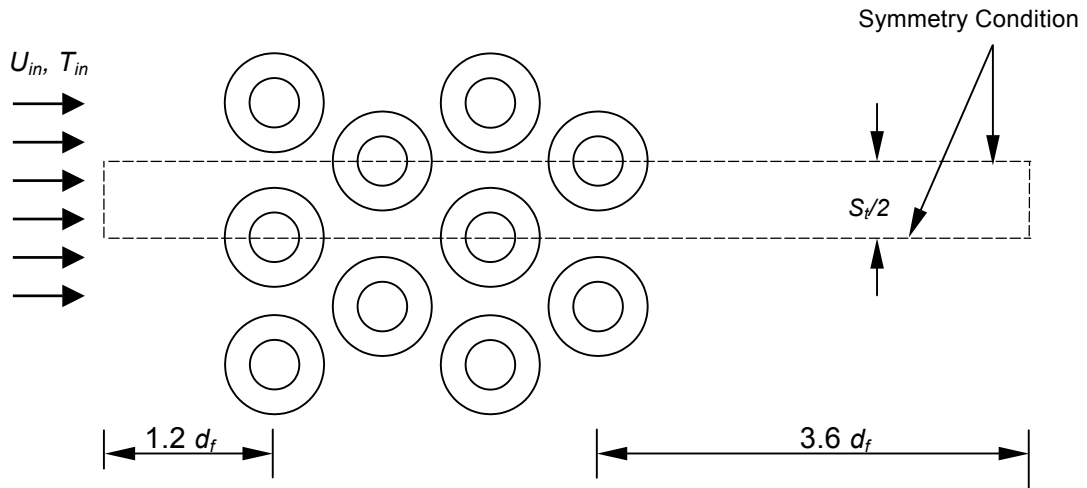
	i1	i2	i3	i4	i5	i6	i7	i8	i9
Tube outside diameter, d	24	24	24	24	24	13.59	28	24	24
Fin diameter, d_f	34	38	44	34	34	23.59	38	34	34
Fin height, h_f	5	7	10	5	5	5	5	5	5
Fin thickness, δ	0.5	0.5	0.5	0.5	0.5	0.5	0.5	0.5	0.5
Fin spacing, s	2	2	2	1.6	4	2	2	2	2
Fin pitch, s_f	2.5	2.5	2.5	2.1	4.5	2.5	2.5	2.5	2.5
Transverse tube pitch, s_t	40.8	45.6	52.8	40.8	40.8	28.308	45.6	47.6	40.8
Longitudinal tube pitch, s_l	40.8	45.6	52.8	40.8	40.8	28.308	45.6	47.6	47.6
Number of row, n	4	4	4	3,4,5	4	4	4	4	4

All dimensions are in mm.

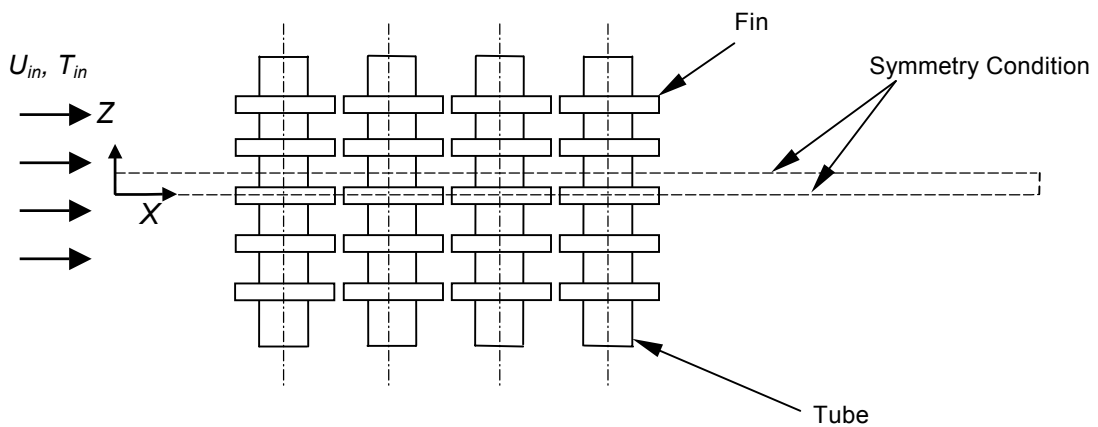
Table 4.1 Dimensions of bundles used in numerical investigation.



(a) In-line Arrangement



(b) Staggered Arrangement



(c) Top View

Figure 4.2 Computational domains.

To avoid possible approximation effects in the flow boundary condition, it had been justified for down stream by 5 times and 3.6 times fin diameter, respectively. However, there are no periodic vortex streets in the wake for both cases. Therefore, the upstream boundary of the computational domain is located 1.4 times fin diameter from the centre of the first row while the downstream boundary is set as 3.6 times fin diameter from the last row centre line (e.g., [65, 66]).

4.2.3 Grid Generation

In this study, a general curve linear coordinate grid generation system based on body-fitted coordinates was used to discrete the computational domain into a finite number of control volumes. The geometries of the problems are carefully constructed. All cases were modelled and meshed with the GAMBIT [12]. FLUENT also comes with the CFD program that allows the user to exercise the complete flexibility to accommodate the compatible complex geometries. The refinement and generation of the grid system is important to predict the heat transfer in complex geometries. In other words, density and distribution of the grid lines play a pivotal role to generate accuracy. Due to the strong interaction of mean flow and turbulence, the numerical results for turbulent flows tend to be more dependent on grid optimisation than those for laminar flows [11].

A significant factor in the accuracy of the numerical computation is the near-wall region treatment. For example, the possible separation phenomenon due to an adverse pressure gradient greatly relies on the resolution of the boundary layer upstream at the point of separation [11]. With proper control of the grid density, the computational domain can be considered for two main regions. The mesh sizes are made finer near the fin and tube wall to resolve the secondary flows (horseshoe vortices, flow separations) where the high gradients are expected (e.g., [29, 39]). The coarse mesh sizes were selected for the case where the flow is relatively uniform. The resultant grid is shown in Figure 4.3. Figure 4.3(b) is also prepared for the grid generation in the z direction of computational domain. The grid generations for staggered and in-line arrangements are shown in Figure 4.4, respectively.

The effects of grid resolution were examined depending on the individual problem. Even there are some limitations on the CPU time and computer resources, 50,000 to 150,000 cells were used to discrete the computational domains. Quite a number of pre testes for the grid independence was conducted for the purpose of

improving the accuracy of the results. To determine the grid independence of the results, care is necessarily to be taken because the relative errors in the averaged Nusselt numbers between such grids should be less than 5 %. If necessary, the grids have been refined with subsequent repeat of the numerical simulation. On the other hand, for minimization of the computational effort, the coarsest grid was applied as possible as it can in the computational domain.

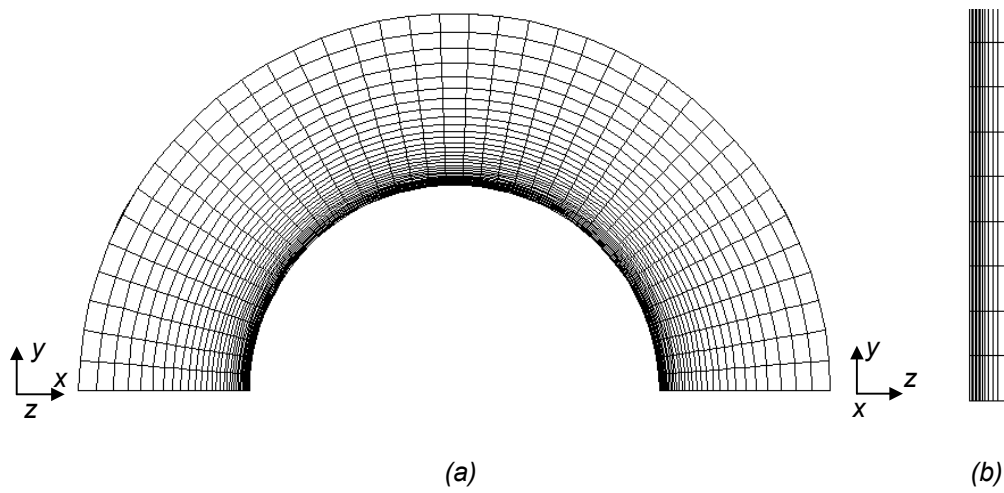


Figure 4.3 Grid generation (a) near tube, (b) at z - direction of the domain.

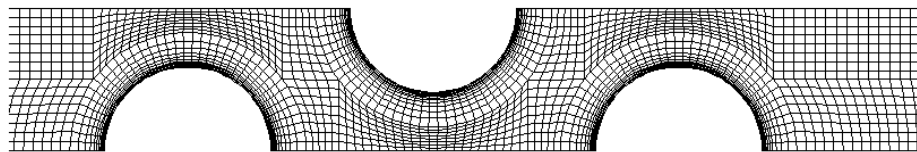


Figure 4.4 (a) Grid generation for the staggered arrangement.

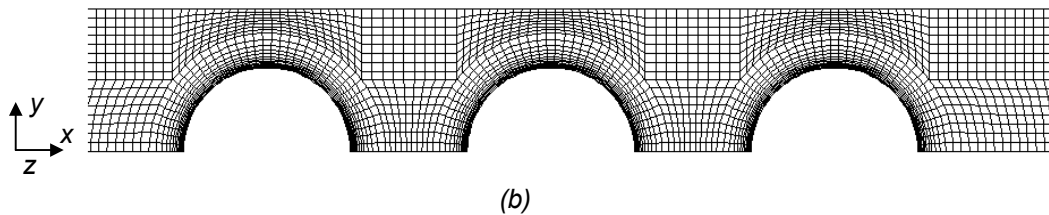


Figure 4.4 (b) Grid generation for the in-line arrangement.

4.2.4 Choosing the Physical Properties

The definition of physical properties (thermal conductivity, density, viscosity, specific heat) of fluids and solids is a necessary factor for setting up the model. In this study, the air is forced to pass between the fins, which transfers heat, and possibly moisture to the fin and tube surface, from where the heat is conducted to the coolant. However, in this study, it is assumed to be the dry air and no attempts were prepared for condensation effects. For the solid's part, aluminium is chosen for both the tube and the fin.

4.2.5 Boundary Conditions

In order to evaluate the heat and momentum transfer of circular finned-tube bundles, some preliminary conditions of the physical model have to be defined appropriately. For the numerical approach to the problem, the boundary conditions are required to set for all boundaries of the computational domain. At the upstream boundary conditions, the air entering the computational domain is assumed to have uniform velocity U_{in} , temperature T_{in} (308.15 K) and turbulent intensity I (1 %). The velocity components in the y and z directions are considered to be zero. The fluid region consists of the entrance, outlet, and bundle zone. The solid region includes the fin. At the solid surfaces, no-slip conditions for the velocity are specified. Heat convection to the fin and heat conduction in the fin is considered.

Constant temperature T_w (283.15 K) is assigned at the tube surface and all velocity components are considered to be zero. To simplify the calculation, the flow and thermal fields are assumed to be symmetric in the mid plane between the fins, mid plane of the fin itself, centre plane of tube and at the half of the transverse pitch from this tube as shown in Figure 4.2. At the symmetry planes assume a zero heat flux. The normal velocity component at the symmetry plane is zero, i.e. no convective flux across that symmetry plane. Thus, the temperature gradients and tangential components of the velocity gradients in normal direction are set to be zero.

- Inlet:

$$U = U_{in} = \text{constant}$$

$$T = T_{in} = \text{constant}$$

$$I = 1\%$$

- Outlet: Static pressure
- Tube: no-slip condition
 $T = T_w = \text{constant}$
- Fin: no-slip condition
Coupling of conduction and convection
- Symmetry Plane: Velocity components in normal direction = 0
Temperature gradients in normal direction = 0
Gradient of tangential components of velocity in normal direction = 0

The previous investigations of compact heat exchangers are set to be laminar flow [22] and compared to the turbulent flow, a smaller pressure drop is expected in laminar region. However, the turbulent flow is supposed to mix well and to get the more intensive heat transfer while incomplete mixing of the fluid occurs in laminar flow. As previously described in the literature review, the actual flow patterns of a circular finned-tube heat exchanger are of the complex entity, which is not easy to figure exactly. It should be noted that turbulent effects and unsteady conditions should be considered as well since the flow field is so complex in finned-tube heat exchangers [29].

When considering for a circular finned-tube heat exchanger under the proposed range of Reynolds numbers, the flow in the finned-tube bundle has to be assumed to be a three-dimensional, unsteady, incompressible turbulent flow. For the benefit of accuracy, pre- tests were made with the turbulent flow condition for the whole domain and consequently the results were obviously high when comparing with experimental data. Nir [46] reported that the fins represent 80-95 % of the heat transfer surfaces in modern finned-tube banks and the heat transfer phenomenon at the fin surface may be considered as a process in channels. Moreover, Yudin et al. [80] also noted that the flow in a bundle with high fins comes close to the nature of flow in the channel. Therefore, for the convenience of calculation, the flow between the fins is considered as a channel flow to be computed as laminar while the other parts of the bundle will be treated as turbulent regions.

4.2.6 Control Parameters

It is noteworthy that proper numerical control and modelling techniques are necessary for to speed up convergence and stability of the calculation. With a control-volume-based technique, FLUENT converts the governing equations to algebraic forms that can be solved numerically. This control volume technique consists of integrating the governing equations inside each control volume, yielding discrete equations that conserve each quantity on a control-volume basis [11]. For discretization of equations, the user needs to select the respective numerical schemes. The first order upwind numerical scheme is selected to simulate the problems.

For the aspect of pressure-velocity coupling, The Pressure-Implicit with Splitting of Operators (PISO) is selected. PISO pressure-velocity coupling scheme is a part of the SIMPLE family and it is highly recommended for all transient flow calculations. PISO is based on the higher degree of the approximate relation between the corrections for pressure and velocity. An approach to judging convergence is setting as the convergence criterion.

4.2.7 Computing Time

It can be easily noted that when dealing with three-dimensional unsteady turbulent flow, the simulation may take longer than for steady flow problems. One typical calculation with sufficient mesh sizes took about three days to get an acceptable solution whereas just a few hours for the laminar flow cases. When simulating of complex turbulent flows, the complicated geometry of the heat exchanger and associated grid resolutions may impose restrictions on the computational time step. It showed that the dense grid resolution would restrict the time step. To determine the time step size, FLUENT [11] reported that there is no stability criterion that needs to be met. However, FLUENT recommends that the time step should be at least one order of magnitude smaller than the smallest time constant in the system being modelled. By observing the number of iterations needed to converge at each time step, the time step size is able to be judged. The ideal number of iterations per time step is 10 to 20. For the purpose of accuracy it should start with a smaller time step. Thus all the tests are processed with the time increment $\Delta t = 0.001$ sec at initial condition and then, gradually it is increased as the calculation proceeds.

Numerical simulations were performed with a SGI – Indigo 2 (1 CPU R8000, 175 MHz, 256 MB RAM) and Dogbert workstation (2 CPU R12000, 2300 MHz, 768 MB RAM). Time-marching calculations are stopped when either a steady or periodic flow was encountered, or in case of a time-periodic solution when it becomes approximately constant. FLUENT provides for post processing and it is also able to track the convergence during the solution process.

4.2.8 Algorithm

In order to simulate, the following procedures of analysis are performed:

1. Start the FLUENT with 3D solver
2. Read an existing grid file and feed into FLUENT
3. Check the grid (e.g., concerning the dimension of the calculation domain, the cell volume, the number of nodes and area of each cell)
4. Choose the suitable type of solver:

Fluent supplies three types of solver for solving the discrete equation. Basically, the specific characteristics of the investigation (incompressible and mildly compressible flows) are dealt with “segregated solver”. This solver solves the continuity, momentum, energy and species equations sequentially (i.e., Segregated from one another) while the other two solvers solve these equations simultaneously (i.e., coupled together) applied for high-speed compressible flow. Here the segregated solver has been selected.

5. Choose the model:

To calculate the flow field, select the $k-\varepsilon$ (RNG) model and for the near fin treatment, set standard wall functions. For coupling heat transfer (convection and conduction), activate the energy equation.

6. Define the properties of following material:

- Components of dry air
- Aluminium

Detailed material properties are shown in the Appendix A.

7. Define the boundary conditions (see section 4.2.5)

8. Define the control parameter:

The following under-relaxation factors are set.

- | | |
|------------------------------|-----|
| • Pressure | 0.3 |
| • Energy | 1.0 |
| • Momentum | 0.7 |
| • Turbulent kinetic energy | 0.8 |
| • Turbulent dissipation rate | 0.8 |

Select the reference of discretization of differential equations,

- | | |
|----------------------------------|----------------------------|
| • For pressure | choose, STANDARD |
| • For momentum | choose, First order upwind |
| • For pressure-velocity coupling | choose, PISO |
| • For energy | choose, First order upwind |
| • For turbulent kinetic energy | choose, First order upwind |
| • For turbulent dissipation rate | choose, First order upwind |

Set the convergence criteria,

Continuity = 0.001	$k = 0.001$	$\varepsilon = 0.001$
x, y, z velocity = 0.001	Energy = $1e^{-6}$	

9. Initialisation of flow field.

10. Calculate the solution.

11. Save the result.

5 Results and Discussion

This chapter mostly deals with the results of the investigations of the main characteristics that affects the heat transfer and pressure drop of circular finned-tube banks. In addition to describing the substantial geometric parameters and their performance characteristics, local heat transfer and flow results are illustrated and discussed separately.

5.1 Evaluation of Nusselt and Euler Numbers

FLUENT evaluates the Nusselt number and Euler number as follows:

The outlet air temperature T_{out} was calculated as a mass average temperature at the outlet position of the calculation domain.

$$T_{out} = \frac{\int T \rho \bar{u} \cdot d\bar{A}}{\int \rho \bar{u} \cdot d\bar{A}} = \frac{\sum_{i=1}^n T_i \rho_i \bar{u}_i \cdot \bar{A}_i}{\sum_{i=1}^n \rho_i \bar{u}_i \bar{A}_i} \quad (5.1)$$

The enthalpy flow rate of air at the inlet and outlet were calculated as,

$$\dot{H} = \int \tilde{h} \rho \bar{u} \cdot d\bar{A} = \sum_{i=1}^n \tilde{h}_i \rho_i \bar{u}_i \cdot \bar{A}_i \quad (5.2)$$

with the specific enthalpy

$$\tilde{h} = \int_{T_{ref}}^T c_p dT \quad (5.3)$$

where FLUENT set as $T_{ref} = 298.15$ K.

Enthalpy flow rates of the inlet \dot{H}_{in} and outlet \dot{H}_{out} positions of the computational domain (Equation 5.2) were determined by the aid of FLUENT and then the air-side heat transfer rate of the bundle was calculated according to Equation (5.4).

$$\dot{Q} = \dot{H}_{out} - \dot{H}_{in} \quad (5.4)$$

By this air-side heat transfer flow rate, the heat transfer coefficient of the air-side h can be evaluated by means of the Equation (5.5) where A_t is the tube surface area, A_f is the fin surface area and η is the fin efficiency.

$$h = \frac{\dot{Q}}{(A_t + \eta A_f) LMTD} \quad (5.5)$$

In here assume the heat transfer coefficient at the fin and base-tube is the same. LMTD is the log mean temperature difference,

$$LMTD = \frac{T_{in} - T_{out}}{\ln \frac{T_{in} - T_w}{T_{out} - T_w}} \quad (5.6)$$

The inlet air temperature and base-tube surface temperature were set as boundary condition with $T_{in} = 308.15$ K and $T_w = 283.15$ K (see in section 4.2.5). The outlet air temperature, T_{out} was evaluated from the Equation (5.1). The base-tube surface area, A_t , and the fin surface area, A_f were calculated as

$$A_t = \pi d(S_f - \delta).n, \quad A_f = \left(\frac{\pi}{2} (d_f^2 - d^2) + \pi d_f \cdot \delta \right) n \quad (5.7)$$

The fin efficiency, which is needed for the determination of the heat transfer coefficient, arises as a result of iterative calculations of Equation (5.8) and (5.9) and the heat transfer coefficient from the Equation (5.5). As Equation (5.8), the fin efficiency η_f approaches its maximum and minimum values of 1 and 0, respectively, as h_f approaches 0 and ∞ . The value of ψ was derived from the Equation (5.10) individually.

$$\eta = \frac{\tanh(\psi m h_f)}{\psi m h_f} \quad (5.8)$$

$$m = \sqrt{\frac{2h}{k_f \delta}} \quad (5.9)$$

$$\psi = 1.0 + 0.35 \ln\left(1.0 + 2.0 \frac{h_f}{d}\right) \quad (5.10)$$

The method for calculation of the fin efficiency was taken from VDI-Wärmeatlas [68] in which the heat transfer coefficient h over the fin surface is assumed to be a constant mean value. Though it is not uniform in practice, such uncertainties are not reflected in Equation. 5.5 (Kearney and Jacobi [32], and Sparrow and Samie [59]).

The dimensionless number for air-side heat transfer in the finned-tube bank was defined and calculated depending on the Reynolds number and geometric parameters. For many cases the Nusselt number, the Colburn j factor, Stanton number are used to express the heat transfer coefficient and the characteristic length is not the same. Tube outside diameter, hydraulic diameter, fin spacing, equivalent diameter were varied from experiment to experiment.

In here the Nu number was used as

$$Nu = \frac{hd}{k_a} \quad (5.11)$$

The properties of air (thermal conductivity, dynamic viscosity) at inlet temperature are displayed in the Appendix A. The influence of geometric parameters and the inlet air parameter on the pressure loss and resistance for the in-line and staggered bundles are investigated as

$$Eu = \frac{\Delta p}{\rho U_{max}^2} \quad (5.12)$$

where $\Delta p = p_{in} - p_{out}$

The static pressure at the inlet and outlet of the computational domain were evaluated as

$$p_{in,out} = \frac{\int p d\bar{A}}{\int d\bar{A}} = \frac{\sum_{i=1}^n p_i \bar{A}_i}{\sum_{i=1}^n \bar{A}_i} \quad (5.13)$$

5.2 Local Heat Transfer and Flow Results

The results and discussions are divided into three topics accordingly. The present study includes the nature of boundary layer developments, local velocity and temperature variations between the two adjacent fins and over the fin surface, the horseshoe vortices system, the occurrence of the flow separation on the tube and wake behind the tube. Since the convection boundary layer development is the most influential factor of the local heat transfer and flow behaviour, the flow visualization results particularly concerning the nature of the horseshoe vortex flow patterns will be discussed firstly. Secondly, the temperature boundary layer development between the fins and the temperature distributions over the fin surface and within the fins are outlined. Finally, the flow and temperature distributions near the fin surface and on the mid-plane between fins will be covered.

5.2.1 Local Flow Behaviour

The temperature and velocity boundary layers on the fin and tube surfaces are strongly dependent on the spacing between the fins and the corresponding velocity. Therefore, the numerical results will be presented which are carried out for three different fin spacings (1.6 mm, 2 mm and 4 mm) for a fixed fin height of 5 mm and tube diameter of 24 mm. In addition, it may be useful to discuss the natures of velocity distribution of the first and second rows, respectively.

Staggered Arrangement

Figure 5.1 shows velocity distributions between the fins of the first row for three different spacings of the staggered array at ($\theta = 0^\circ$) corresponding to the stagnation point of each tube for $Re = 8.6 \times 10^3$. For the narrowest fin spacing of $s = 1.6$ mm, two boundary layers grow from the leading edge of the fins. According to the flow visualization results, the velocity boundary layers at the fin base and tube surface are seen to be thicker. Owing to the adverse pressure gradient effect, a horseshoe vortex system is developed near the junction of tube and fins for all three spacing cases. A boundary layer will be formed when the fluid stream meets the leading edge of the fin surface. As the fluid goes on, the thickness of the boundary will be amplified. Hence, the local heat transfer coefficient may change from point to point of the finned surface. In addition, the velocity is reduced in the upstream region and the flow forms the

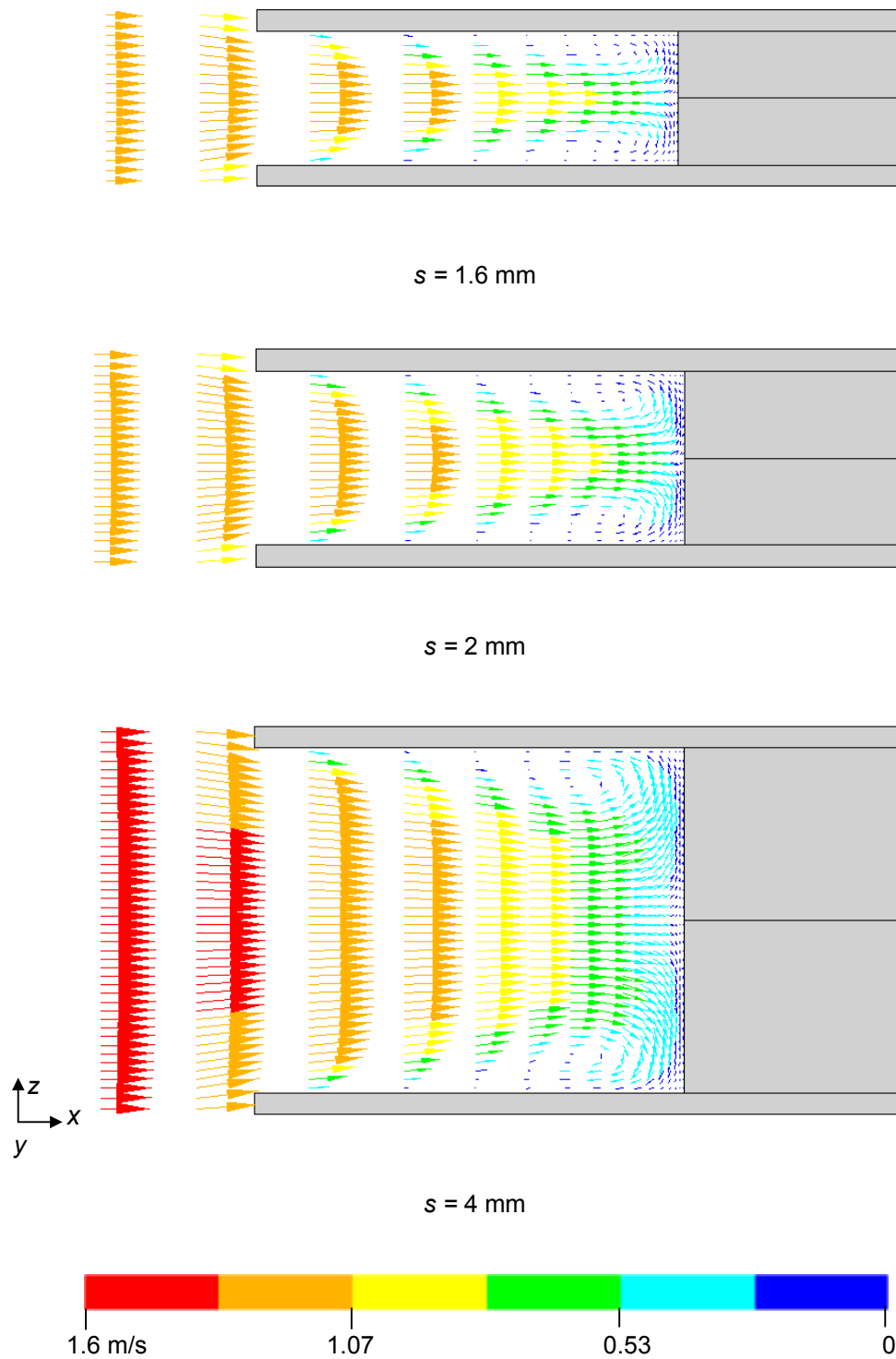


Figure 5.1 Velocity distributions between the fins of first row of staggered arrangement at $Re = 8.6 \times 10^3$.

horseshoe vortices that caused a rather complicated flow pattern. For larger fin spacings cases ($s = 2$ and 4 mm), similar flow behaviour is recognized. The horseshoe vortex effect is more pronounced in the largest fin spacing cases.

When increasing the Reynolds number to 4.3×10^4 , the horseshoe vortex system can be observed for the above three different pitches of staggered first rows as for the low Reynolds number case. The velocity distributions between the fins of first row for the Reynolds number 4.3×10^4 are shown in Appendix B.1. The intensity of the vortices becomes stronger for the high velocity and the vortex positions are nearly the same for all fin spacing changes because of the fixed geometry, i.e. fin height, and tube diameter are constant.

It is a well known phenomenon that the deeper rows were affected by the upstream rows. It is true especially for the in-line array where the second rows are in the dead region of the first rows. In the staggered array, the first row acting as a turbulence promoter as well as the velocity is increased for the second row because of the blockage effect of first row [54]. Appendix B.2 is prepared for the flow patterns between the fins of second row of staggered tube arrangement at high $Re = 4.3 \times 10^4$. It is almost inevitable that the velocity boundary layer at the fin base and tube surface region becomes thinner. The reason lies in which the influence of the stronger horseshoe vortex system is apparently more prominent than the first row.

Horseshoe Vortex System

The existence of the horseshoe vortex system is evident in the heat transfer pattern studies (Hu and Jacobi [21], Jones and Russell [27], Saboya and Sparrow [52, 53], and Sheu and Tsai [58]). The numerical flow visualization shows a single large horseshoe vortex, the smaller secondary counter rotating vortices (proposed by Goldstein and Karni [16] and Goldstein et al. [17]) are absent in the flow. They illustrated the schematic drawings of a horseshoe vortex system, which consists of the large and main vortex $V1$, the secondary, small vortex $V2$, and even smaller vortex $V3$. Goldstein and Karni [17] claimed that the smallest vortex $V3$ appeared around the front portion of the cylinder above the intense $V2$. The magnified flow patterns near the fin-tube junction of present numerical results are described in Appendix B.3 (a).

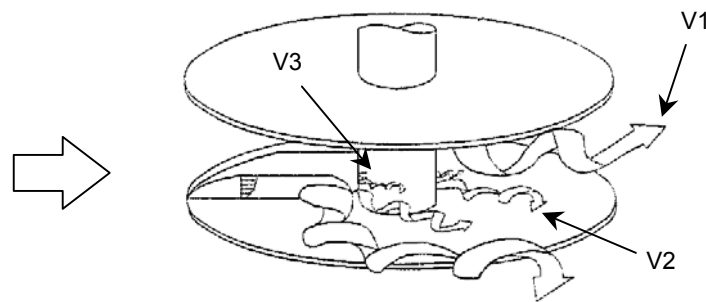


Figure 5.2 Schematic flow patterns of horseshoe vortices around a circular cylinder between annular fins [63].

The experimental investigations of horseshoe vortices were performed mostly with a cylinder that was mounted on a flat plate (e.g., Baker [3], Goldstein and Karni [16] and Goldstein et al. [17]). Baker [3] stated that the horseshoe vortex system depends on the velocity and the tube diameter effect. When considering a narrowly spaced finned-tube exchanger, the spacing between fins will play an influential role on the horseshoe vortex system. For this regard, the structure of flow and the thermal fields in the fin and tube heat exchanger were obtained numerically and experimentally with cases of different fin pitches by Kaminski [29], Romero et al. [51], Sung et al. [63], and Torikoshi et al. [64]. The distribution of the velocity between the fins, by the ratio of fin spacing to tube diameter were shown by Torikoshi et al. [64].

A comparison was performed between the geometry of the lowest $\frac{s}{d}$ ratio of [64] and the case $s = 4$ mm of the present numerical investigation, since both the ratio is in the region of ($\frac{s}{d} = 0.17$). The present results obviously differ from those obtained by [64], since there is no horseshoe vortex system visible in their figures. Probably, this is a result of low velocity effect ($Re = 400$) and it is found that their flow patterns are similar to Schwind's vortex regime one [3]. However, a similar flow pattern without horseshoe vortex system is also observed in the numerical simulation of the first row of bundle ($s8$)(see Appendix B.3 (b)). In this case, the main flow cannot penetrate deeply since the fin spacing to tube diameter ratio of this bank is 0.03.

Sung et al. [63] examined the occurrence of the horseshoe vortex system in accordance with fin spacing changes. They exposed Schematic flow patterns of horseshoe vortex system around the circular cylinder between annular fins in the

Figure 5.2. They have analyzed such vortex characteristics by utilizing the mass transfer data at $3.3 \times 10^4 < Re_\alpha < 8 \times 10^4$ and over the ranges, $0 < \frac{S}{h_f} \leq 0.40$. In a manner similar to Goldstein and Karni [16], Sung et al. found that the smaller vortex $V3$ occurs at $\frac{S}{d} = 0.05$ for the wide fin spacing, $\frac{S}{h_f} = 0.4$, a geometry which is equivalent to the present $s = 2$ mm bundle (s2). However, it is not possible to observe the secondary horseshoe vortex $V3$ in the results of the present simulation. Since these vortices are very small, an appropriate numerical simulation may need extremely fine grids. Therefore, it is time-consuming and beyond the scope of the present work.

Surprisingly, at $Re = 4.3 \times 10^4$, a second horseshoe vortex system occurs at third and fourth rows of the fin spacing 4 mm bundle (s7). Figure 5.3 has been prepared to illustrate this point. The size of the second vortex is nearly the same as the first vortex of fin-tube junction. Two vortices occur at $\frac{S}{d} \approx 0.083$. Although, it is difficult to find the responsible flow features, here are three possible reasons for the presence of these vortices. The higher Reynolds number, the larger fin spacing effects, and the wake effect of the preceding rows could cause such vortices. Unfortunately, no experimental data of the flow visualization are available to verify these horseshoe vortex occurrences.

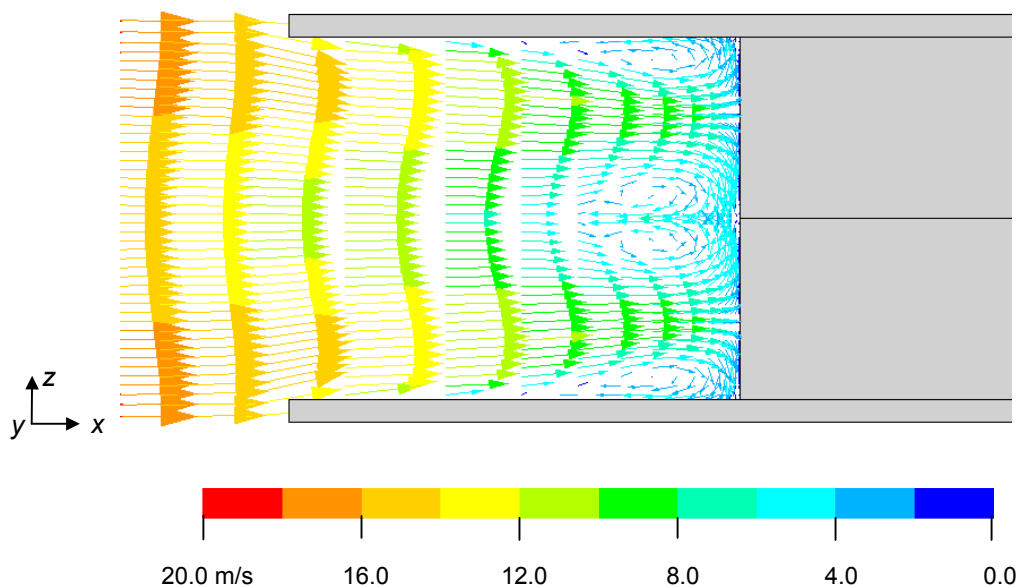


Figure 5.3 Flow pattern for the fourth row of bundle (s7) at $Re = 4.3 \times 10^4$.

In-line Arrangement

Attention will now be turned to the in-line arrangement. Analysis of the first row of the in-line array figures, which are presented in Figure 5.4, shows the same manner as results of first rows of staggered arrangement. The Reynolds number in Figure 5.4 is 8.6×10^3 . This trend continues for the higher Reynolds number (see Appendix B.4). As expected, the horseshoe vortices are more prominent than at the lower Reynolds number. From Appendix B.4, it is seen that the velocity distributions between the fins of first rows of in-line array at $Re = 4.3 \times 10^4$ are almost identical to the flow visualization results of the first rows of the staggered array at high Reynolds number. Therefore, it can be concluded that the flow patterns at the first rows for the tested three different fin spacings are similar regardless of tube arrangements and velocity. These results confirm the result of Kearney [31] and Konstantinidis et al. [33] that the first row is not influenced by any rows downstream.

Observation of the flow patterns of second rows of the in-line array shows different behaviour from those of the second rows of staggered array. Flow patterns between the fins of second row of in-line array are visualized and shown in Appendix B.5 for $Re = 4.3 \times 10^4$. There are reverse flows upstream of second rows instead of the horseshoe vortices that appeared in the first rows of in-line array and second rows of staggered array. Because of the arrangement of in-line tubes, the most of the second row fin surface exists in the wake region of the first row. Brauer [7] proposed that the inactive heat transfer regions (“dead” regions) of the in-line array are noticeably larger than the staggered array. Flow visualization results of the flow patterns in the bundle will be presented and discussed in the section 5.2.3.

In considering the results of second rows, it is appropriate to mention that there may develop a horseshoe vortex system if the longitudinal pitch is long enough. In this case, the ratio of the longitudinal tube pitch to fin diameter is 1.7. A further inspection of the figures of Appendix B.5 indicated that the velocity is augmented for a larger gap distance ($s = 4$ mm) due to the flow resistance between the fins being reduced. A similar reverse flow pattern occurred at the third and the fourth rows. From this point of view, it is noted that the in-line array has less performance of heat transfer than the staggered one since the upstream and downstream of the fin surface of tube rows are lie within “wake flows” except for the first row. The horseshoe vortices develop in all staggered rows; however, only for the first row in the in-line tube array.

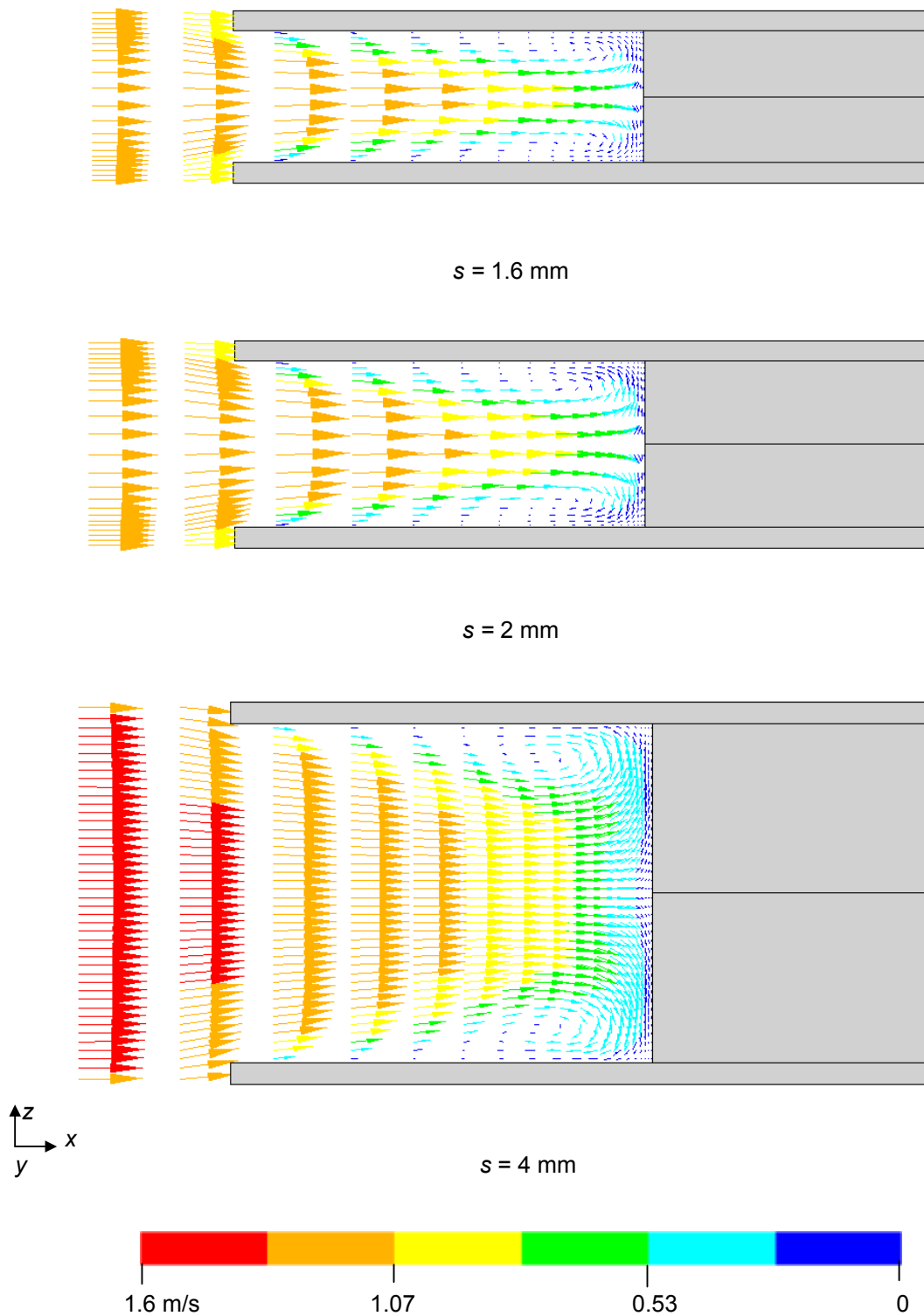


Figure 5.4 Velocity distributions between the fins of first row of in-line arrangement at $Re = 8.6 \times 10^3$.

5.2.2 Local Temperature Distribution

The aforementioned discussion mainly emphasised on the horseshoe vortex system. The presence of the horseshoe vortices evidently caused effects on to the thermal boundary layer formation since the temperature gradient at the surface depends on the flow field. The results obtained from the three different spacing changes are utilized for the analysis of the thermal boundary layer development. Therefore, our discussion shall now be necessarily started with the thermal boundary layer development for the first and fourth rows, respectively and then, the temperature distribution over the fin surface and within the fin will follow later.

Thermal Boundary Layer Development for Staggered Arrangement

Examination of Figure 5.5(a), which corresponds to the first row for three different fin spacings of the staggered array at ($\theta = 0^\circ$) for the $Re = 8.6 \times 10^3$ shows the thermal boundary layer developments between the fins. It is seen that at the narrowest fin spacing ($s = 1.6$ mm) bundle, two boundary layers grow to touch each other. Thus, the main flow cannot sufficiently penetrate to reach the tube surface. The temperature gradient decreases at the fin base and tube surface as shown in the figure. This will lead to decrease of the convection heat transfer coefficient.

For the case of moderately spaced fins ($s = 2$ mm), the thermal boundary layers are slightly thinner than in the case of the narrowly spaced fins ($s = 1.6$ mm) and as a result, the heat transfer coefficient is found to be increased at the ($s = 2$ mm) bundle. Moreover, it is observed that the boundary layers interacting point is shifted markedly compared to the narrowest fin spacing bundle. However, it is noticed that two thermal boundary layers developing separately for $s = 4$ mm bundle (s_7), which is the largest fin spacing case. In this case, the boundary layer developed on the tube surface is considerably thinned. This attributes to higher temperature gradient at the tube than in the former bundles. According to the horseshoe vortex that occurs at the fin-tube junction, the temperature gradient at which tends to be higher again. Therefore, boundary layer developments between adjacent fins and tube surface are mainly dependent on the fin spacing. Moreover, a higher heat transfer rate is obtained for thinner boundary layer. It confirms the result of Goldstein and Karni [16] that the mass transfer rate around a tube is influenced by the thickness of the boundary layer.

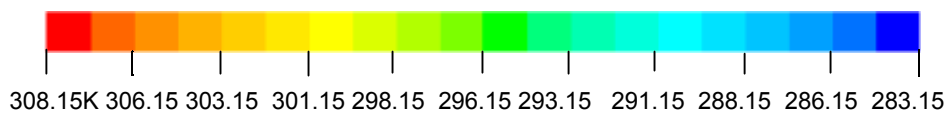
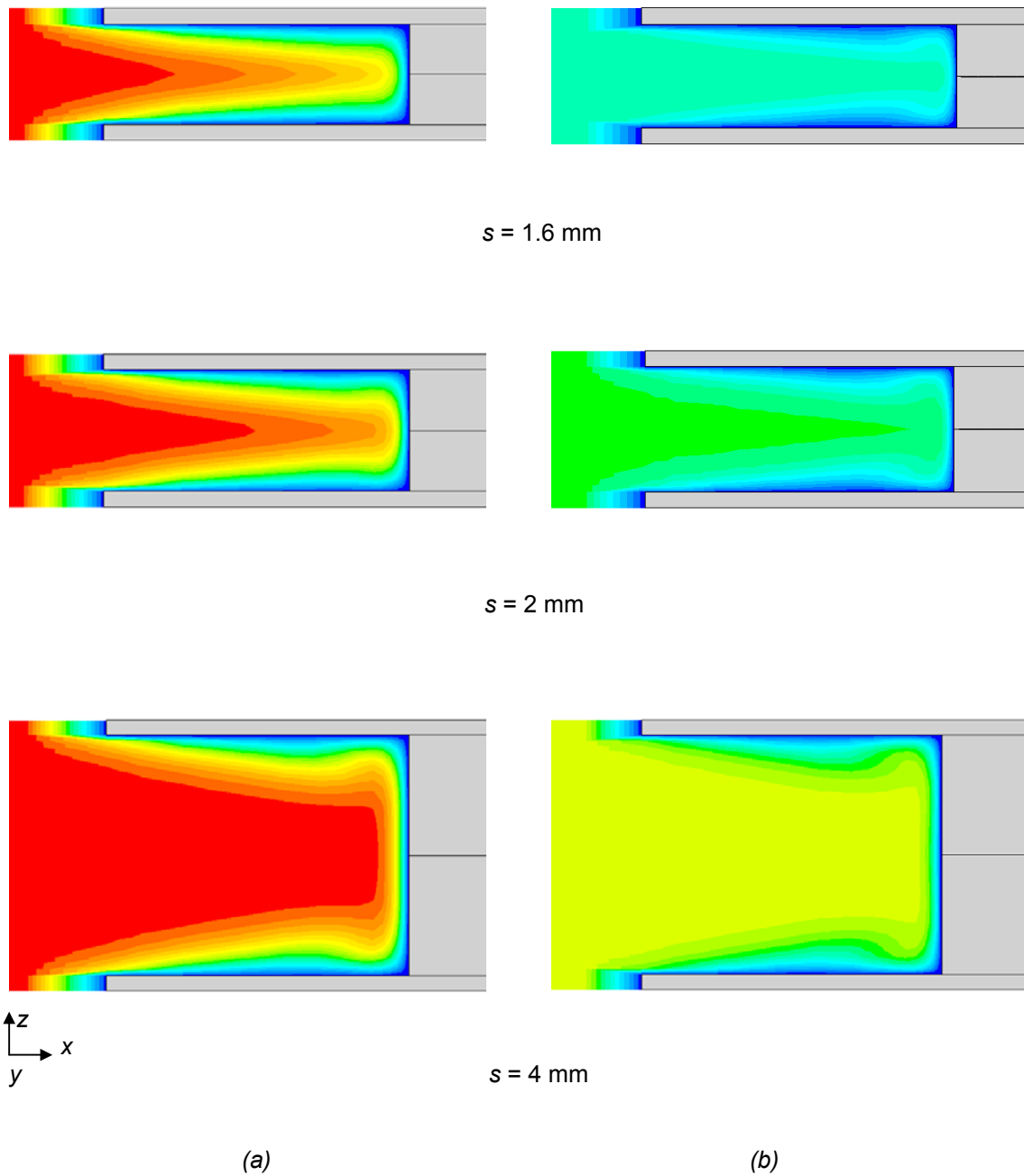


Figure 5.5 Temperature distributions between the fins for staggered arrangement at $Re = 8.6 \times 10^3$ (a) first row and (b) fourth row.

Now attention is turned to the fourth row positions of the staggered array, and Figure 5.5(b) displays the temperature field ahead of the fourth row. The temperature boundary layers of the fourth rows are thinner than those of the first rows for the Reynolds number 8.6×10^3 . It is clearly seen from the fourth row figures that the boundary layers are developing separately even for the narrowest fin spacing. Further inspection of the figures shows that the temperature between the fins is decreased significantly compared to the first row results. Naturally, the main air stream becomes cooler for subsequent rows.

Further increase of the velocity ($Re = 4.3 \times 10^4$) proved that two thermal boundary layers develop separately even at $s = 1.6$ mm bundle which is shown in Appendix B.6 (a). Consequently, it can be concluded that the velocity influences the thermal boundary layer development of the first row as expected. At $s = 4$ mm, the thermal boundary layer development on the tube surface is different from the smaller fin spacings. It is seen from Appendix B.6 (b) that the temperature gradient at $s/2$ of the bundle ($s/2$) is reduced. It is owing to the second horseshoe vortex appearance, which is already shown and discussed in Figure 5.3.

Figure 5.6 shows the effect of flow impingement of the vortices on the tube surface of bundle ($s/2$). Local Nusselt number distribution along the tube surface of the first and fourth row for fin spacing 4 mm at ($\theta = 0^\circ$) is provided in this figure. The x-axis represents the gap between the fins from the fin-tube junction to the symmetry line $s/2$ (at $s = 2$ mm). The definition of the local Nusselt number is based on the inlet temperature as Romeo-Méndez et al. [51]. On the other hand, Fiebig et al. [10] and Jang et al. [24, 25] used the local bulk mean temperature as a reference. It should be noted that the magnitude of Nusselt number will be different with the reference temperature taken. However, the similar trend will be maintained, which is the main purpose of the present presentation. Kaminski [29] presents Romeo's statement on local Nu number in equation form as follows,

$$Nu = \frac{\left. \frac{\partial T}{\partial x} \right|_w}{T_{in} - T_w} \cdot d \quad (5.14)$$

For the first row of the bundle ($s/2$), the lowest local Nu number is revealed at the fin-tube junction, which agrees with Romeo (see Figure 5.6); however, the maximum local Nu number of Romeo-Méndez et al. is at $s/2$. The Reynolds number for

Romeo-Méndez et al. is only 630, but the current results are investigated for the much higher $Re = 4.3 \times 10^4$. The present results indicated that the local Nu number increases from $s = 0$ along the tube surface due to the higher velocity caused by the horseshoe vortex and attains the maximum at $s = 0.75$ mm. A precise inspection of Figure 5.3 confirms that a higher velocity attains due to horseshoe vortices at that point. Beyond the $s = 0.75$ point, the local Nu number decreases gradually to the symmetry line because of the lower velocity. The similar trend and the same peak point position are observed for the fourth row.

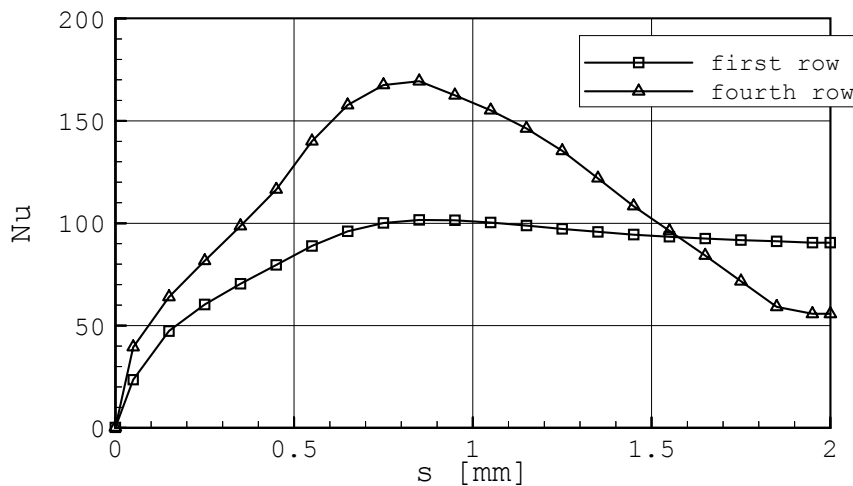


Figure 5.6 Variations of local Nu number along the tube surface of bundle ($s7$) at ($\theta = 0^\circ$) for $Re = 4.3 \times 10^4$.

As per the first row result, the local Nu number decreases up to the symmetry plane having the lower Nu number. This is an effect of the occurrence of a lower temperature gradient in that region, which is already described previously in the explanation of the thermal boundary layer development. Moreover, the decreasing rate of the local Nu number of fourth row is more significant than in the first row.

Thermal Boundary Layer Development for In-line arrangement

Now attention will be focused on the in-line tube arrangement and the first and fourth row results are shown in Figure 5.7 for $Re = 8.6 \times 10^3$. A study of the figures shows that the development is the same as in the staggered arrays for the first row. However, there is a difference between the fourth row results of the staggered and in-line arrays. Because of the in-line tubes position, the temperature difference between air and fins is considerably lower than for the staggered array. The fourth row has a lower temperature gradient than the first row when comparing the fourth and the first

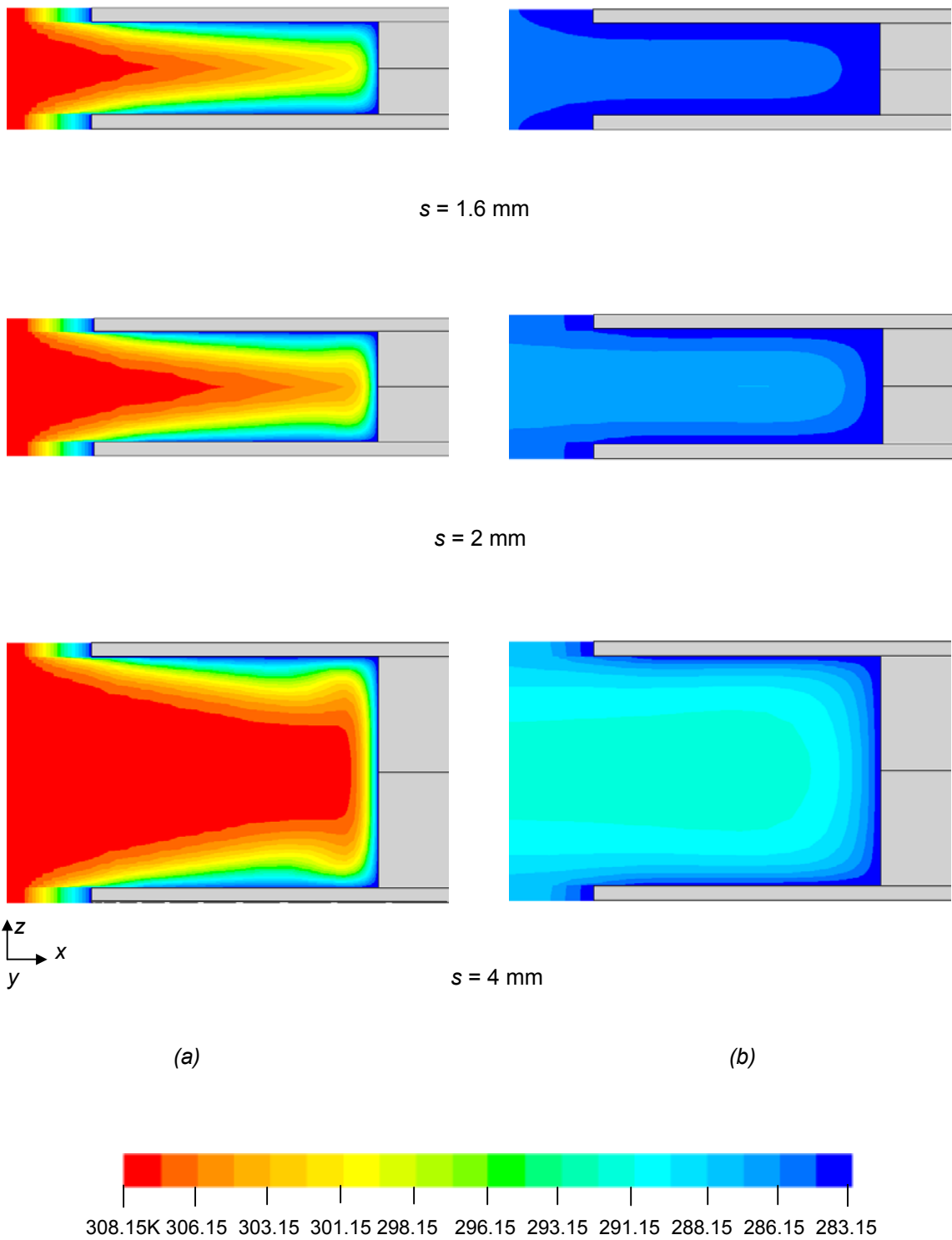


Figure 5.7 Temperature distributions between the fins for in-line arrangement at $Re = 8.6 \times 10^3$ (a) first row and (b) fourth row.

row of the in-line array. For the case of lowest fin spacing, the air temperature near the tube surface is almost the same as the temperature of tube surface. The temperature gradient is increased for the largest fin spacing case compared to the lowest spacing where a higher velocity value is firmly established.

In summary, the thermal boundary layers on the fin and tube surfaces are found to be developing by the nature of the fin spacing and velocity. Moreover, an overview of these figures shows that the thermal boundary layer development starts from the leading edge of the fin and gradually increases in size along the fin height. Therefore, the thicker the boundary layer, the higher the fin height is.

Temperature Distribution over the Fin Surface and within the Fin

The discussion of the temperature distribution should start from the fin surface of staggered finned-tubes. At $Re = 4.3 \times 10^4$, the temperature contours on the fin surface and middle surface of the fin for first, second and fourth row of the bundle (s3) is shown in Figures 5.8. The highest temperature gradient is seen along the radial direction at ($\theta = 0^\circ$) for the first row. According to Figures 5.5, 5.6, Appendices B.6 and B.7, the thinner boundary layers are observed at the fin tip. The fin surface temperature contours of Jang et al. [25], and Neal and Hitchcock [45] agree with the numerical results. This trend continues for the second and fourth rows and as expected, there is a larger temperature gradient at the second row for both over the fin surface and within the fin. Remember that the higher velocity impinges at the second row due to its position in the staggered array. If one carefully studies the figures, the surface temperature of the downstream part of the fin is rather similar to the surface temperature of the tube (283.15 K) especially for the fourth row. It is relevant to note that there are no blockage effects for fourth row since its position is at the last row of the bundle. Therefore, the temperature contours of the fourth rows downstream illustrate a larger low temperature area than the preceding rows.

For the in-line array, the results from the investigation of bundle (i2) are presented in Figure 5.9. The temperature distribution of the first row in the upstream range is nearly identical to the first row of staggered arrangement. However, there is a lower temperature gradient downstream due to the tube arrangement. This is because of the tube wake effect and as a result, lower temperature contours are seen in the radial direction of the stagnation point of the successive row. A close look at the figures indicates that the highest temperature gradient of the second row occurs at the point

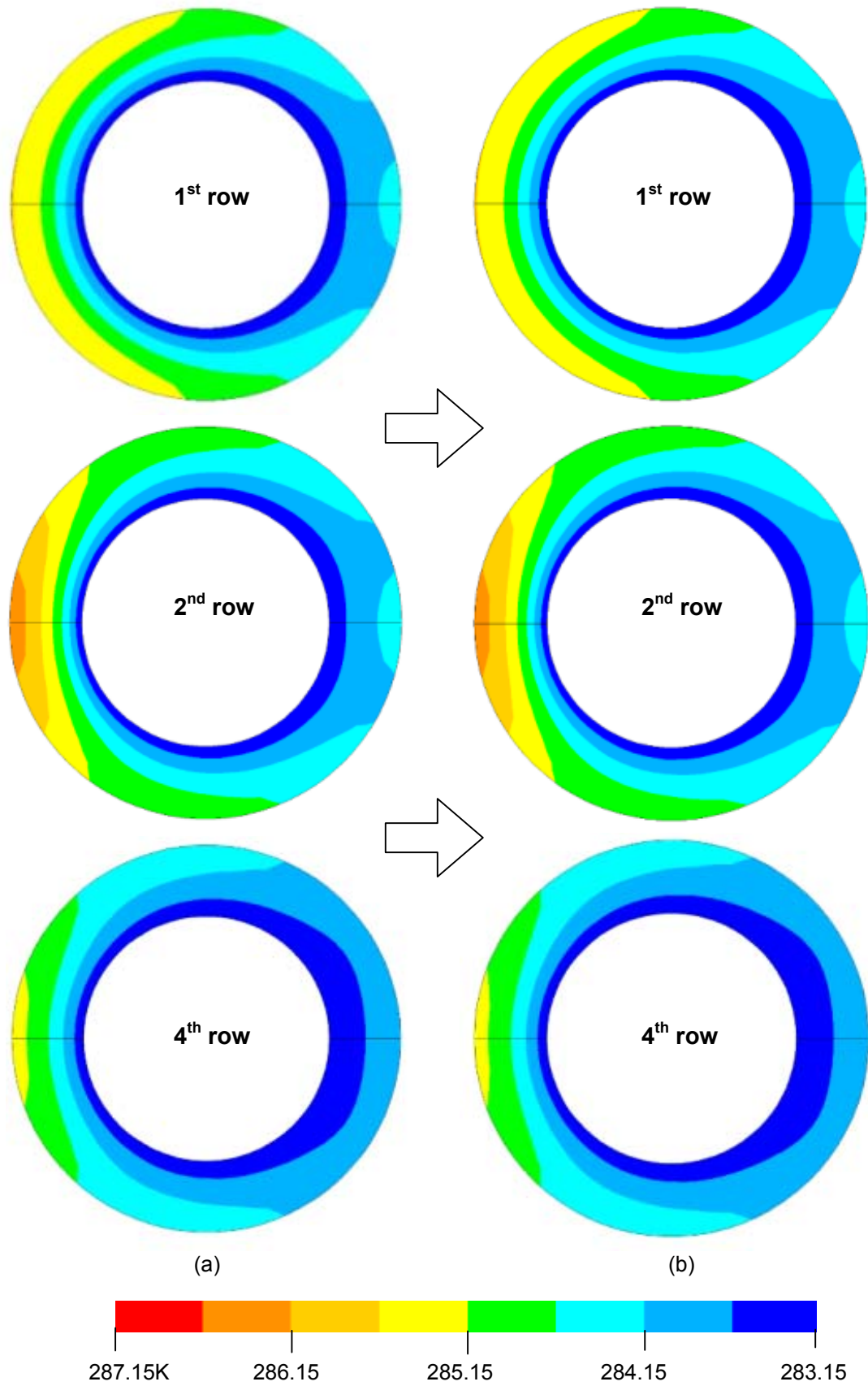


Figure 5.8 Temperature contours for staggered arrangement at (a) over fin surface and (b) within fin of bundle (s3) at $Re = 4.3 \times 10^4$.

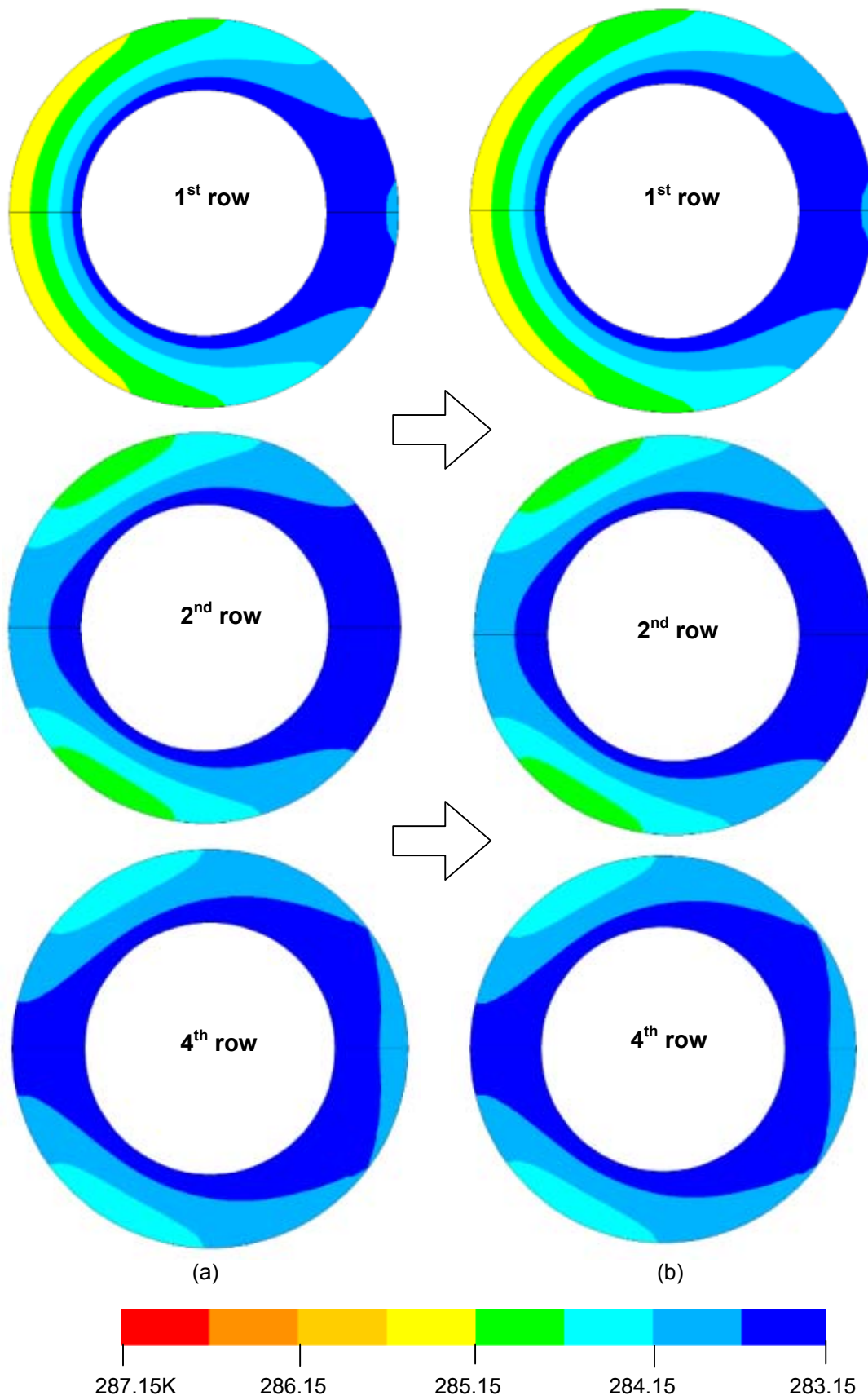


Figure 5.9 Temperature contours for in-line arrangement at (a) over fin surface and (b) within fin of bundle (i2) at $Re = 4.3 \times 10^4$.

where the mainstream of air is impinged (see Figure 5.11). For this reason, Kearney [31] suggested that the in-line fins exhibit enhanced heat/mass transfer at the lateral fin tips and thus, the heat transfer coefficient of the in-line bundle may become comparable to the staggered arrangement for sufficiently high fins. Figure 5.9 is associated with the fin height 7 mm and an additional explanation on the effects of fin height will be presented in the section 5.3.1. Temperature contours of the second row approved that the in-line array heat transfer coefficient is less improved than the staggered array since deeper rows are in the wake regions. Moreover, the temperature gradient of the fourth row becomes smaller and it is evident that the dead area becomes larger up and down stream of the fourth row.

It is learned from the Figures 5.8 and 5.9 that there is no significant difference of the temperature profiles over the fin surface and within the fin for both tube arrays. Temperature contours of Figures 5.8 (b) and 5.9 (b) are observed in the centre plane of the fin. Therefore, it is noted that the fin thickness effect is not an influential factor for the computed geometries. Another point that should be noted is the conductivity of the material used. As previously mentioned, in the present numerical simulations, aluminium, which has high thermal conductivity, is selected for both fin and tube materials.

5.2.3 Velocity and Temperature Distribution Near the Fin Surface Plane and on the Mid-Plane Between the Fins

The distribution of velocity and temperature in the bundles are essential for understanding of the local flow phenomenon. The relevant results will be presented for two planes. The near the fin surface plane is located at $s/20$ mm and the mid-plane refers to a centre plane between two fins at $s/2$ mm. The temperature and velocity distributions in the finned-tube bundle rely on the geometry and the inlet velocity.

Velocity Distribution

The flow pattern is the basic factor controlling the temperature distribution and the heat transfer rate of the bundle. The velocity patterns in near the fin surface plane and in the mid-plane of the bundles, s_6 ($n = 3$) and i_4 ($n = 3$) are provided in Figures 5.10 and 5.11, respectively.

Figures 5.10 and 5.11 show that the velocity distributions in the near the fin surface plane and in the mid-plane are quite different. The velocity in the mid-plane of both tube arrays is stronger than in the near fin surface plane. The velocity near the fin surface plane is weak because of the boundary layer development on the fin surface. In addition, downstream of the tube higher velocity appears on the mid-plane rather than near the fin surface. It is more evident in the staggered array of Figure 5.10. A detailed inspection of Figures 5.10 and 5.11 shows that the main stream of the staggered array is imposed upon higher percentage of the fin surface than in the in-line array and relatively a smaller wake region is emerged. As previously described in the explanation of the local flow and thermal boundary layer developments between the fins, the velocity at the second row of staggered arrangement is found to be larger than in the first row.

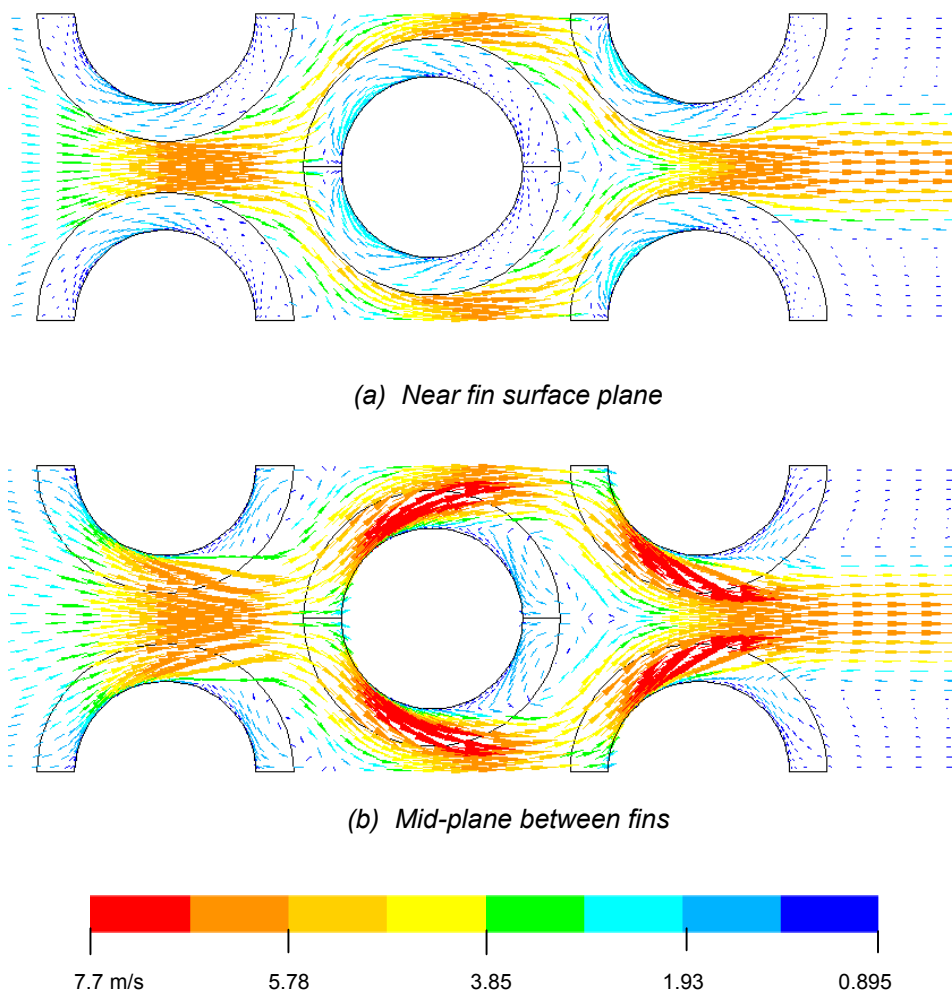
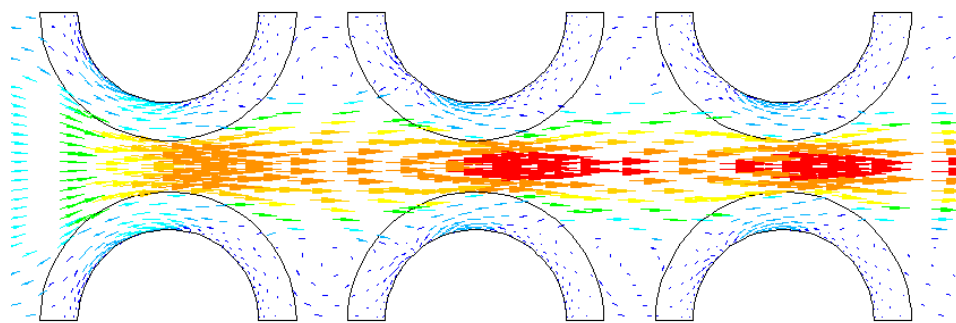
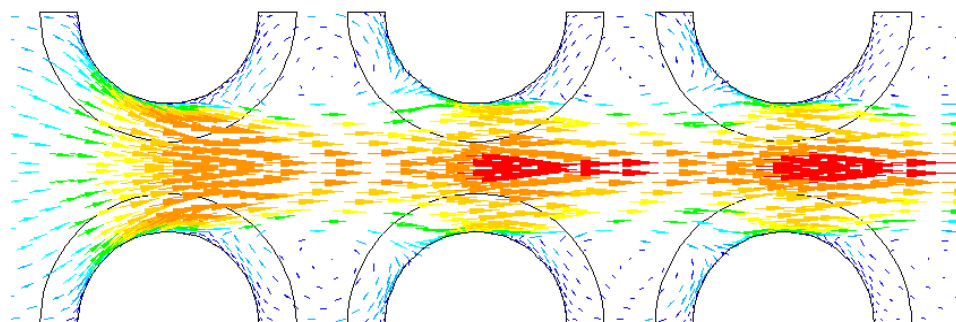


Figure 5.10 Velocity distributions for bundle s6 ($n=3$) at $Re = 8.6 \times 10^3$.

As shown in the Figure 5.11, a large portion of the fin surface area of only the first row of the in-line array is exposed to the main flow. A larger flow recirculation region or dead zone is formed between the two adjacent tubes for the in-line arrangement as Brauer [5, 6], Jang et al. [24], Kaminski [29] and Kearney, [31] noted. Figure 5.11 proves clearly the existence of reverse flow patterns upstream of deeper rows. Furthermore, these velocity data confirm that a bypass stream exists between the tubes with the in-line arrangement in accordance with fin tip-to-tip clearance. For the staggered arrangement, the main flow passes through every finned-tube row and the flow is mixed well. From an overall inspection of the figures, the first row upstream region for both tube arrangements is found to be almost identical as expected.



(a) Near fin surface plane



(b) Mid-Plane between fins

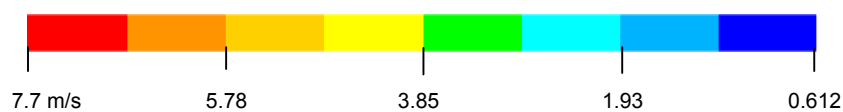


Figure 5.11 Velocity distributions for bundle *i4* ($n=3$) at $Re = 8.6 \times 10^3$.

As already mentioned in the explanation of the temperature distribution on the fin surface, the higher fin with the in-line array may improve the mean heat transfer coefficient [31]. It is true when a larger portion of the fin is exposed to the main flow for larger fin height; however, as the fin height increases, the boundary layer is expanded. Moreover, it is necessary to recall that in the in-line array, the active heat transfer surface area is smaller than that of the staggered array since the up and down stream parts of a fin surface are in the low velocity region.

There appears some difference compared with the results of Sparrow and Chastain [60] since forward-edge separation and second horseshoe vortex in the upstream are absent in the numerical results. They observed that the local flow phenomena on the fin surface depend on the effect of the angle of attack. In their experiment, a single high fin with the fin to tube diameter ratio = 3.03, is used. Because of the high fin effect and the use of a single fin in the free flow may produce the different patterns.

Boundary Layer Separation

The nature of boundary layer development, horseshoe vortices, and the downstream flow condition are also described previously in the literature review along with the occurrence of the flow separation. Depending on the Reynolds number and geometrical parameters, the flow separation on the tube occurs. The flow separation point on the tube emerged where the fluid momentum is too weak to overcome the adverse pressure gradient and the boundary layer detached from the tube surface. By the nature of these flow separations, local heat transfer and fluid mixing will increase especially upstream of the tube and decrease in a very low performance wake region located downstream of the tube. As seen in the above figures, low heat transfer is expected in the wake region since the velocity is low and recirculating flow appears.

The separation point can be seen in front of that point where the fluid near the tube surface is in the reverse direction of the main stream, as shown in the Figure 5.12. Figure 5.12 is prepared to exhibit the detailed flow patterns of the boundary layer separation on the mid-plane of the first row of the bundle (s_3) at $Re = 1.7 \times 10^4$. In all cases, the flow separation on the tube surface is observed shortly after ($\theta = 90^\circ$). This flow pattern is similar to the result of Neal and Hitchcock [45], which is already shown in Figure 2.2.

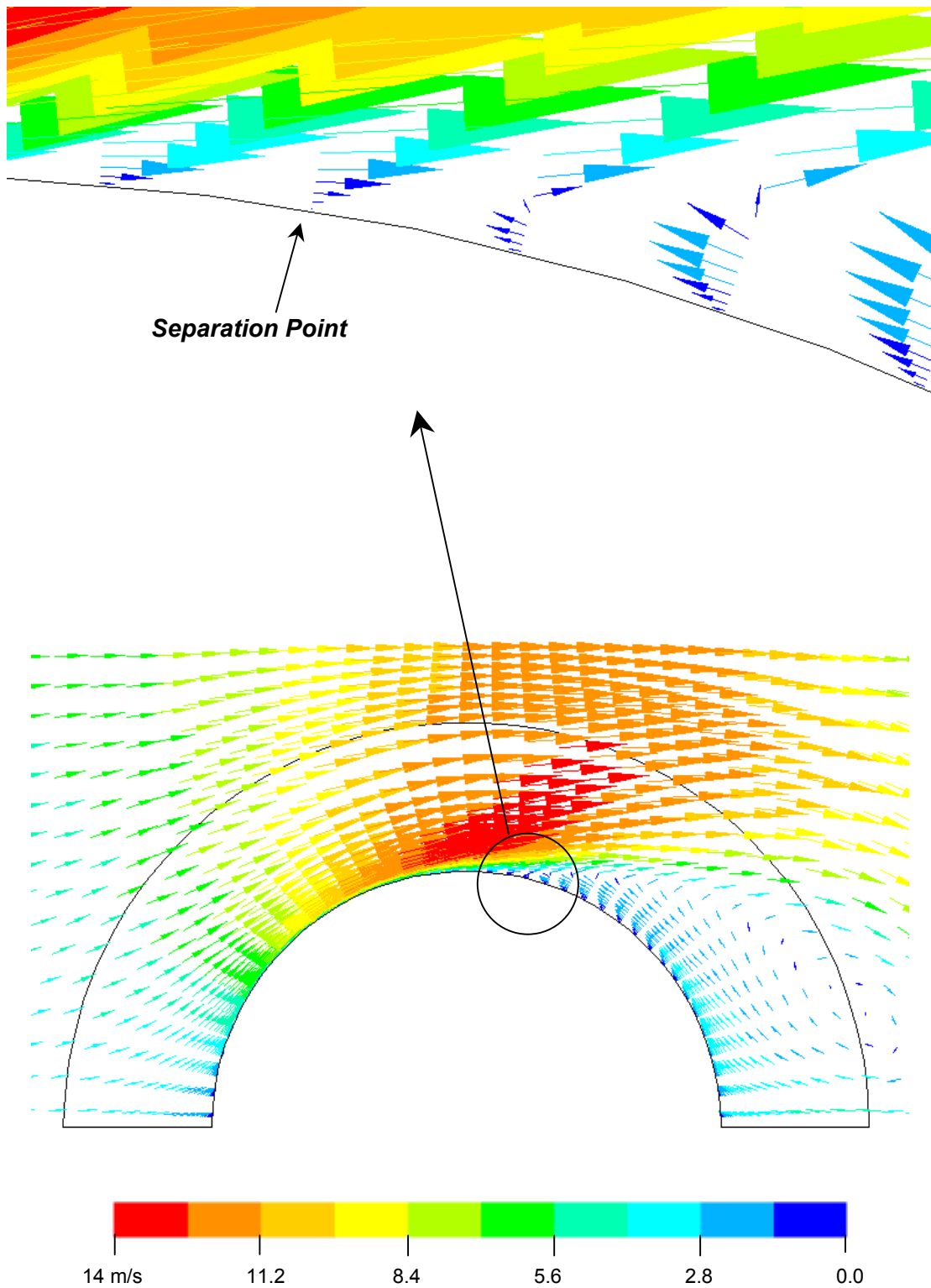


Figure 5.12 Boundary layer separation point of first row of bundle (s3) at $Re = 1.7 \times 10^4$.

Temperature Distribution

Representative results of the temperature contours near the fin surface plane and on the mid-plane of the first three rows for bundles, s6 ($n=3$) and i4 ($n=3$) are shown in Figure 5.13 and 5.14, respectively. These figures show that the temperature distributions within the bundle are significantly different from the first to third row for both the near fin surface plane and the mid-plane between the fins. It is seen that the temperatures on the mid-plane between the fins are higher than near the fin surface plane for both tube arrangements as the results of velocity distributions. Weierman et al. [76] documented temperature profiles in the wakes of both tube arrangements. Apparently, the numerical results agree with Weierman et al. in that the lowest temperature value exists behind the tubes, and the highest temperature exists between the tubes on the mid-plane transverse to the air flow direction. The temperature gradient near the upstream fin tip is higher due to the thin boundary layer thickness. For each fin, there is a larger temperature gradient in radial direction near

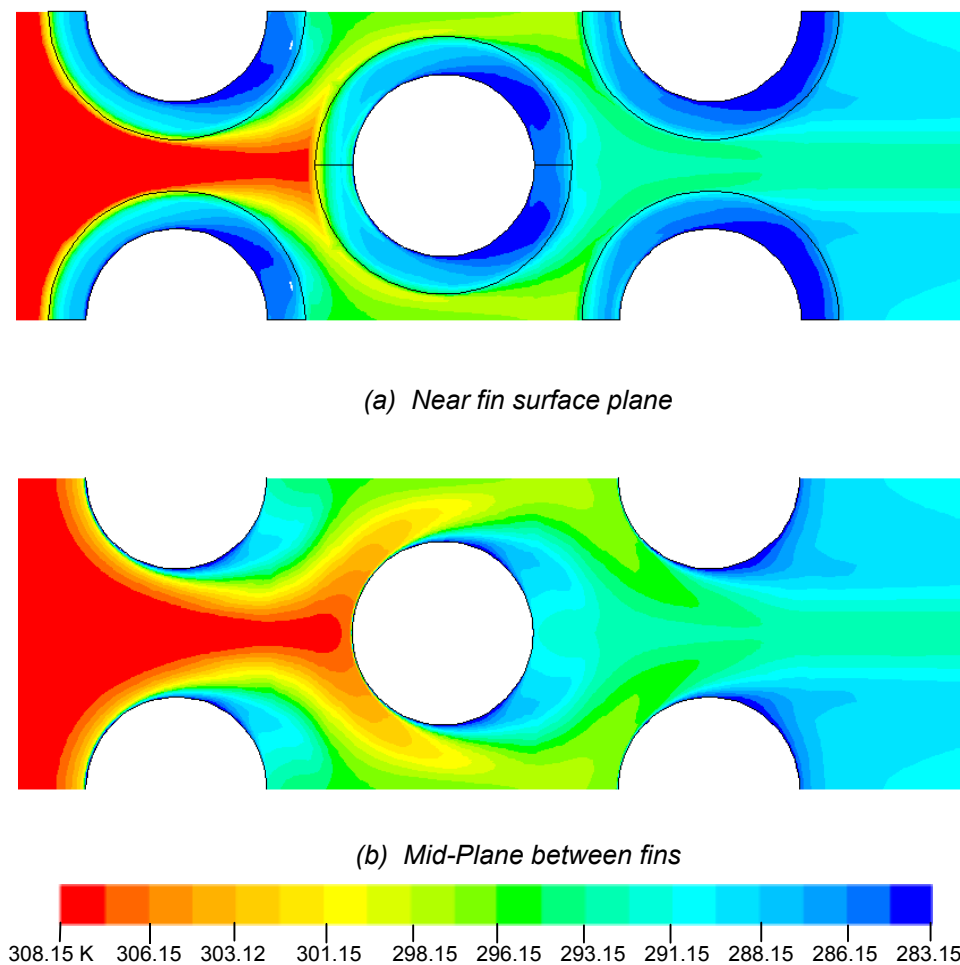
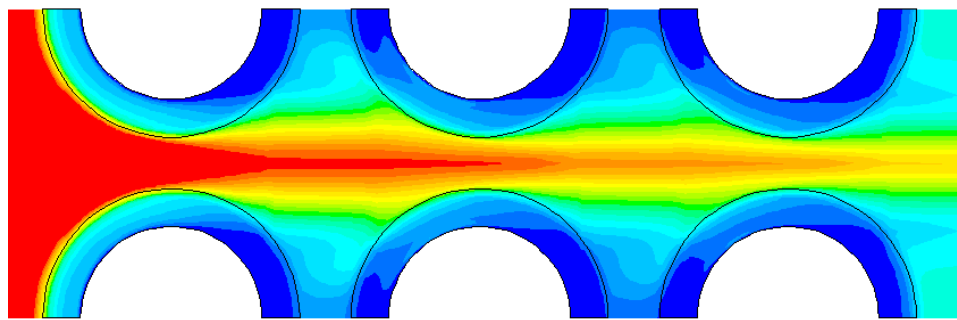


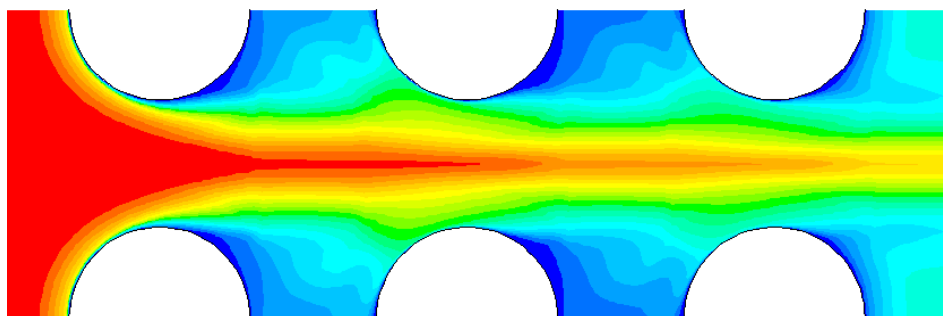
Figure 5.13 Temperature distributions for bundle s6 ($n=3$) at $Re = 8.6 \times 10^3$.

the stagnation point for the staggered tube arrangement. For both tube arrangements, the temperature gradient down stream along the fin is lower than the upstream due to the wake flow.

As can be observed in Figure 5.14, a high temperature stream passes through the in-line bundle without mixing well. It is also confirmed that because of the proceeding rows of in-line array locating in the wake region, the temperature difference between the fin and air is lower than for the staggered rows. The numerical results are consistent with the flow visualizations of Jang et al. [25] and Kaminski [29] and also the experimental investigation of Weierman et al. [76]. Moreover, it is interesting to note that there will be only a small amount of hot air that can be cooled down at higher Reynolds number. A long flow path with the inlet air temperature is expected for higher velocity for both tube arrangements.



(a) Near fin surface plane



(b) Mid-plane between fins

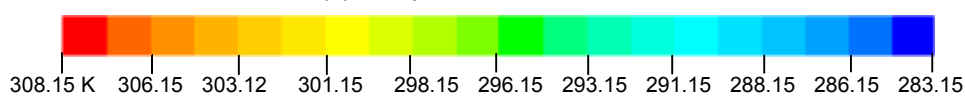


Figure 5.14 Temperature distributions for bundle *i4* ($n=3$) at $Re = 8.6 \times 10^3$.

5.3 Results of Geometric Parameters Effects

Investigations were performed by only varying the intended geometric parameter while other parameters were fixed throughout the related investigations. Totally 29 finned-tube banks were probed and, 19 of them were used for investigating the effects of finning parameters. The rest was used for the effects of tube arrangement and bundle depth.

The results are organized in the following manner. Firstly, the investigation is focused on the heat transfer rate \dot{Q} , and then, on the fin efficiency η , and the heat transfer coefficient h , and finally on the pressure drop Δp . These results are plotted as functions of the relevant geometric parameters for three different Reynolds numbers and presented for staggered and in-line bundles. The discussions for the results are presented with the figures when possible. In a second step, for determination of the optimum geometry, comparisons are prepared in terms of the bundle performance parameter K that is defined by Ackerman and Brunsvold [1], and Kaminski [29].

$$K = \frac{\dot{Q}}{N} \quad (5.15)$$

$$N = \Delta p \dot{V} = \Delta p \frac{\dot{m}_a}{\rho_{in}} \quad (5.16)$$

Equation 5.15 concerns with the gain in the heat transfer rate \dot{Q} from bundles to the power consumption N . The maximum value of this ratio indicates that a given bundle is the optimum one from the point of view of the power input.

5.3.1 Results of Fin Height Effect

To demonstrate the fin height effects, numerical investigations were carried out for five staggered (s1 to s5) and three in-line (i1, i2 and i3) tube bundles. For each case, tests were performed under a consideration of varying only the fin height with constant fin thickness (0.5 mm), fin spacing (2 mm), and constant outside diameter of the tube (24 mm).

Figure 5.15 proves clearly that the heat transfer rate is directly effected by the fin height for both tube arrays since increasing the fin height will raise the heat transfer

surface area of the bundle. As expected, Figure 5.15 shows that the heat transfer rate of the staggered tube array is higher than that of the in-line tube array. The fact that the use of a higher fin gives a higher heat transfer rate is accompanied by slightly decreasing air temperatures at the outlet of the finned-tube bundle.

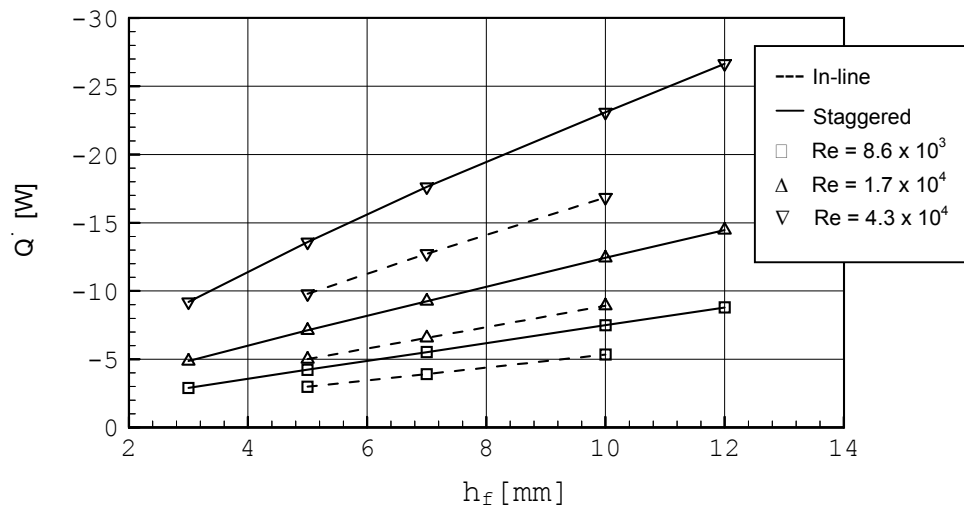


Figure 5.15 Effect of fin height on the heat transfer rate for staggered and in-line tube bundles.

Representative results by Equation (5.8) for the fin height effect on the fin efficiency for both tube arrangements are presented in Figure 5.16 where the expected result is confirmed that the fin efficiency decreases for increasing the fin height for both tube arrangements. Since the fin efficiency is inversely proportional to the parameters (ψ , m , h_f), the efficiency will become smaller whenever these parameters are increased, especially the fin height. For the staggered finned-tube bundle, the fin efficiency decreases by 6.8 % (at $Re = 8.6 \times 10^3$) and 14.2 % (at $Re = 4.3 \times 10^4$) when rising from $h_f = 3$ mm to 12 mm. A similar decrease occurs in the in-line bank by about 2.1 % to 5.5 %, respectively when the fin height varies from 5 mm to 10 mm.

It is seen that the fin height effect on the efficiency increase is noticeable at high Reynolds numbers because the boundary layer gets thinner compared to the lower velocity case. As a result, the temperature gradient along the fin becomes higher. It should be noted that the effect of heat transfer coefficient on the fin height depends on the temperature and velocity boundary layers. The boundary layers become thicker and thicker whenever the height of fin is enlarged and it is expected that the thicker the boundary layer, the smaller the heat transfer coefficient will be.

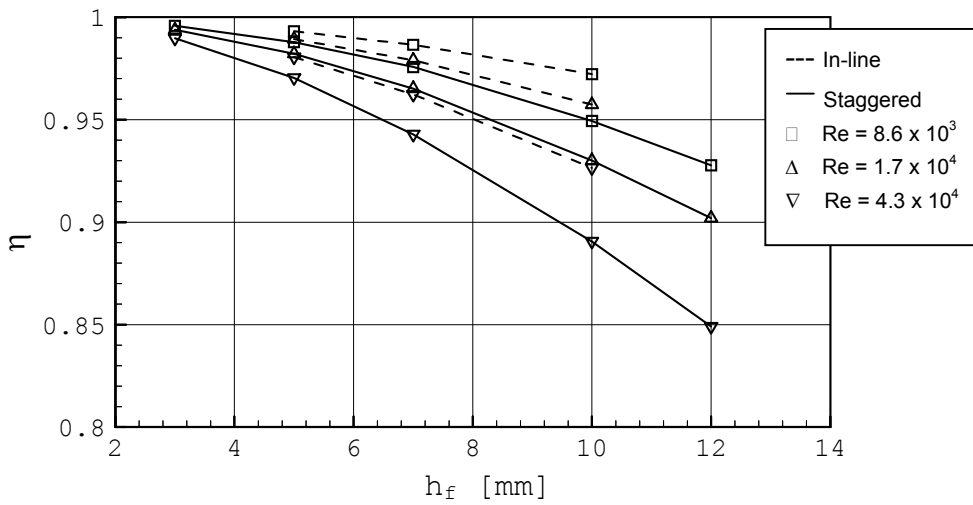


Figure 5.16 Effect of fin height on the fin efficiency for staggered and in-line bundles.

The analysis of the numerical results on the fin height effect for both tube arrays agrees well with the experimental data in that rising the fin height provides a decreased heat transfer coefficient and increased pressure drop of the circular finned-tube bundle (see Figures 5.17 and 5.18). It is discovered in Figure 5.17 that the average heat transfer coefficient of the low fin ($h_f = 3$ mm) bundle is about 12.2 % and 20.3 % higher than for the high fin ($h_f = 12$ mm) of the staggered tube bundle at low and high Reynolds numbers, respectively.

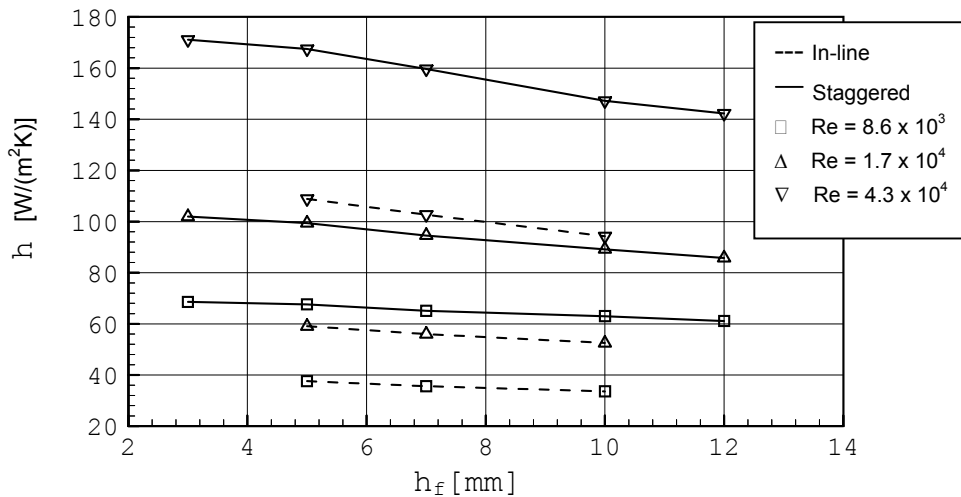


Figure 5.17 Effect of fin height on the heat transfer coefficient for staggered and in-line bundles.

A similar phenomenon is observed in Figure 5.17 for the in-line tube arrangement where the average heat transfer coefficient decreases for the fin height variation from $h_f = 5$ mm to 7 mm and 10 mm by about 5.2 % and 10.6 %, respectively (at low Re) and 5.7 % and 13.44 % (at high Re). The same approach is performed for

the staggered arrangement where the decrease to be about 3.7 % and 6.8 %, respectively (at low Re) and 4.7 % and 12.1 % (at high Re). It will thus be seen that the in-line tube arrangement is more influenced by the fin height changes. Kearney [31] showed that this result may not be sensitive when $\frac{d_f}{d} = 4$; unfortunately, no conclusion can be reached for this case since the present study is confined to $\frac{d_f}{d} \leq 2$.

To get a clear image of the effects of fin height on the pressure drop, Figure 5.18 is presented with the pressure drop ratio of individual fin height to ($h_f = 5$ mm). For both tube arrays, it is common to find that the pressure drop of the bundle increases with the fin height, since the boundary layer thickness increases as the fin height is increased for the same Reynolds number. The trend of the graph of staggered array is found to be similar with the available experimental data (Brauer [6], Mirkovic [43], Stasiulevičius and Skrinška [62], and Yudin et al. [80]). For the staggered tube array, the pressure drop increases about 26.7 % and 7.1 % for varying h_f from 3 mm to 12 mm at $Re = 8.6 \times 10^3$ and 4.3×10^4 , respectively.

This result shows that the percentage increment of the pressure drop is higher at low Re where the boundary layer is thicker. The expectation is confirmed that the pressure drop of the staggered arrangement is higher than in the in-line arrangement for the same Re and fin height. At low Reynolds number ($Re = 8.6 \times 10^3$), the pressure drop of the bundle (s2) is about 66.5 % higher than by bundle (i1). These results agree well with those obtained by Brauer [6] who showed that the pressure drop of the staggered bank at $Re = 10^4$ is about 65 % higher than the in-line bank of $h_f = 5$ mm.

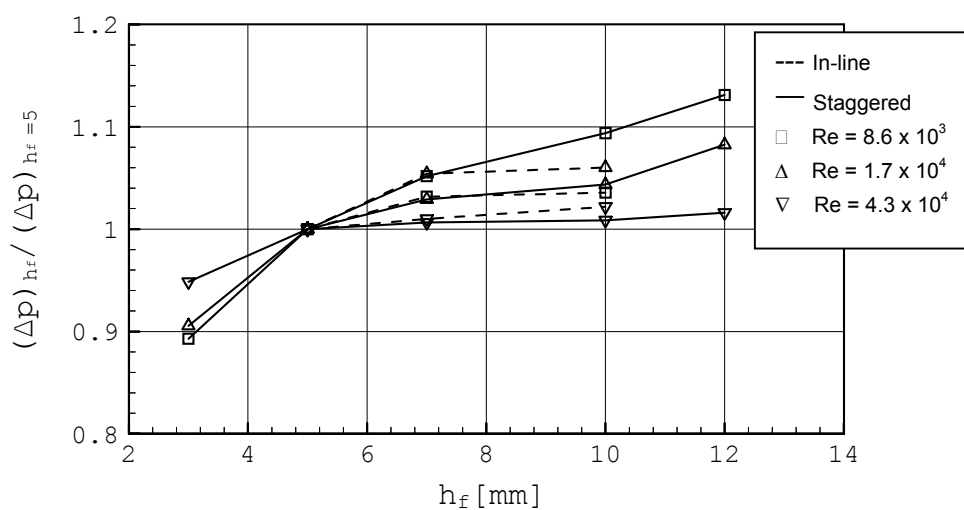


Figure 5.18 Effect of fin height on the pressure drop for staggered and in-line bundles.

According to the basic heat exchanger design, a required total heat transfer surface area A must be realized without decreasing the heat transfer coefficient and increasing the pressure drop. With this in mind, Figure 5.19 is developed to get an optimum value of the fin height of staggered and in-line bundles with an expression of the performance parameter ratio based on individual fin height to $h_f = 5$ mm.

At low Re , the minimum value of the fin height ($h_f = 3$ mm) gives the highest performance for staggered tube arrangement although a different trend is discovered for the in-line tube arrangement as the high performance of the bundle results from the increase of the fin height. This trend is true for $Re = 8.6 \times 10^3$ and 1.7×10^4 ; however, for the highest Reynolds number, the trend is changed and the optimum fin height is at $h_f = 7$ mm for both finned-tube arrangements. Moreover, it is surprising to learn that the in-line finned-tube bundle performance is better than one of the staggered bundle within the tested geometry ranges. The differences of the effects of the layout of the tubes on heat transfer and pressure drop will be discussed separately.

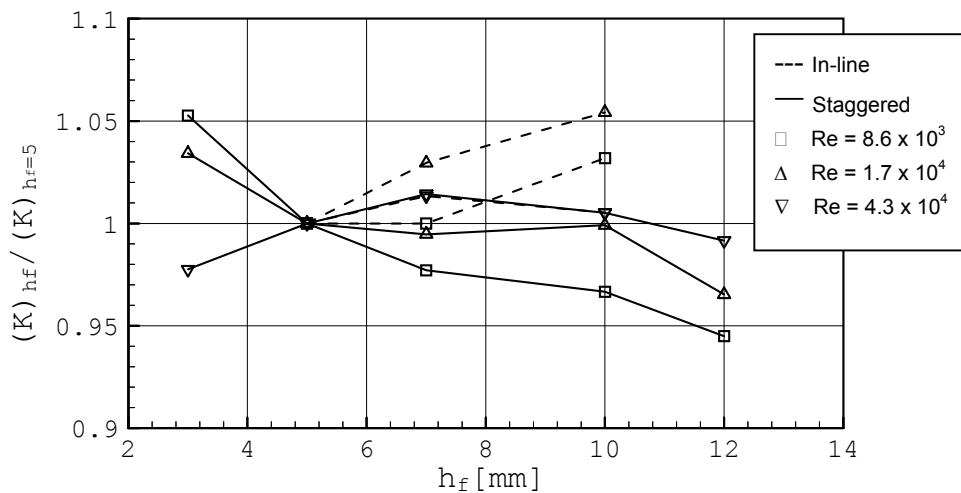


Figure 5.19 Performance parameter of the fin height effect for staggered and in-line bundles.

In summary, the fin height effect on the heat transfer and on pressure drop is very similar for both finned-tube arrangements. Generally, the lower fin height gives a better efficiency, a higher heat transfer coefficient and a smaller pressure drop. Boundary layer development according to the Reynolds numbers is a dominant factor for the effects of fin height and according to the fin geometry, the boundary layer development depends also on the space between the fins.

5.3.2 Results of Fin Spacing Effect

A complete understanding of the fin spacing effect and its relation to heat transfer and pressure drop behaviour of finned-tube bundles is needed. Therefore, the effect of the fin spacing was investigated for the eight bundles with the two fin heights; namely fin height 5 mm for bundles (s2, s6, s7, i1, i4, i5) and height of 10 mm for bundles (s4 and s8). It should be mentioned that numerical investigations were based on a single fin pitch as indicated in Figure 4.2 (c). Therefore, the results may probably differ especially for the cases of fin pitch and thickness effects when considering for the unit length of tube instead of one pitch unit. When the fin spacing is increased, the fin surface area keeps constant and only the base tube surface area will slightly grow. Therefore, a larger mass flow rate of air is expected for the larger fin spacing bundle.

As shown in Figure 5.20, the heat transfer rate increases with the fin spacing for both tube arrays due to enhancement of the total surface area. This effect amounts to 12.4 % ($Re = 8.6 \times 10^3$) and 7.9 % ($Re = 4.3 \times 10^4$) where the fin spacing is changed from 1.6 mm to 2 mm in the staggered tube arrangement, but 13.5 % and 10.2 %, respectively for the in-line finned-tube bundle.

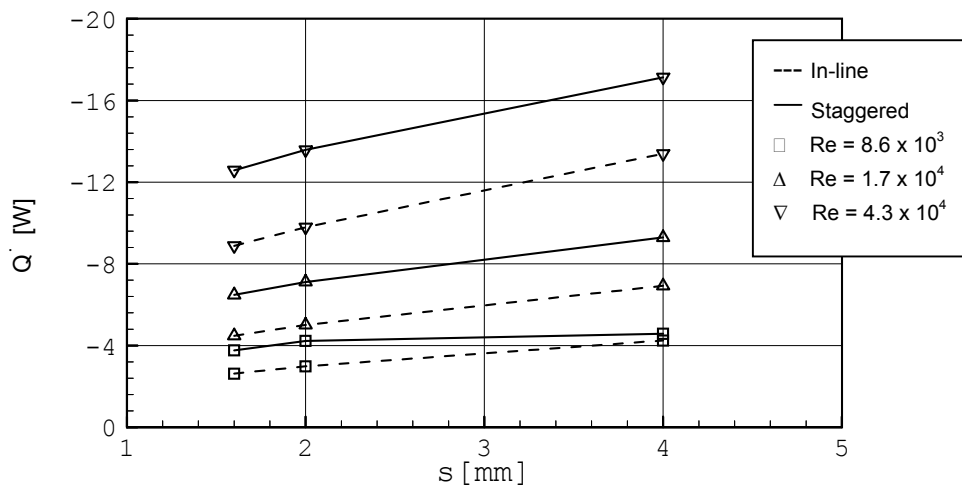


Figure 5.20 Effect of fin spacing on the heat transfer rate for staggered and in-line bundles.

Attention is now turned to the fin efficiency and one can see in Figure 5.21, that there are only small effects for both arrays. For both tube layouts, the fin efficiency slightly decreases with the Reynolds number. This decrease is because of the heat transfer coefficient is higher at increased Re (see Equation 5.8). Figure 5.21 reconfirms the fact that the in-line bank fins are more efficient than those in the staggered bank for the same Re since the in-line tube array gives the lower heat transfer coefficient.

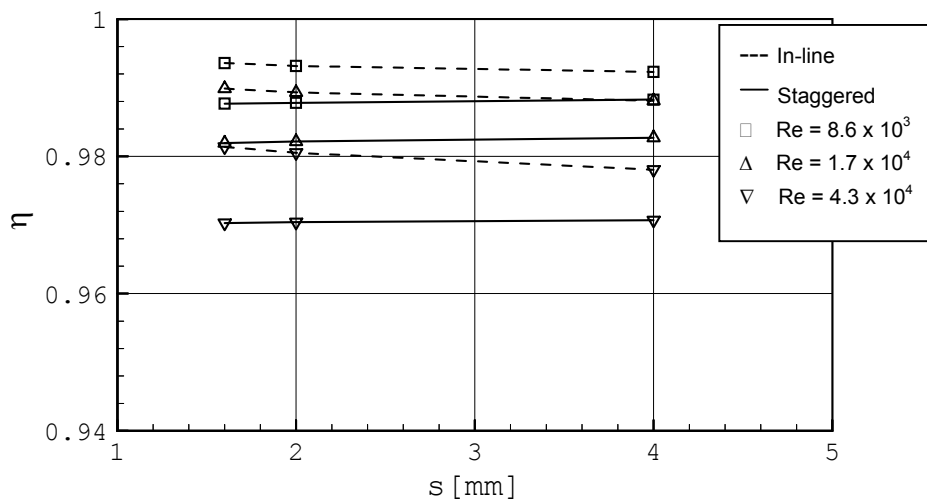


Figure 5.21 Effect of the fin spacing on the fin efficiency for staggered and in-line bundles.

A careful evaluation of Figure 5.22 shows that the heat transfer coefficient of the staggered tube array is slightly changed as the fin spacing increases for the low finned bundles with three different fin spacing (1.6 mm, 2 mm and 4 mm). It is noted that the numerical result agrees with the result of Antuf'ev and Gusev [2] who showed that the heat transfer coefficient of the smaller fin spacing, $s = 1.2$ mm is superior than the higher fin spacing $s = 1.7$ mm for the 19 mm tube and 3 mm fin height (the Re range was $2 \times 10^3 \leq Re_{\alpha} \leq 1.6 \times 10^4$).

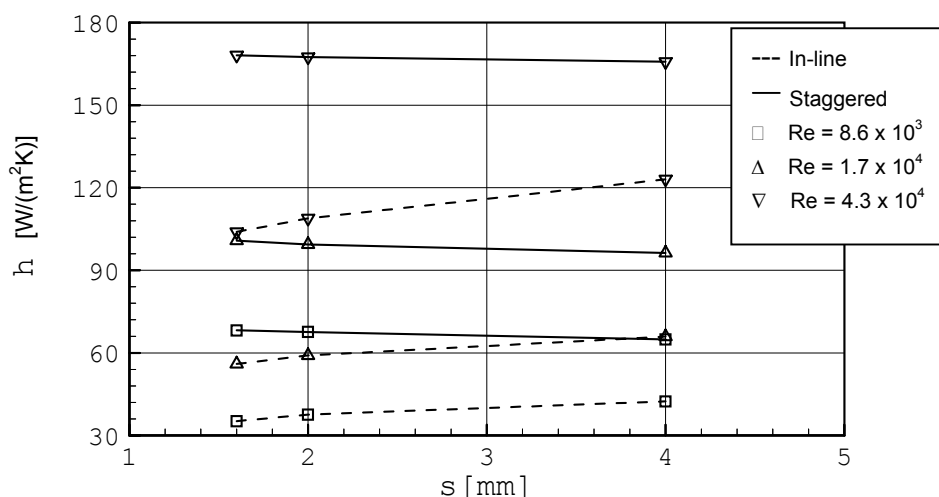


Figure 5.22 Effect of fin spacing on heat transfer coefficient for staggered and in-line bundles.

However, at high Re the differences of the heat transfer coefficient between these three bundles tend to be negligible, as the difference is less than 1 %. Experimental data (Kuntysch et al. [34], Stasiulevičius and Skrinška [62], Watel et al.

[70, 71] reported that if the fin spacing exceeds about twice the boundary layer thickness at the base of fin, the influence of s on the heat transfer coefficient is small. These results are well consistent with the numerical investigations of the staggered tube array in which most of the boundary layers between the fins of the above bundles are found to be departing each other.

Further analysis of the experimental data (Kuntysh et al. [34], Stasiulevičius and Skrinska [62], Watel et al. [70, 71], and Yudin et al. [80]) on the fin spacing effect showed some different trend: the Nusselt number increases with the fin spacing when fin spacing is less than two times of boundary layer thickness. Therefore, for purpose of verification, further calculations (bundles s4, and s8) were performed with the higher fin height (10 mm), in which the fin spacing was varied from 0.7 mm to 2 mm. In this case, the heat transfer coefficient increases with the fin spacing and the boundary layers between two adjacent fins are found to touch each other. Therefore, it is appropriate to mention that the effect of fin spacing is largely influenced by the boundary layer development in the system. It is also noted that the increase of heat transfer coefficients is more significant at low Re because the thickness of boundary layer decreases with the increased Re . It was suggested earlier (in section 5.2.2) that at low Re , the boundary layers built up on the two adjacent fins and interact with each other. Due to the merging of the two boundary layers between the fins, the horseshoe vortices around the tube are suppressed and the heat transfer coefficients decrease. Therefore, the effect of reducing of the fin spacing depends principally on the velocity of air, which rules the boundary layers.

The numerical simulation for the in-line tube array is showing the different conclusion. The heat transfer coefficient of the bundle increases with the enlargement of fin spacing. This trend may attribute to the in-line array geometry where the deeper rows lie in the wake region of the previous tubes. Due to the wider fin spacing, an increased mass flow can penetrate the in-line tubes surfaces and the stronger reverse flow, which enhanced heat transfer, appear in the wake as previously described in the section 5.2.1. When increasing the fin space from 2 mm to 4 mm, the percentage increment of heat transfer coefficient of the in-line bank is about 13 %.

Similar to the experimental results of Jameson [23], and Ward and Young [69], Figure 5.23 shows that the pressure drop decreases for both tube arrays while increasing the fin spacing. When increasing the fin spacing, the strong interactions of

the boundary layers between the fins are reduced and resulting friction losses were considerable. As expected, the staggered tube array gives a larger pressure drop at higher Reynolds number.

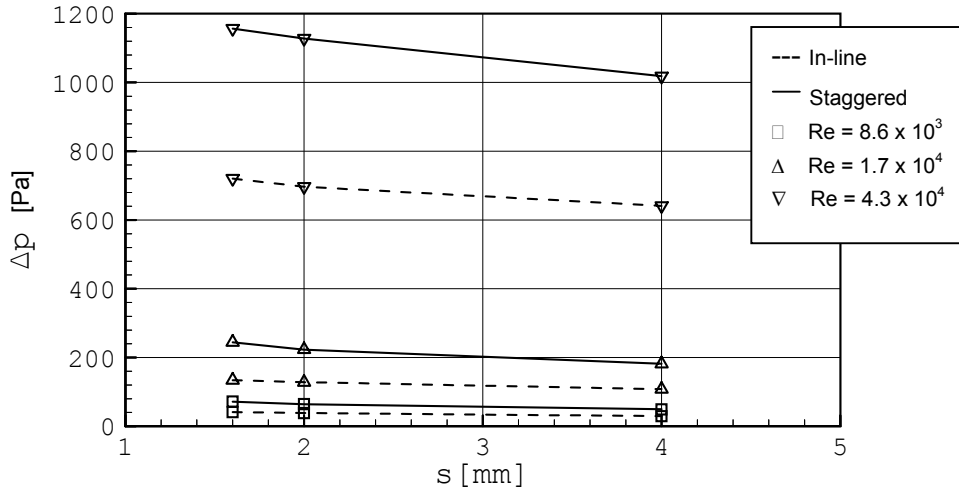


Figure 5.23 Effect of fin spacing on the pressure drop for staggered and in-line bundles.

Figure 5.24 shows the bundle performance of staggered and in-line tube arrays based on the fin spacing. It is understood from the figure that the in-line bundle has a better performance than the staggered bank. The single trend observed from the figure is that the bundle performance slightly decreases when the fin spacing is increased. Therefore, the optimum spacing for the in-line tube bank is at the lowest value of 1.6 mm.

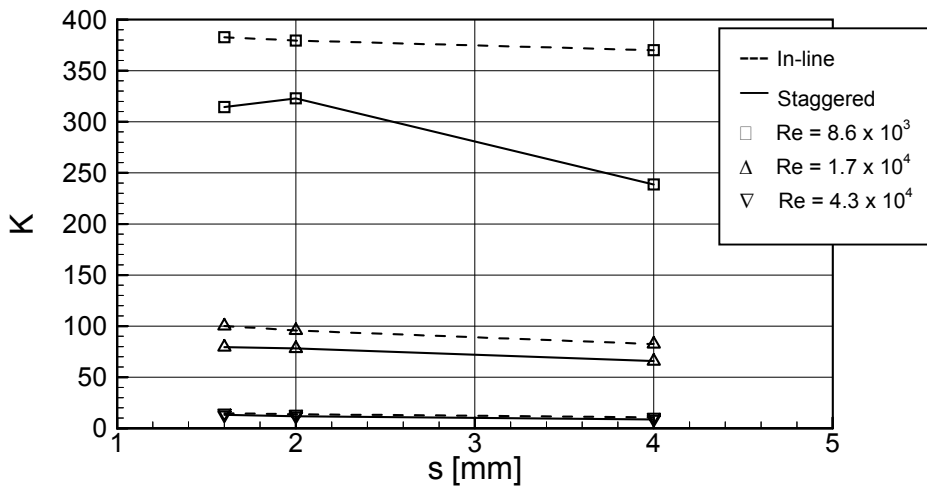


Figure 5.24 Performance parameter of the fin spacing effect for staggered and in-line bundles.

As explained above, the large fin spacing enhances the heat transfer rate and reduces the pressure drop. However, the simultaneous rise of the volume flow rate of air is substantially high enough to decline the performance of the finned tube bundle (see Equation 5.15). The similar trend is achieved at the $Re = 4.3 \times 10^4$ and 1.7×10^4 for the staggered tube array as the optimum fin spacing has the smallest value. On the other hand, the maximum performance is attained at $s = 2$ mm for the low Re and further increase in the fin spacing provides lower performance.

5.3.3 Results of Fin Thickness Effect

One of the present objectives is to find out the effect of the thickness of the fins and for this purpose, it was investigated only for the staggered finned-tube bank. Circular fins with the constant fin thickness (fin tip and fin base thickness is unique) are used in this study. Three bundles (s_2 , s_9 , and s_{10}) are considered where geometrical parameters are identical except for the fin thickness, which is varied from 0.3 mm to 0.6 mm.

Figure 5.25 shows that the thicker fin provides the higher heat transfer rate, which increased by a comparatively small amount in the staggered finned-tube bundle. The influence of the fin thickness effect is more pronounced at high Reynolds number. When increasing the fin thickness from 0.3 mm (bundle s_9) to 0.5 mm (bundle s_2) at $Re = 4.3 \times 10^4$, the heat transfer rate is improved by about 4.2 %, while it remains about 3.2 % at $Re = 8.6 \times 10^3$.

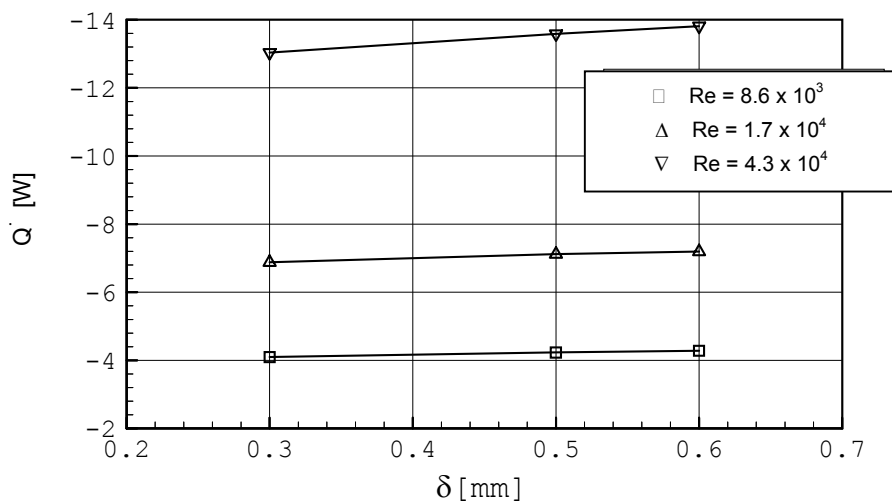


Figure 5.25 Effect of fin thickness on the heat transfer rate for staggered bundle.

Like the heat transfer rate effect, the same trend for the fin efficiency is discovered in Figure 5.26. It proved the definition of the fin efficiency (Equation 5.8) where the fin efficiency increases with the larger fin thickness. The temperature gradient in the fin decreases as the fin thickness increases. Higher percentage increment of the fin efficiency is found at higher Reynolds number, increasing however, at $Re = 4.3 \times 10^4$ by only 1.9 % when the fin thickness changes from 0.3 mm to 0.5 mm.

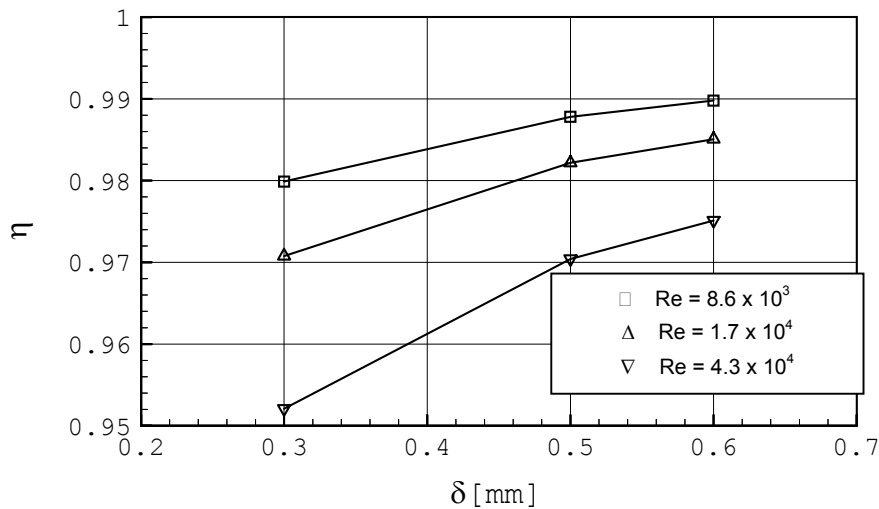


Figure 5.26 Effect of fin thickness on the fin efficiency for staggered bundle.

There is also need to emphasize the heat transfer coefficient variations, can be caused by the fin thickness changes. Inspection of Figure 5.27 shows clearly that the heat transfer coefficient of the staggered tube bank is remarkably insensitive to the changes of the fin thickness. Therefore, the effect of the fin thickness on the staggered tube bundle may be neglected in the practical considerations.

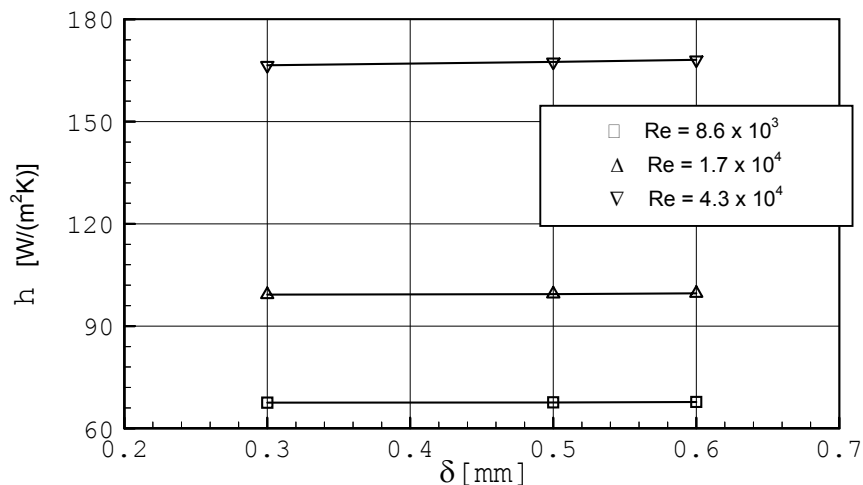


Figure 5.27 Effect of fin thickness on the heat transfer coefficient for staggered bundle.

This result agrees with the previous analytical result of Stasiulevičius and Skrinska [62]; however, it differs from those of Briggs and Young [8], and Ward and Young [69]. In deed, Ward and Young [69] did not conduct the test properly for this effect; however, it can be traced a trend from their correlation that heat transfer coefficient increases with the fin thickness. Briggs and Young [8] showed contrary to [69] that the heat transfer coefficient decreased approximately 8 % when raising the fin thickness by four times. Briggs and Young's finding on the fin thickness effect is excluded for the pressure drop behaviour and therefore, it is of interest to observe the pressure drop changes and Figure 5.28 represents the numerical results. Apparently, the changes of the fin thickness do not affect considerably the pressure drop since the flow distribution in the bundle is not much different.

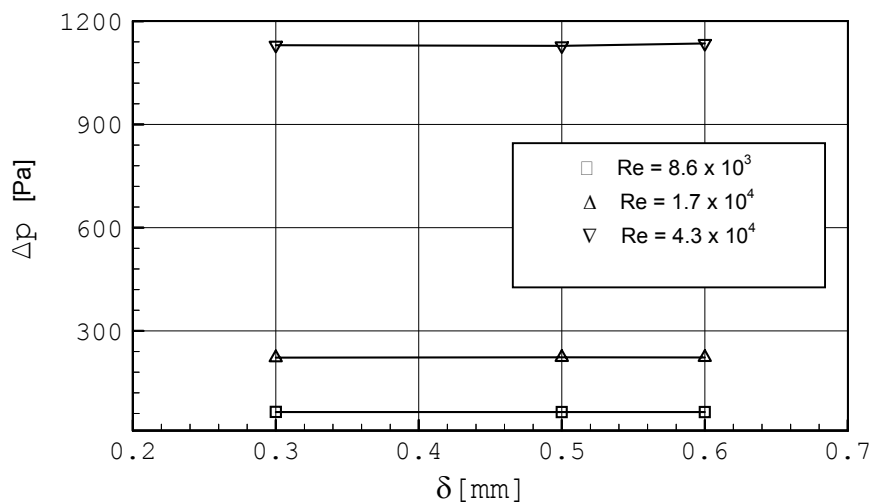


Figure 5.28 Effect of fin thickness on the pressure drop for staggered bundle.

Since there is no significant effect on the heat transfer coefficient and the pressure drop, the same conclusion is reached for the performance graph of fin thickness effect (see Figure 5.29). It is useful to note that the lower performance is observed at high Reynolds numbers as in the previous results of fin height and fin spacing changes. This behaviour is a result of the fact that higher pressure drop is expected at higher Reynolds numbers. Consequently, the analysis of results on the fin thickness within the investigated range of Reynolds numbers agrees with Stasiulevičius and Skrinska [62] in that the fin thickness changes do no influence all the interested behaviours of the finned-tube bundle except for its weight and cost.

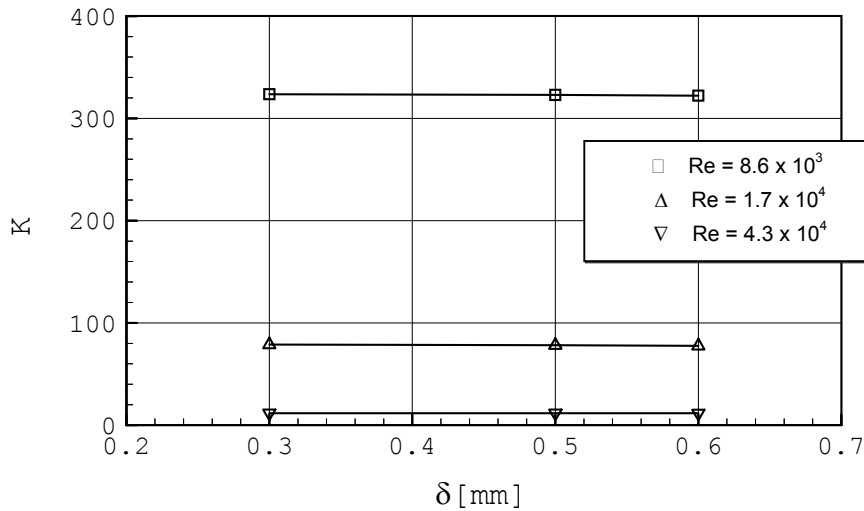


Figure 5.29 Performance parameter of the fin thickness effect for staggered bundle.

5.3.4 Results of Tube Outside Diameter Effect

The role of the tube diameter in changing the heat transfer and fluid flow characteristics of the circular finned-tube bank is required to be emphasized. As noted earlier, the numerical investigations for the effect of tube diameter were performed for three different diameters (13.59 mm, 24 mm, 28 mm) and for the fixed other geometric parameters of three bundles (s2, s11, s12) of the staggered tube array, and three in-line bundles (i1, i6, i7). As shown in Figure 5.30, the average heat transfer rate decreases as the tube diameter increases for both staggered and in-line tube bundles.

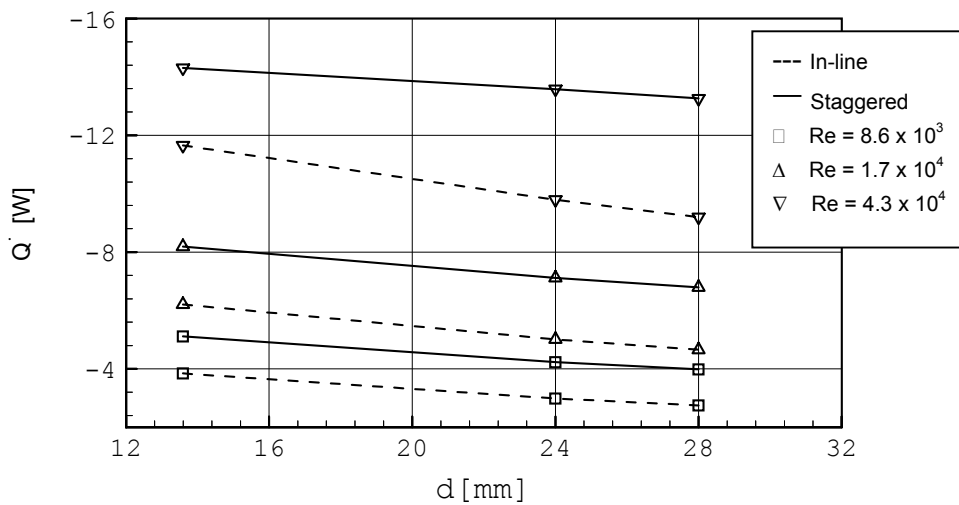


Figure 5.30 Effect of tube outside diameter on the heat transfer rate for staggered and in-line bundles.

In addition, the average air temperature at the outlet decreases as the tube diameter increases. By Reynolds number definition, the inlet velocity for a smaller tube diameter is higher for the same Re . For the staggered arrangement, increasing the tube diameter from 13.59 mm to 24 mm achieves a decrease of the average heat transfer rate up to about 17 %, and 22.3 % for the in-line array.

Attention is next turned to Figure 5.31 and to the fin efficiency results of tube outside diameter changes for both tube arrays. Figure 5.31 illustrates that the fin efficiency slightly increases with the tube diameter. The fin efficiency increases only by 2.6 % for the staggered array when changed from the smallest to the largest tube diameter, and 2.5 % for the the in-line array. The increased temperature gradients in the fin are responsible for the increased fin efficiency.

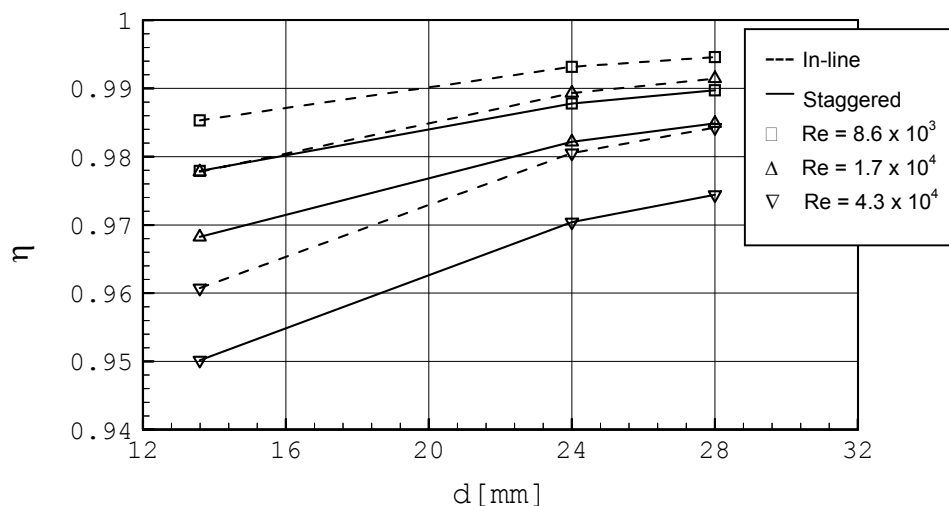


Figure 5.31 Effect of tube outside diameter on the fin efficiency for staggered and in-line bundles.

It is seen that the average heat transfer coefficient considerably depends on the value of the tube outside diameter. In view of Figure 5.32 shows that the heat transfer coefficient declines as the larger tube outside diameter in both staggered and in-line finned-tube bundles. For the staggered tube arrangement, increasing the tube diameter from 13.59 mm to 24 mm resulted in a decrease of the heat transfer coefficient up to about 38 %. This result agrees with Ward and Young [69] findings the average heat transfer coefficient is inversely proportional to the tube diameter. For the in-line arrangement, the heat transfer coefficient decreases up to about 48 %. Therefore, it can be concluded that there is a stronger tube outside diameter effect for the in-line array. This behaviour is a result of the fact that the wake region of the in-line tubes becomes larger whenever tube diameter increases.

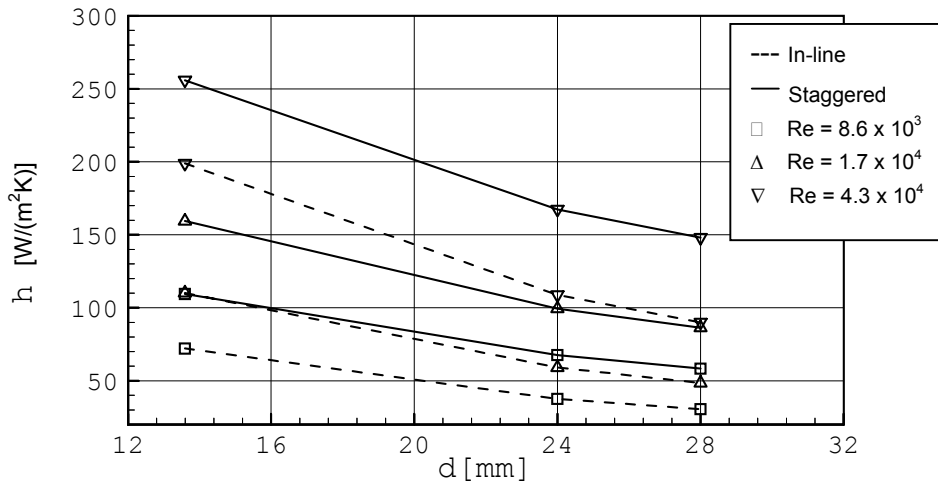


Figure 5.32 Effect of tube outside diameter on the heat transfer coefficient for staggered and in-line bundles.

For the same Re , the inlet velocity in case of the smaller diameter is higher than for the larger diameter. Due to this behaviour, the pressure drop also decreases with the rising tube diameter for both in-line and staggered bundles, as show in Figure 5.33. As the tube diameter increases from 13.59 mm to 24 mm, the pressure drop decreases up to 66.7 % for the in-line array and up to 61.1 % for the staggered arrangement.

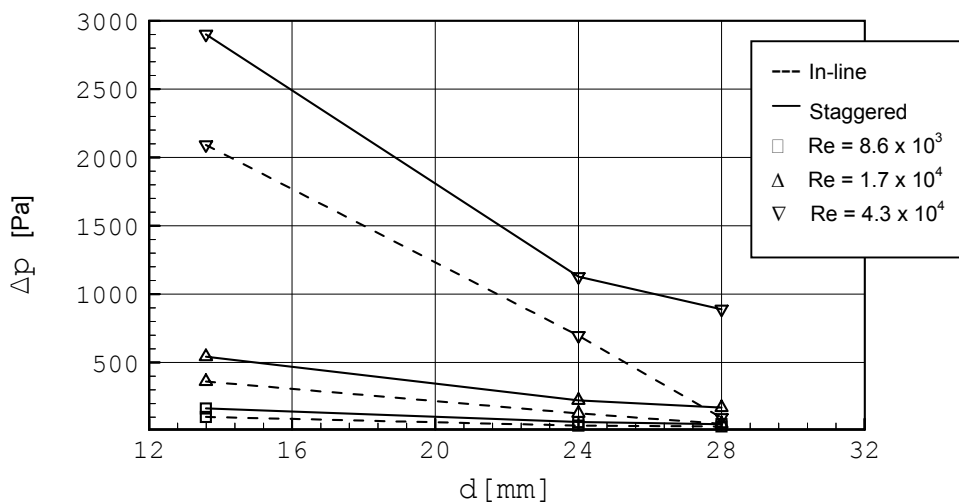


Figure 5.33 Effect of tube outside diameter on the pressure drop for staggered and in-line bundles.

Different results are obtained in this work when comparing with Mirkovic [43] who found that both heat transfer and pressure drop increases with the tube diameter for constant transverse and longitudinal pitches. This difference may be due to the fact

that the ratio of the transverse tube pitch to the fin diameter, $\frac{S_t}{d_f}$ is set to be constant in the present study. For this reason, the tube pitch also increases when the tube diameter is increased. For the case of constant tube pitches, the velocity at the narrowest cross-section increases with the increase of tube diameter. In this respect, the heat transfer and pressure drop are increased with the tube diameter. In the present study, the inlet velocity is higher for the case of a smaller tube diameter at the same Reynolds number.

The Reynolds number definition of Figure 5.34 is the same as for the above figures and it is observed that the most advantageous tube diameter is the largest value of 28 mm for all reference Reynolds numbers. This behaviour is quite noticeable at $Re = 8.6 \times 10^3$ and it should however, be stressed that the effect of tube diameter on the performance of tube bundles is quite insensitive to the Reynolds numbers. Moreover, the performance parameters at $Re = 4.3 \times 10^4$ are virtually the same for staggered and in-line tube arrangements.

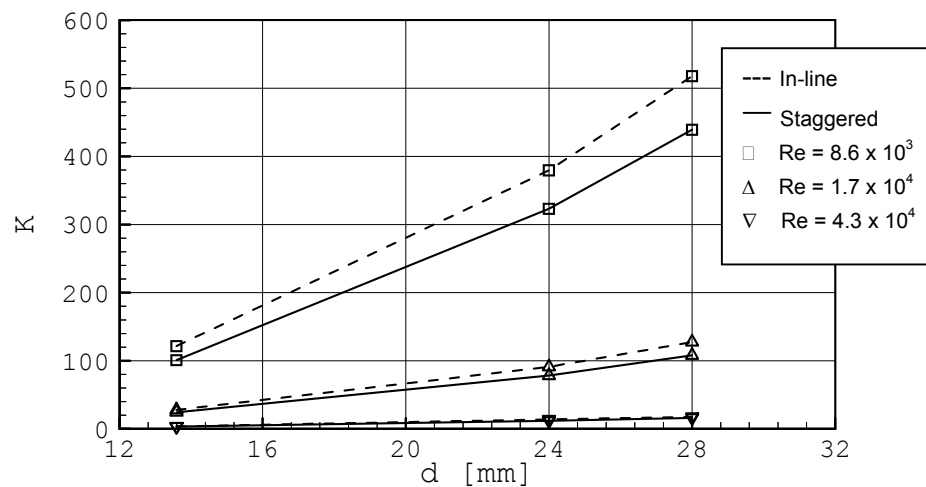


Figure 5.34 Performance parameter of the tube outside diameter effect for staggered and in-line bundles.

5.3.5 Results of Tube Spacing Effect

A large number of opinions have been put forward concerning the effect of longitudinal and transverse tube pitches in circular finned-tube heat exchangers. However, in the numerical investigation all staggered bundles were considered as the

equilateral tube pitch bundles and therefore, the direct comparison with the experimental results are unfeasible. For the effect of tube spacing, six numbers of finned-tube bundles, three for staggered tube arrangement (s2, s13, s14) and three for in-line bundles (i1, i8, i9) were examined. The diagonal tube pitch rather than the transverse and longitudinal pitches was selected because both tube arrangements can be conveniently displayed in one figure.

The heat transfer through the bundle is related to the tube arrangement. The variation of heat transfer due to changes of the tube arrangement mostly can be considered with the variation of air flow patterns. The influences of the tube spacing on the heat transfer rate for staggered and in-line tube arrays are characterized in Figure 5.35. It is seen that the heat transfer rate increases at first with the diagonal pitch of the staggered array, although, a further increasing in S_d (by increasing transverse tube pitch S_t) does not affect significantly in terms of heat transfer rate.

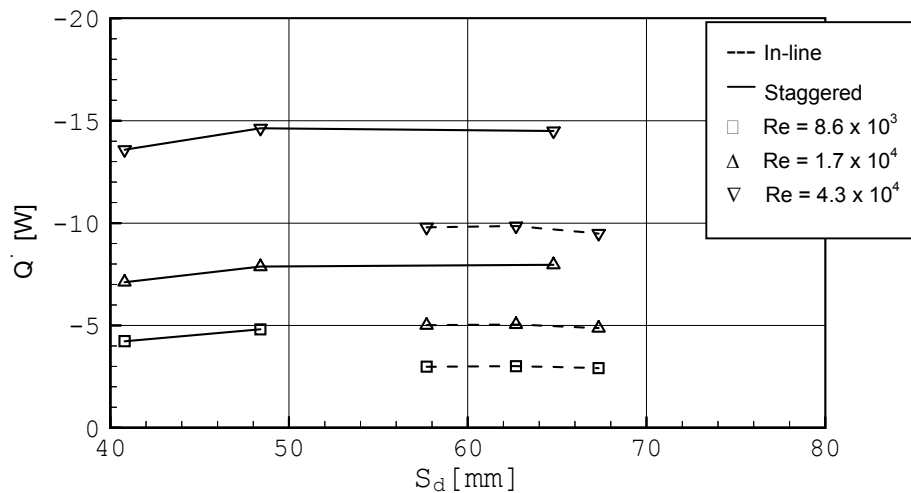


Figure 5.35 Effect of tube spacing on the heat transfer rate for staggered and in-line bundles.

The extent of increase is appreciated since the average air temperature at the outlet increases with the tube spacing because of the bypass flow through fin tip clearance. As a consequence of the equilateral pitch setting, the longitudinal pitch will vary proportionally in accordance with the transverse tube pitch changes. The negative effect on the heat transfer coefficient will be exhibited later. As shown in Figure 5.35, it is seen that increasing S_d from 62.7 mm (i9) to 67.32 mm (i8), (only varying the transverse tube pitch) the heat transfer rate is slightly decreased. It reflects that the velocity of air increases as through narrow fin tip-to-tip spaces that accompany the reduction in transverse pitch.

As illustrated in Figure 5.36, the changes of tube spacing of both tube arrangements produce no real significance effect on the fin efficiency. The fin efficiency is lower at the higher Reynolds number, which tends to increase the heat transfer coefficient. Sparrow and Samie [59] showed that fin efficiency is smaller with respect to the lower $\frac{S_t}{d_f}$ value. For a similar Re , it is seen that the lower efficiency changes occurred for larger $\frac{S_t}{d_f}$ values. Unfortunately, this behaviour is applied in [59] only for one-row arrays and it should be noted that unheated tubes were also used in the experiment.

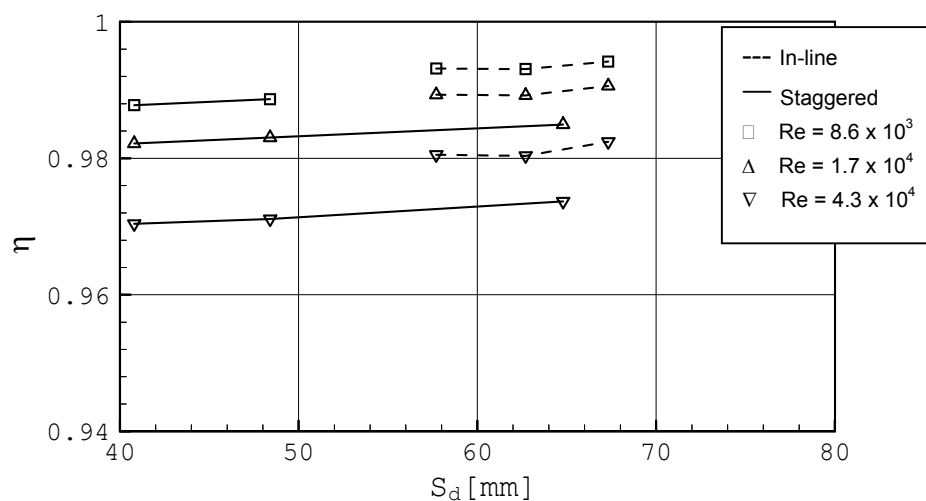


Figure 5.36 Effect of the tube spacing on the fin efficiency for staggered and in-line bundles.

The heat transfer coefficient is decreased as tube spacing increases for both tube arrangements. This trend is shown in Figure 5.37. When the tube spacing of the staggered bundle increases from $S_d = 40.8$ mm (s2) to $S_d = 48.4$ mm (s13) the heat transfer coefficient decreases by approximately 4.9 % at $Re = 1.7 \times 10^4$. When comparing bundles (s13 and s14) in which S_d is increased from 48.4 mm to 64.8 mm, the heat transfer coefficient decreases by approximately 11.5 % at $Re = 1.7 \times 10^4$. Therefore, it is understandable that the higher heat transfer coefficient could be generated at closer tube spacing. The reason is that the influence of the tubes exerted on each other is decreased by increasing diagonal tube pitch, and the tube bundle will tend to behave more like individual finned-tubes in crossflow [46]. The numerical results agree with Neal and Hitchcock [45], and Sparrow and Samie [59].

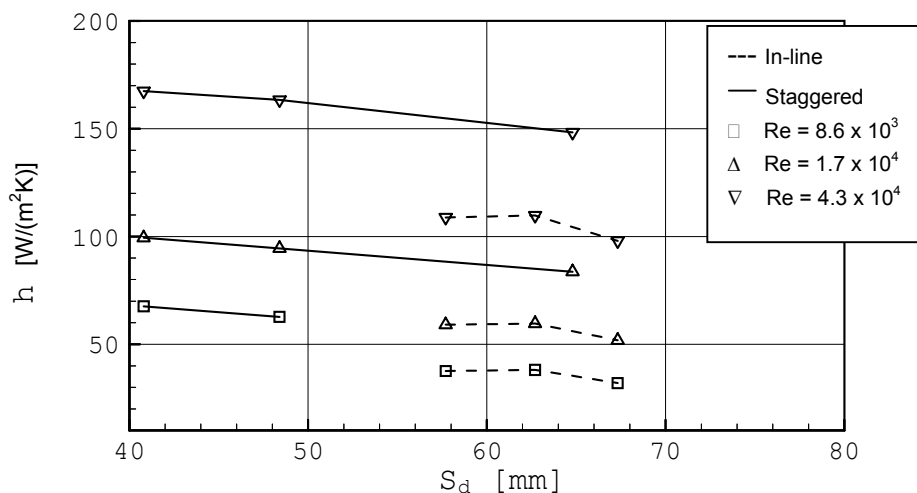


Figure 5.37 Effect of the tube spacing on the heat transfer coefficient for staggered and in-line bundles.

For the in-line arrangement, varying the diagonal pitch from 62.7 mm (i9) to 67.32 mm (i8) generated to decrease average heat transfer coefficient by about 23.7 % at $Re = 1.7 \times 10^4$. In the bundles (i8 and i9), the transverse tube pitch only will change when varying the diagonal pitch. Therefore, it indicates that the transverse tube pitch is more important on in-line tube arrangement than those for the staggered tube arrangement are. A comparison between (i1) and (i9) is performed for the effect of longitudinal tube pitch. The result shows that there is no significant effect on heat transfer coefficient corresponding to S_d changes (from 57.7 mm to 62.7 mm). For this test, the transverse tube pitch is fixed at a constant value while only varying the longitudinal tube pitch. Hence, the changes of S_d are directly proportional to S_l .

Varying tube spacing has a substantial effect on air pressure drop. A decrease in the diagonal tube pitch gives a positive effect on the heat transfer coefficient; however, there is a negative effect on pressure drop. The average bundle pressure drop increases as the diagonal tube pitch becomes closer. This behaviour is valid for both tube arrangements as shown in Figure 5.38. When varying $S_d = 40.8$ mm (s2) to 48.4 mm (s13) of the staggered tube bundle, the percentage pressure drop is lower by about 8.8 % at $Re = 1.7 \times 10^4$. In comparison of bundles (s13 and s14), the pressure loss in bundle (s13) is about 14.2 % lower than that of bundle (s14). In here, the result for pressure drop of staggered banks agrees well with those of Briggs and Young [8], Jameson [23], Robinson and Briggs [50], and Stasiulevičius and Skrinška [62].

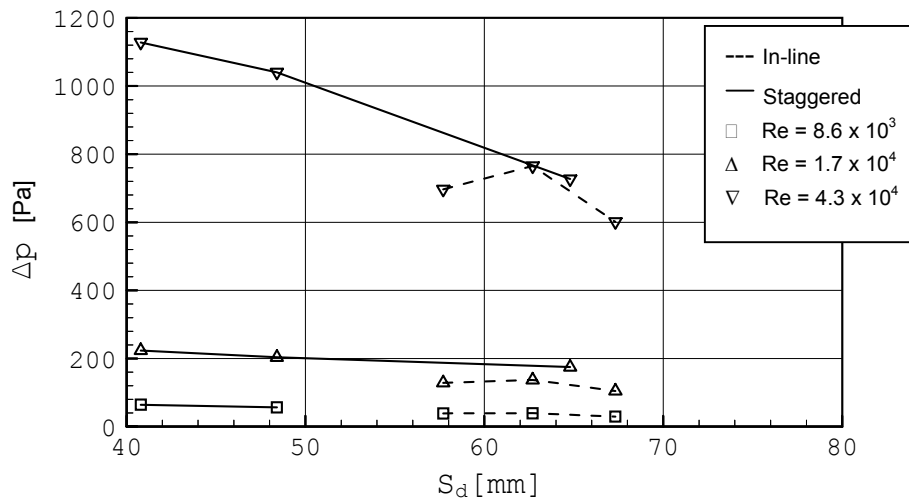


Figure 5.38 Effect of the tube spacing on the pressure drop for staggered and in-line bundles.

The pressure drop of the in-line bundles increases considerably when the transverse tube pitch is decreased. It is reasonable to expect that the smaller fin tip clearance provides the higher velocity. When increasing $S_d = 62.7$ mm (i9) to $S_d = 67.32$ mm (i8), the pressure drop is lower by about 23.7 % at $Re = 1.7 \times 10^4$. Note that the longitudinal pitch is fixed in the bundles (i8) and (i9). For the effect of longitudinal pitch, a comparison is prepared for bundle (i1) and (i9) where transverse tube pitch is fixed. When increasing $S_d = 57.5$ mm (i1) to $S_d = 62.7$ mm (i9) pressure drop is found to be higher by about 6.7 %. Therefore, it is observed that increasing the longitudinal pitch generated a larger pressure drop for a same transverse pitch. This trend is the same as the result reported by Sparrow and Samie [59]. This effect is not significant at low Re ; however, it is also noted at $Re = 4.3 \times 10^4$ with the increment of about 9.8%. This behaviour can be explained by an increase of turbulence intensity in the wake region for rising Re and by this means, a change of the pressure drop.

Figure 5.39 shows how the performance parameter related to the tube spacing changes for staggered and in-line tube bundles for various Reynolds numbers. It is seen that the performance parameter of both finned-tube bundles decreases with increasing the diagonal tube pitch. The larger diagonal tube pitch gives a lower pressure drop; even though, the volume flow rate is high. Thus, the performance is lower than for the smaller diagonal tube pitch.

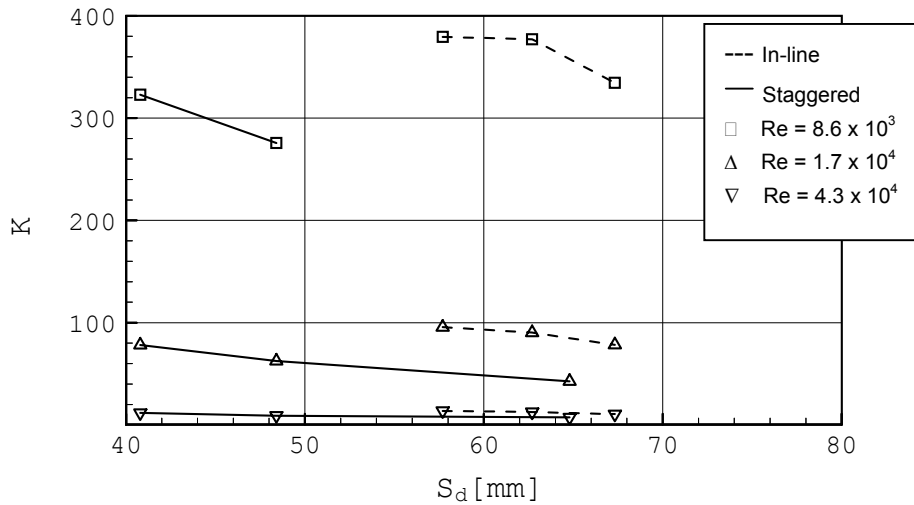


Figure 5.39 Performance parameter of tube spacing effect for staggered and in-line bundles.

5.3.6 Results of Row Effect

A heat exchanger design is often motivated by a desire to minimize the number of rows in a bundle. To determine how to limit the number of rows, the results from all numerical investigations were collected and analysed. In this section, it is subdivided into two parts in respect to the number of rows in the array. The first part deals with the row-to-row effect on heat transfer characteristics and apart from the individual row effects, the bundle depth effect on staggered and in-line tube bundles will be discussed in the second part.

Row-to Row Effects

Figure 5.40 includes results of row-to-row effect on the heat transfer rate and corresponds to the $Re = 4.3 \times 10^4$. It is seen from the figure that the heat transfer rate of all staggered tube bundles increases from the first to the second row and then, decreases in the following rows. A major cause of this decrease is that the air temperature becomes lower for the deeper rows and with it the driving temperature difference. Moreover, according to the staggered tube layout, the position of the second row is in the jet like stream see Figure 5.10 [59]. It is clearly recognised from the Figure 5.40 that the first row is higher than the third and the fourth rows since all numerical investigations were conducted under the forced draft condition. Further examination of Figure 5.40 shows that this trend is convincing until the sixth row of the bundle (s6).

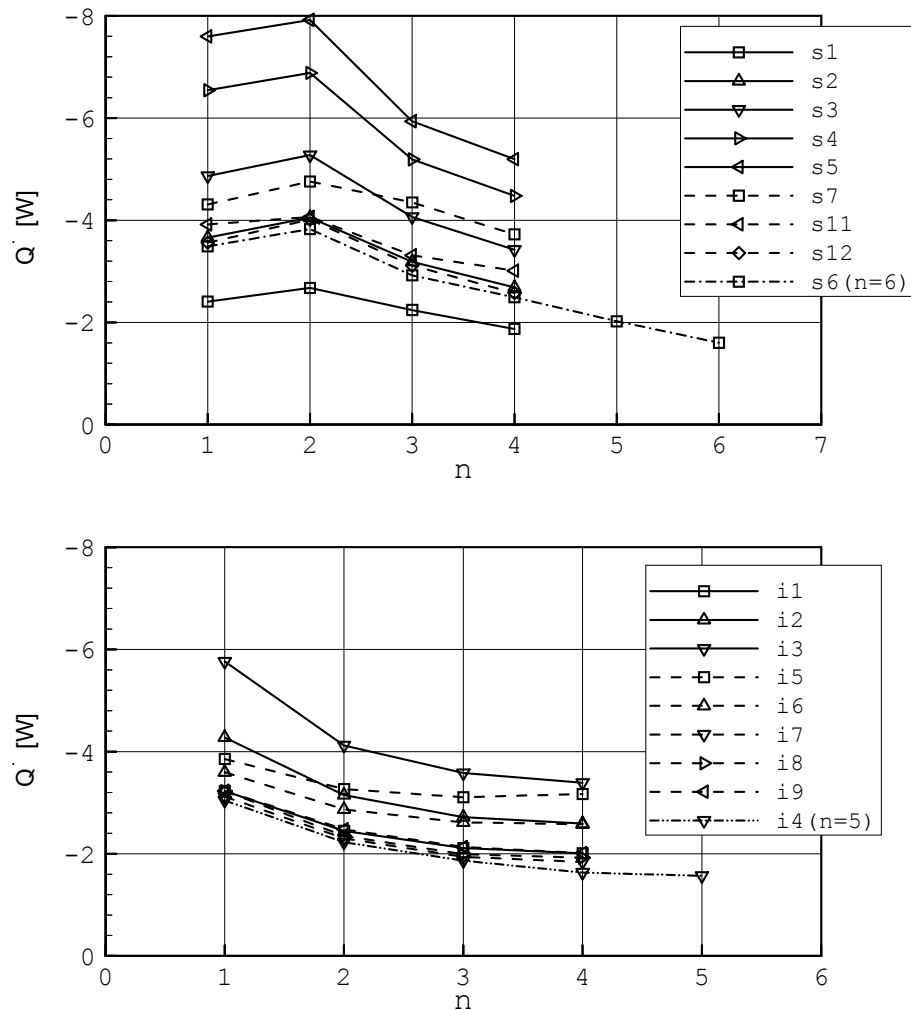


Figure 5.40 Row-to-row effect on the heat transfer rate for staggered (above) and in-line (below) bundles at $Re = 4.3 \times 10^4$.

The different trend of heat transfer rate is discovered for in-line tube bundles. The heat transfer rate of all in-line bundles decreases with the number of rows for all Reynolds numbers. The first row gives the highest rate due to the temperature difference between the air and fins. This temperature difference decreases since there is a bypass effect in the in-line tube bundles.

The fin efficiency results of $Re = 4.3 \times 10^4$ for both arrays are presented in Figure 5.41. For the staggered array, the efficiency ranges from 0.845 to 0.996. The trend of Figure 5.41 may be questionable in that the first row gives the highest efficiency; however, the temperature gradients in the fins of the first row are higher than of the other rows. The lowest fin efficiency is established at the second row and then it increases as the rows become deeper.

The fin efficiency of the in-line arrangement increases with the number of the rows and it decreases with the Reynolds number. The efficiency values displayed in Figure 5.41 are generally high, with the overall range from 0.908 to 0.99. This suggests that these small deviations from unity may be the result of using the high thermal conductivity aluminium fins.

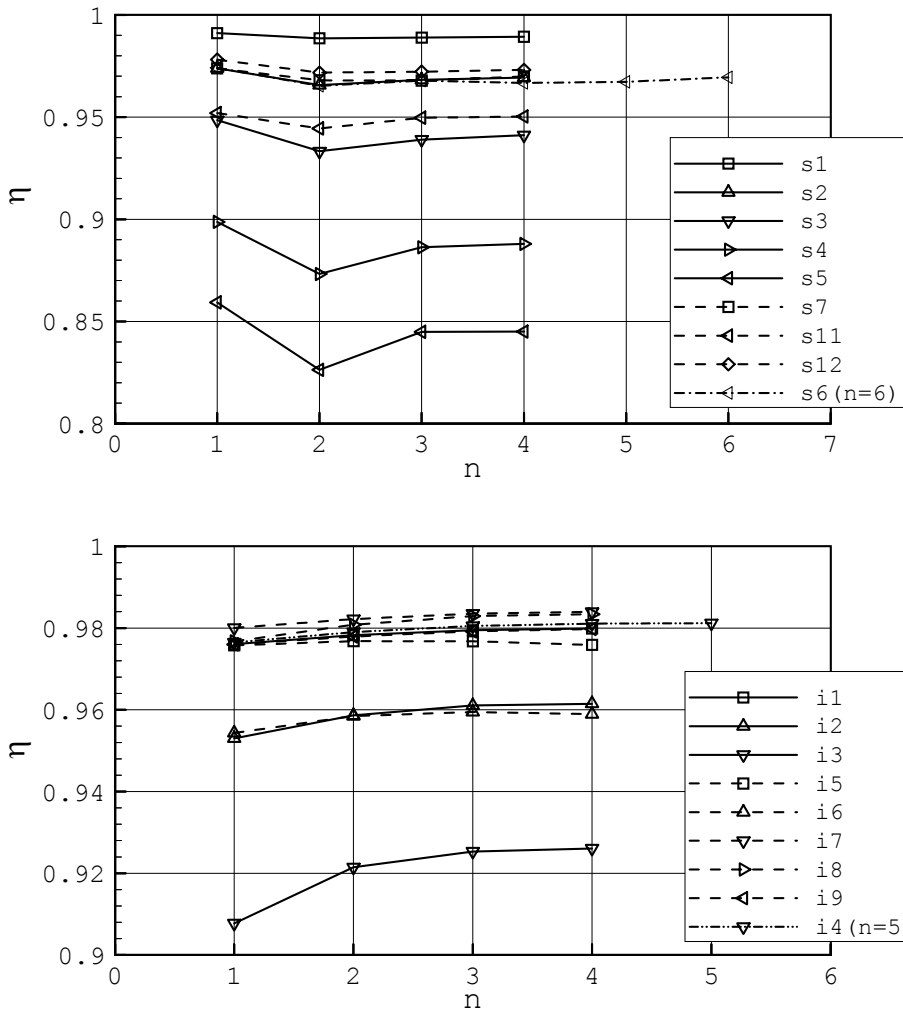


Figure 5.41 Row-to-row effect on the fin efficiency for staggered (above) and in-line (below) bundles at $Re = 4.3 \times 10^4$.

The variations of the heat transfer coefficient from row-to-row of the staggered bundles are presented in Figure 5.42. The heat transfer coefficient of the first row is the smallest value relative to the others and the maximum heat transfer coefficient occurs mainly at the second row. This is caused by the formation of the tubes in this arrangement. Since the efficiency of the fins is inversely proportional to the heat transfer coefficient, the heat transfer coefficient of the second row for staggered array is the highest. The heat transfer coefficient of second row is about 35.6 % and 46.5 %

higher than the first row for the bundle (s6) at $Re = 8.6 \times 10^3$ and 4.3×10^4 , respectively, while 23.2 % and 30.5 % for the bundle (s7). However, in the latter bundle where the fin spacing is increased to 4 mm, the third row heat transfer coefficient is slightly higher (about 0.6 %) than the second row at $Re = 4.3 \times 10^4$. This is because of the second horseshoe vortices that appeared in this case. When concerning on the number of rows, the fin spacing effect (bundle-s7) shows a different trend to other geometry changes.

A comparison with the data of Neal and Hitchcock [45] for the second and the sixth row shows, however, a different trend. The numerical result of the heat transfer coefficient of the sixth row is about 14.2 % lower than the second row at $Re = 4.3 \times 10^4$, $\frac{S_t}{d_f} = 1.2$ and $\frac{S_l}{d_f} = 1.04$. However, Neal and Hitchcock showed that the heat transfer coefficient of the sixth row is about 1 % higher than the second row of the equilateral triangular tube pitch. The Reynolds number used in their investigation was 1.25×10^5 and the transverse and longitudinal pitches to fin diameter ratios were 1.3 and 1.13. It is unclear which type of air drafting to the system was applied in their [45] experimental investigation. According to Gianolio and Cuti [14]'s comparison between the forced and induced draft data, yields different trends for both of them. In the induced draft, the heat transfer coefficient increases with the rows number. For the forced draft, the heat transfer coefficient is greatest at the second row and then, decreases gradually with the row numbers. The numerical simulation results have the same trend as the results in [14] since the current simulation was under the consideration of a forced draft.

The variations of the heat transfer coefficient with the number of rows of the in-line bundle are also depicted in Figure. 5.42. Contrasting to the staggered bundle results, the highest heat transfer coefficient occurs at the first row of every bundle. The heat transfer coefficient is typically very low in the wake region where the deep rows are found to lie. This result agrees with the work of Brauer [6], and Kuntysh and Stenin [37].

For the fin height increase bundles (i1, i2 and i3), the percentage decrease of the heat transfer coefficient of the first to second row is increased. The same behaviour for the tube spacing changes (i1, i8 and i9) is also observed in the figure. This behaviour is more noticeable on the transverse pitch than the longitudinal pitch. It can be explained that the increased transverse tube pitch gives more bypass flow between the tubes.

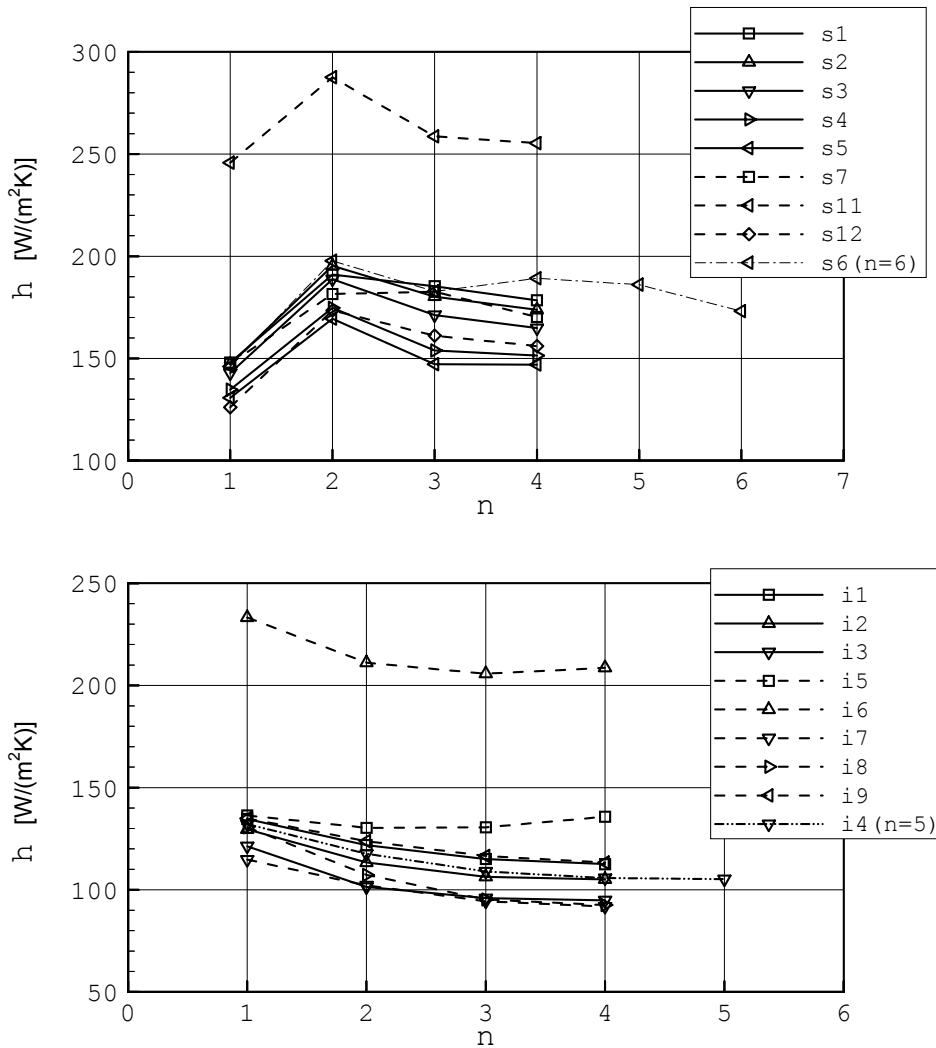


Figure 5.42 Row-to-row effect on the heat transfer coefficient for staggered (above) and in-line (below) bundles at $Re = 4.3 \times 10^4$.

Figure 5.42 shows the same trend of investigated results except for the widest fin spacing bundle (i5). For this bundle, the heat transfer coefficient at first row is 14 % and 4.4 % higher than that at the second row for $Re = 8.6 \times 10^3$ and 4.3×10^4 , respectively. For the narrowest fin spacing bundle (i4), the heat transfer coefficient at the first row is about 27 % and 11 % higher than at the second row, respectively. This is contrary to the published data of Sparrow and Samie [59]. They showed that the second row exceeds the first row by up to 35 %. This is likely a result of different means of determination of the tube wake region. The authors supposed that more turbulence effect was expected in the second row and their Re range is from 1.3×10^4 to 5.7×10^4 . However, the numerical results show that low velocity regions appear up and down stream of the second row and the temperature difference between fin surface and air is lower (see Figures 5.7 and 5.11). Therefore, it is quite feasible to say

that the heat transfer coefficient of the first row is higher than the deeper row for the in-line array.

It should be noted that the heat transfer coefficient becomes stable starting from the fourth row for the entire range of Reynolds numbers for both in-line and staggered tube arrangements. It is approved with the staggered tube results of Ward and Young [69] and the in-line tube results of Brauer [6].

Average Bundle Depth Effect

Row-to-row effects on heat transfer behaviour of staggered and in-line tube bundles have been described above and the average bundle depth effect on the heat transfer and pressure drop will be discussed from now on. As can be seen in Figure 5.43, the heat transfer rate increases with the number of rows when the bundle depth becomes deeper for both finned-tube bundles. Due to the fact that the temperature difference between the air and the surface temperature of the finned-tube bundle is decreased with heat transfer area.

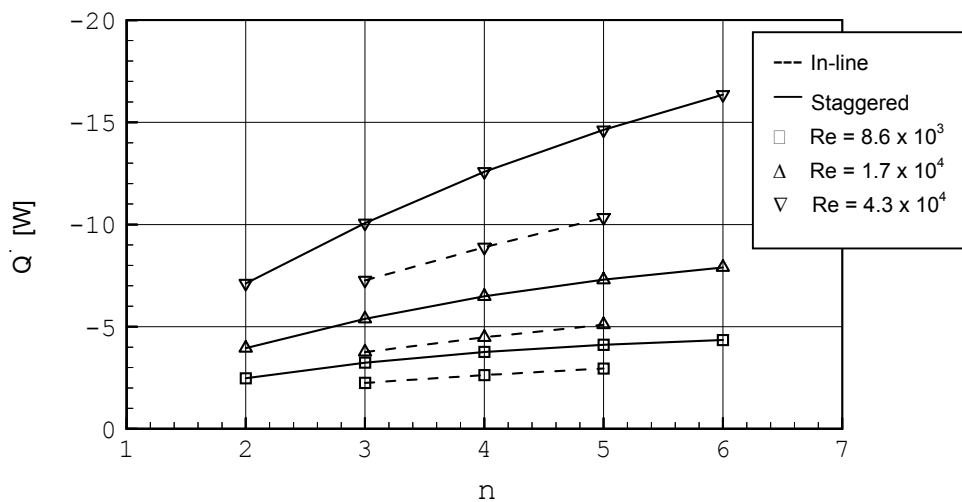


Figure 5.43 Effect of the number of rows effect on the heat transfer rate for staggered and in-line bundles.

Figure 5.44 shows the number of rows effect on the fin efficiency, which proves to be approximately constant when the bundle depth increases for both finned-tube arrangements. Therefore, it can be concluded that the rows number effect has no real significance on the fin efficiency.

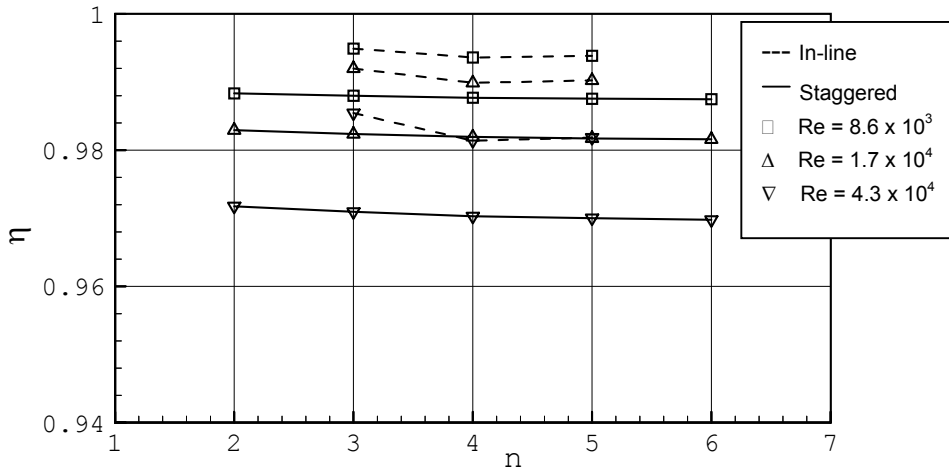


Figure 5.44 Effect of number of rows on the fin efficiency for staggered and in-line bundles.

Figure 5.45 shows that the heat transfer coefficient increases with bundle depth in the staggered array. For the staggered bundle, every row is affected by the mainstream. However, for the in-line bundles, the heat transfer coefficient increases at first and then, there is no further increase for deeper bundles. Consequently, the horseshoes vortex system occurs in every row and the local heat transfer coefficient is higher as the average heat transfer coefficient is increased. Increasing the staggered bundle depth from two-row to four-row yields the heat transfer coefficients to rise by about 6.5 %. However, the increment of the heat transfer coefficient is only about 1.1 % when the bundle depth is increased to five-row from four-row. Therefore, it can be indicated that the heat transfer coefficient becomes stable at the fourth row of the staggered tube bundle and the same conclusion is reached for the in-line tube banks.

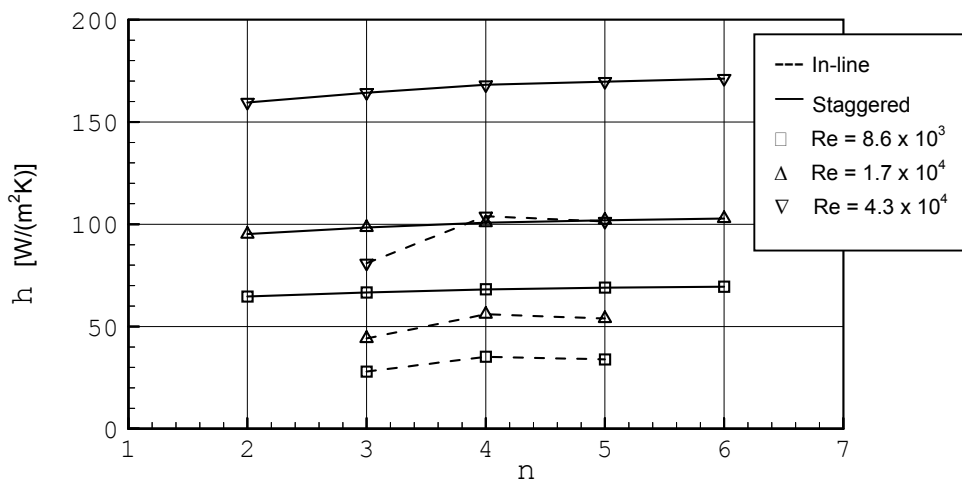


Figure 5.45 Effect of the number of rows on the heat transfer coefficient for staggered and in-line bundles.

Bundle depth effect on pressure drop for bundles s6 ($n = 2$) to s6 ($n = 6$) and i4 ($n = 3$) to i4 ($n = 5$) are shown in Figure 5.46. It is seen that the pressure drop increases linearly as the bundle depth becomes deeper for both staggered and in-line arrangements. In all cases, only the depth of bundle is varied while other geometric parameters were set constant. At low Re , the percentage of increment pressure drop is greater than the high Re . It can be seen that the in-line bank provides the lower pressure loss than the staggered bank for the same Reynolds number and geometry. This may indicate that the in-line tube bundles may offer a higher performance than the staggered banks.

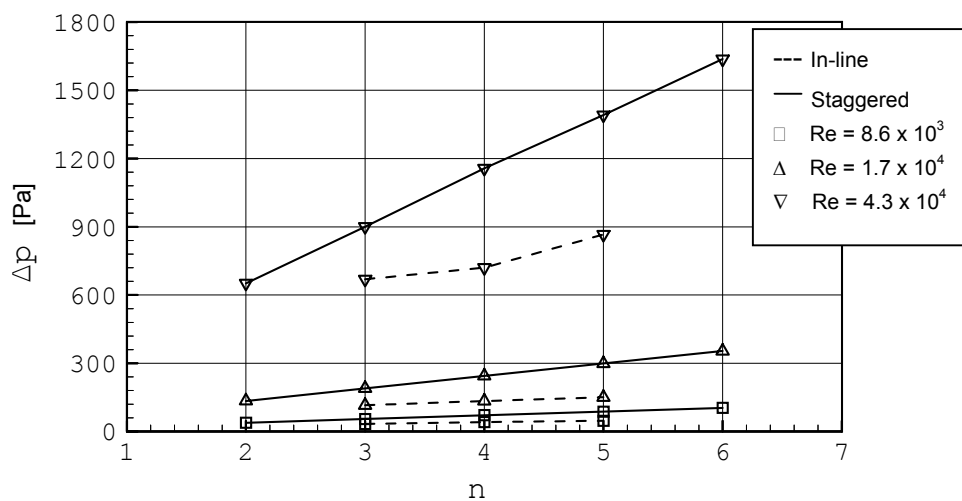


Figure 5.46 Effect of number of rows on the pressure drop for staggered and in-line bundles.

The performance parameter of the staggered array decreases with bundle depth at $Re = 8.6 \times 10^3$ and 1.7×10^4 as shown in Figure 5.47. As bundle depth increases, both the heat transfer rate and pressure drop increase. However, the pressure drop increase is stronger than the heat transfer rate gains. Therefore, a good performance is obtained at shallow bundle depth for above Reynolds numbers. However there are no significant changes for higher Reynolds number. For the in-line banks the bundle performance decreases with the bundle depth at $Re = 8.6 \times 10^3$. At $Re = 1.7 \times 10^4$ and 4.3×10^4 , the performance parameters are constant regardless of the bundle depth. Moreover, it can be seen from the figure that the performance parameters of staggered and in-line tube arrangements are nearly identical at the highest Reynolds number ($Re = 4.3 \times 10^4$). Therefore, the difference of the performance parameter between staggered and in-line tube arrangements becomes reduced when Reynolds number is increased.

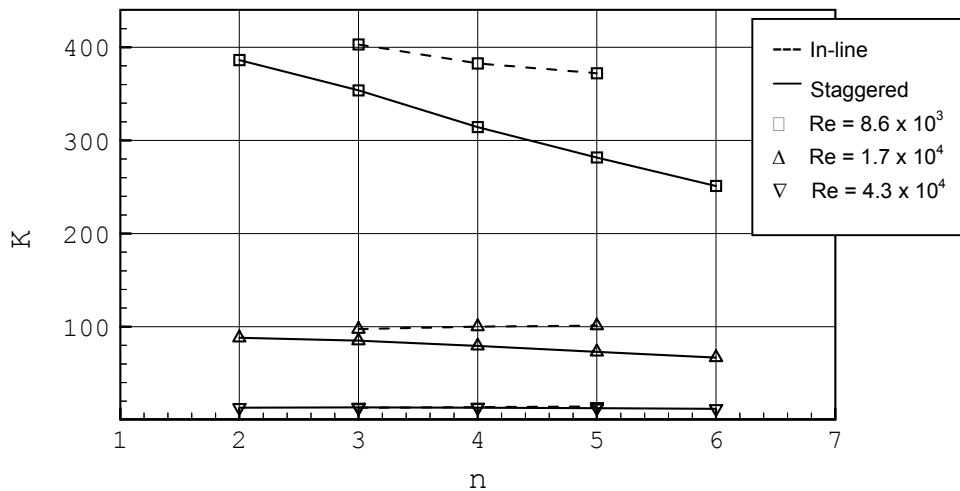


Figure 5.47 Performance parameter of the rows effect for staggered and in-line bundles.

5.3.7 Results of Tube Arrangement Effect

It was noted by a number of investigators in this field that the staggered tube layout has a better heat transfer performance. However, the importance for developing the effectiveness of a heat exchanger is required not to underestimate the pumping power. Moreover, the correct selection of the optimum size of a finned-tube bundle for a given and specific application depends on pumping power, weight and fabricating cost [62]. To demonstrate which tube layout is more advantageous, the bundle performances are calculated for both finned-tube arrays by Equation 5.15. The performance graphs for geometric parameters have already been presented in the aforementioned sections accordingly. The comparisons may not be clearly conclusive unless it is based on the thermal and power input. However, the current method is also widely used for comparing the performance of heating surfaces as it is convenient and it reflects both the thermal and hydraulic effects.

As described in the objective, this study was not only emphasized on the staggered tube arrangement, but a total of nine in-line tube banks were also concerned, since the available relevant literature is markedly limited to experiments on the staggered array. An analysis of the performance parameter figures shows obviously that the in-line tube array has a better performance than the staggered array at low Reynolds number. For this point, a quantity of explanations is revealed here for the typical geometry variations such as fin height, fin spacing and tube diameter corresponding to $Re = 8.6 \times 10^3$.

According to a comparison between the in-line and staggered arrays for a fin height of 5 mm, the heat transfer rate of staggered array (bundle s2) is about 41.7 % higher than those of the in-line array (bundle, i1). The same trend is obtained by Ackerman and Brunsvold [1], Hashizume [20], Kaminski [29], Neal and Hitchcock [45], Rabas and Huber [49], and Sparrow and Samie [59]. Remember that the bundle performance not only relies on the heat transfer rate but also on the pressure drop. Therefore, unless the staggered tube array had better results in the heat transfer rate, a great loss (66.5 %) of the pressure drop is found for a same Reynolds number. As stated earlier, the in-line tube array had advantages for low Re and the margin between the in-line and staggered arrays becomes narrower as the Re is increased and at $Re = 4.3 \times 10^4$, the performance of both bundles is approximately the same. Once the velocity is increased, the pressure drop increases stronger than the heat transfer rate for the in-line array and thus, the lower performance can be obtained.

A comparison of the staggered and in-line array based on the fin spacing shows that the heat transfer rate of the former is moderately higher. For example, the maximum enhancement (relative to the in-line array) is 43.2 % for the staggered array at $s = 1.6$ mm. However, a comparison of the two arrays reveals marked differences in terms of the pressure drop results by about 74.3 %. Further examination on the tube diameter effects show a similar trend as in the previous investigations. At $d = 13.59$ mm, the pressure drop of the staggered array is 60.2 % higher than the in-line while only 33 % higher for the heat transfer rate. Therefore, it is confirmed that at low Reynolds number only in-line tube configuration would be considered as the optimum surface for a given geometry since the pressure drop severely affected the heat transfer enhancement.

This result agrees well with the work of Ackerman and Brunsvold [1] and Kaminski [29] since similar performance criteria were applied in their investigations. Ackerman and Brunsvold [1] showed that the in-line tube arrangement provides the higher performance than the staggered arrangement for similar tube geometry. Moreover, it is found that the performance parameter attains maximum at low Re . However, this method gives no indication of the amount of surface required by any arrangement to transfer a given amount of heat [1].

Weierman [76] reported that the staggered array had a good performance although his comparison was based on four-row staggered and seven-row in-line bundles with the same pressure drop values. If compared to the same rows number,

i.e., four-row staggered to four-row in-line tubes, the result may be different. However, Kuntysh and Stenin [37] showed that the four row staggered array has a better efficiency than the four row in-line array for the same specific power required.

The relevant qualitative findings of these comparisons are:

- The performance parameter of the in-line geometry is higher when compared under the same condition applied for the staggered array.
- The staggered array clearly yields a higher heat transfer coefficient, while the pressure drop of the staggered array is generally higher than for the in-line arrangement.
- The difference of the heat transfer coefficient between the in-line and staggered arrangement is decreased in the aspect of Reynolds number and fin spacing are increased, and fin height and tube diameter are decreased.
- The difference is also decreased when the bundle depth of both tube arrays increases, except for the five-row in-line bundle.
- Generally, the pressure drop of the staggered banks is higher by a factor of 1.8 than the in-line banks at a low Reynolds number. This pressure drop increment is declined as Reynolds number increases.

The flow characteristics, the local effects on the heat transfer and pressure drop of the circular finned-tube heat exchangers and the results of geometry variables effects are already described above. Alternatively, the numerical simulation results made possible the analysis on the local and average aspects and provides for the more resourceful correlations on both the heat transfer and pressure drop characteristics. For this reason, correlating the numerical results to obtain better sense of correlations will be presented in the next chapter.

6 Correlations and Data Comparison

A set of correlations based on numerical investigation results and available experimental data is proposed in this chapter. Since different variables were applied in the reduction of the various experimental data, direct comparison to those correlations is more or less ambiguous. Even though, this chapter is also concerned with the comparison of the present numerical results with data in the previous literature and vice versa.

6.1 Heat Transfer Correlations

Using the power law correlations, most of the experimental results are correlated in non-dimensional form in a wide range of Reynolds numbers. The Nusselt number Nu , the Stanton number St , and Prandtl number Pr are typically used for the heat transfer while the Reynolds number Re is for the flow variables. On the other hand, the Euler number Eu and friction factor f is often used to express the correlated equation of pressure drop. For the bundle arrangement, existing experimental investigations for heat transfer coefficient and pressure drop are classified in Appendix D. Stasiulevičius and Skrinska [62] indicated that the available heat transfer correlations were based on how to determine the average convective heat transfer coefficient and ignored the state of non-uniformity in distributions of heat transfer over the fin surface. Beside being impracticable to establish a universal correlation, analyzing the numerical results and discussing with the previous data in the last chapters provide the fact that a correlation should embrace enough considerations such as all parameters of finning geometry, bundle configuration, and flow distribution in the bundle. To encounter these effects, additional terms are used to apply in a preliminary correlation for a single bundle that is based on the power law equation.

In order to achieve an acceptable correlation, the heat transfer correlations were based on own numerical results and the experimental data. Dimensions of experimental finned-tube heat exchangers are shown in Appendix C. However, the heat transfer

results that were obtained by the local thermal simulation method (only one test tube is heated) and segmented fin cases were omitted in these correlations. Moreover, cases with Reynolds number below 4×10^3 or above 7.5×10^4 are not considered. The results are reduced in non-dimensional form and average heat transfer correlations for both staggered and in-line arrangements were prepared.

6.1.1 Staggered Tube Arrangement

Bundles with only one row were not included in this investigation and two correlations for the staggered arrangement are therefore presented here depending on the number of rows. The concept of VDI-Wärmeatlas [68] was applied for this presentation taking the tube diameter and velocity at minimum free flow area as the reference quantities. The average heat transfer correlation for the staggered finned-tube bundles with $n \geq 4$ has the following form,

$$Nu = \underbrace{C Re^a Pr^{1/3} \left(\frac{A}{A_t} \right)^b}_{\text{VDI-Wärmeatlas[68]}} F^c \left(\frac{S_t}{S_d} \right)^d \quad (6.1)$$

Where A = Total heat transfer area, m^2

A_t = Outside surface area of tube except fins, m^2

S_t = Transverse tube spacing, m

S_d = Diagonal tube spacing, m

The exponents of Re and the ratio of total heat surface area to base tube area $\left(\frac{A}{A_t} \right)$ were set as in the VDI-Wärmeatlas [68] correlation, $a = 0.6$ and $b = -0.15$

respectively (see Appendix D.3). The extra terms, F and $\frac{S_t}{S_d}$ were added to the

correlation of VDI-Wärmeatlas. The term $\frac{S_t}{S_d}$ was added for a consideration of the

effect of non-equilateral triangular pitch arrangement which has been found in a very few cases, and F was supplemented for special consideration of the ratio of boundary layer thickness δ_b , and characteristic length expressed as the hydraulic diameter d_h of the finned-tub arrangement.

Following suggestions by Kays and London [30] and later by Nir [46] the hydraulic diameter may be expressed as

$$d_h = \frac{4d_f \cdot A_{ff}}{A'} \quad (6.2)$$

where A_{ff} = minimum free flow area of finned-tube per unit length, m²/m,

$$= S_t - d_f + (d_f - d)(1 - \delta N_f)$$

A' = Heat transfer area of unit length finned-tube, m²/m,

$$= \pi d \left(1 - \frac{\delta_f}{S_f} \right) + \frac{\pi}{S_f} \left(\frac{d_f^2 - d^2}{2} + d_f \delta \right)$$

By rearranging Equation (6.2) as $\frac{A'}{A_{ff}} = 4 \frac{d_f}{d_h}$, to following expression has been developed for optimum representation of the above mentioned boundary layer thickness effects:

$$F = \frac{1}{\frac{A'}{A_{ff}} + 1} \quad (6.3)$$

where $F = f_1 \left(\frac{d_f}{d_h} \right) = f_2 \left(\frac{\delta_b}{d_h} \right)$.

When increasing the diameter of fins, the boundary layer developed on the surface of fins becomes thicker and the factor F becomes smaller. Thus, decline of the heat transfer coefficient and increase of the pressure drop will result.

The correlations are prepared with the results from all numerical configurations (see Table 4.1) except for the bundles (s9) and (s10), which had undergone the test for the fin thickness effect along with bundle (s2). However, it is found that the Nu number difference between these tests is negligible and hence, only bundle (s2) was considered for this correlation. Finally, the air-side heat transfer correlation for the depth of four and more rows has been obtained as following by application of the least square method. For the staggered arrangement, the effect of factor F is of no real significance because the value of exponent is very small:

$$Nu = 0.284 Re^{0.6} Pr^{1/3} \left(\frac{A}{A_t} \right)^{-0.15} F^{-0.075} \left(\frac{S_t}{S_d} \right)^{1.06} \quad (6.4)$$

Equation 6.4 represents the results for four and more row bundles, and it is necessary to modify this expression for consideration of smaller bundles. In this case, the use of some row correction factor is a normal practice. For this

$$\frac{Nu_{n=2,3}}{Nu_{n=4}} = 1 - e^{-j(n-k)} \tag{6.5}$$

has been chosen, with the exponents j and k calculated according to the least squares method from the bundle (s6) yielding the final correlation for the staggered arrangement of two and three rows bundle is,

$$\frac{Nu_{n=2,3}}{Nu_{n=4}} = 1 - e^{-1.11(n+0.488)} \tag{6.6}$$

Reduced numerical finned-tubes heat transfer results are plotted as a function of Reynolds number in Figure 6.1 applying Equations 6.4 and 6.6 :

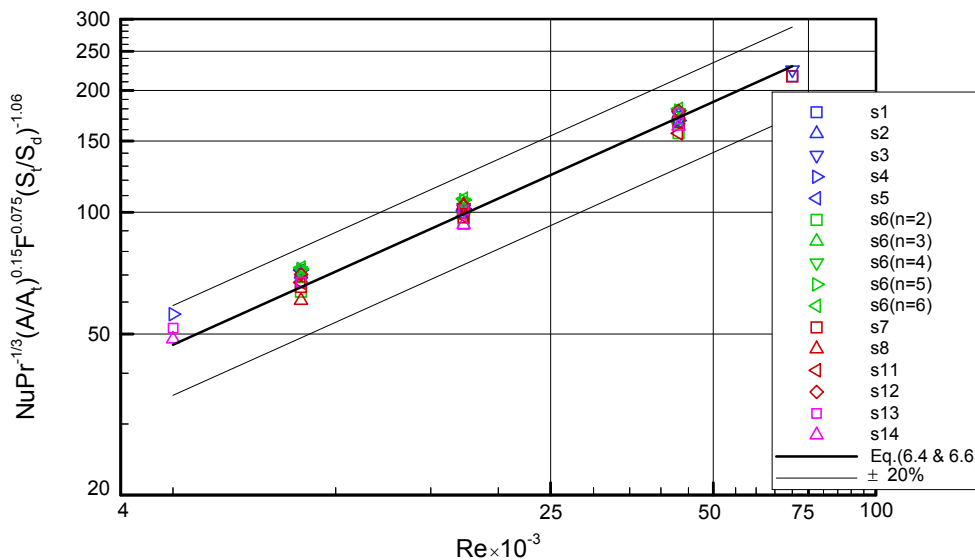


Figure 6.1 Comparison of the numerical results with Equations (6.4 and 6.6).

The deviations of the Nusselt number calculated from Equations (6.4) and (6.6) are described in Table 6.1. 100 % of all numerical results are correlated within ± 20 % and more than 80 % within ± 10 %.

Deviation (%)	$n \geq 4$ Equation (6.4)	$n < 4$ Eqs. (6.4)& (6.6)
$\pm 10\%$	88.37%	83.33%
$\pm 15\%$	97.67%	100%
$\pm 20\%$	100%	100%

Table 6.1 Deviations of heat transfer correlations for staggered arrangement.

6.1.2 In-line Tube Arrangement

As described in the literature review, only a few heat transfer data for the in-line arrangement was found since the staggered tube arrangement gives a higher heat transfer rate. Among them, Brauer [6] particularly studied the in-line arrangements and he provided a large number of performance data on heat transfer and pressure drop. Due to the omission of the fin efficiency effect in his study, too high heat transfer coefficients resulted. Moreover, his investigation was reflected only for the tube area, rather than the total surface area. Hence, in the present study, Brauer's data were reduced to the total surface area in consideration of fin efficiency effects for the improved in-line heat transfer correlation. At this point, the heat transfer correlation for the in-line array is also based on both numerical and experimental results with the following form,

$$Nu = C Re^a Pr^{1/3} \left(\frac{A}{A_t} \right)^b F^c \left(\frac{S_t}{S_l} \right)^d \quad (6.7)$$

For the values of the exponents, the same considerations are given and evaluated as in the staggered arrangement. There is no numerical investigation for less than four row bundles, thus, the final correlation equation for number $n \geq 4$ rows is as follows,

$$Nu = 0.356 Re^{0.6} Pr^{1/3} \left(\frac{A}{A_t} \right)^{-0.15} F^{0.173} \left(\frac{S_t}{S_l} \right)^{-0.475} \quad (6.8)$$

From above equation, it is noted that the effect of factor F is of considerable influence on the in-line array. The numerical results are graphically compared with the above equation in Figure 6.2 and the deviations for the bundle depth $n \geq 4$ are shown in Table 6.2. From here a stronger scattering of the results can be found.

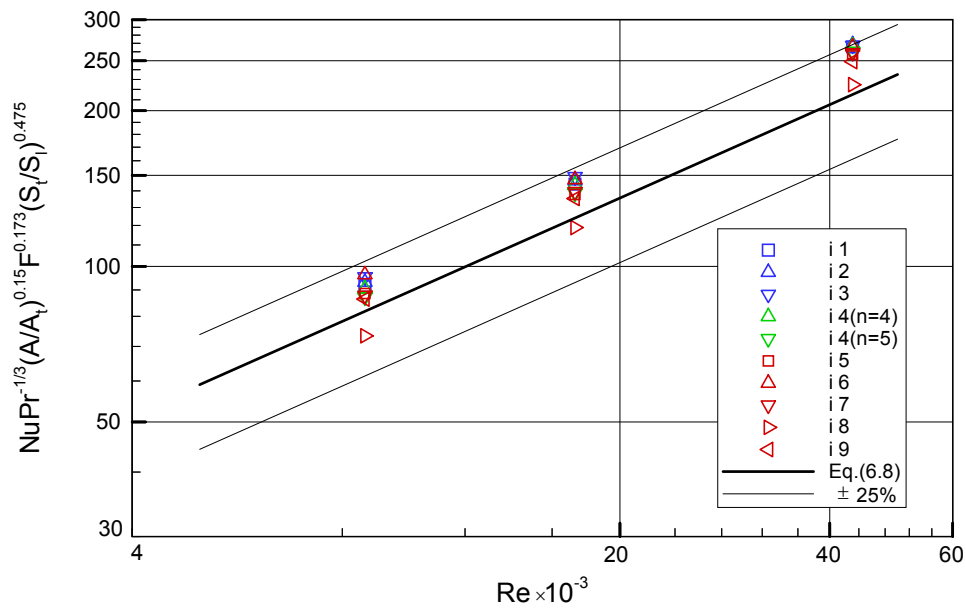


Figure 6.2 Comparison of the numerical results with Equation. (6.8).

Deviation (%)	$n \geq 4$ Eq. (6.8)
$\pm 10\%$	23.33%
$\pm 15\%$	46.67%
$\pm 20\%$	73.33%
$\pm 25\%$	100%

Table 6.2 Deviations of heat transfer correlations for in-line arrangement.

6.2 Pressure Drop Correlations

Although the pumping power is an important determining factor to improve the heat exchanger design, relatively less efforts were performed on this subject. The correlations of the pressure drop for finned-tube banks in both arrays are complicated owing to the geometry factors and the loss of static pressure. The developing procedure for an enhanced pressure drop correlation is the same as correlating the heat transfer results. In the present pressure drop correlations, both isothermal and non-isothermal pressure drop data were encountered. Both numerical results and existing experimental data, shown in Appendix C were correlated by the following expression:

For staggered banks with $n \geq 2$,

$$Eu = C Re^a \left(\frac{A}{A_t} \right)^b F^c \left(\frac{S_t}{S_d} \right)^d .n \quad (6.9)$$

The coefficient C and all exponents were calculated by means of the least squares method. The statistical analysis of the factors incorporated in the relationship point out that the roll of ratio of total heat transfer surface area to based tube surface area, $\frac{A}{A_t}$, was not significant ($b = 0.006$). Therefore, the correlation equation obtained for the staggered array is the following,

$$Eu = 0.75 Re^{-0.24} F^{-0.49} \left(\frac{S_t}{S_d} \right)^{0.64} .n \quad (6.10)$$

It is seen from the above equation that the factor F is substantially affects the pressure drop of staggered finned-tubes. The pressure drop results are presented in dimensionless terms via Eu number defined by Equation (6.10). The numerical results are plotted as a function of Reynolds number in Figure 6.3. The deviation of the Eu number calculated from Equation (6.10) and the simulated results from FLUENT is shown in Table 6.3.

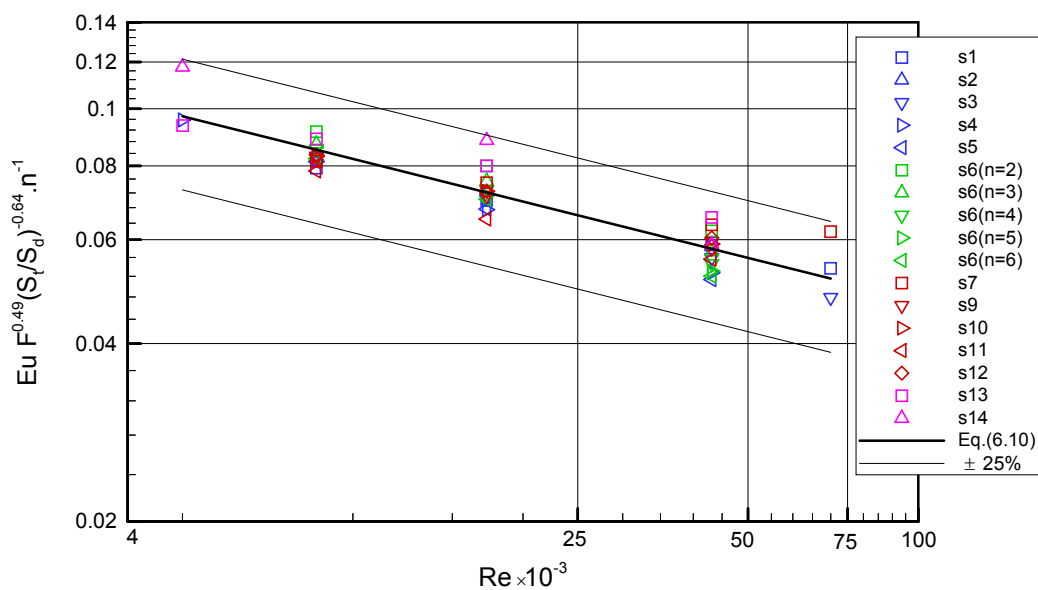


Figure 6.3 Comparison of the numerical results with Equation (6.10).

For an in-line arrangement, the term $\frac{A}{A_t}$ was included in the following equation,

$$Eu = 0.536 Re^{-0.23} \left(\frac{A}{A_t}\right)^{0.068} F^{-0.343} \left(\frac{S_t}{S_d}\right)^{-2.18} .n \tag{6.11}$$

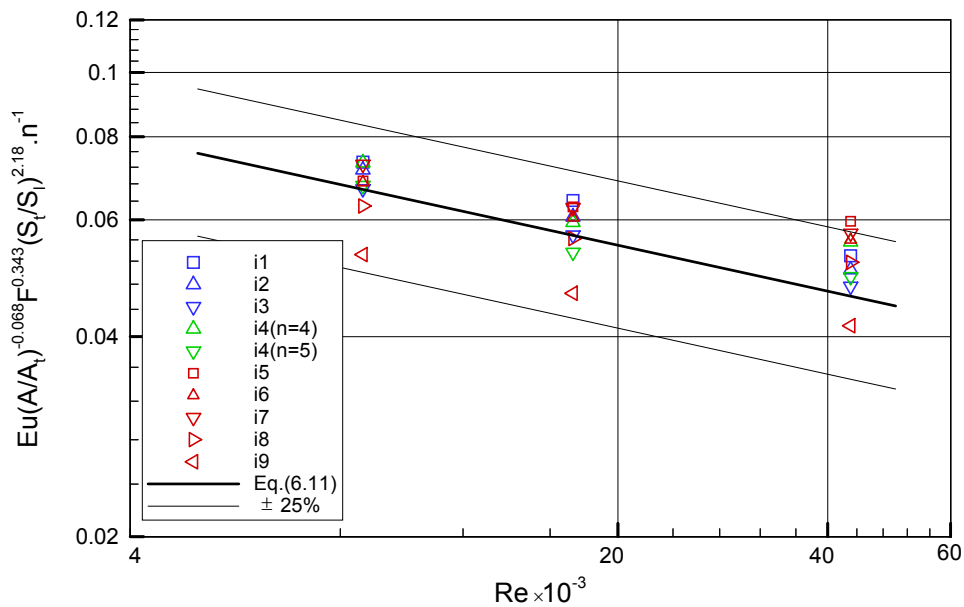


Figure 6.4 Comparison of the numerical results with Equation (6.11).

From above equation, it can be concluded that the effect of factor F is substantial on pressure drop of both tube arrays. A comparison between the numerical results and the correlation is illustrated in Figure 6.4 and the extent of the accuracy of the Equation (6.11) is shown in Table 6.3.

Deviation (%)	$n \geq 2$ Equation (6.10)	$n \geq 2$ Equation (6.11)
± 10%	85.45%	63.33%
± 15%	94.55%	76.67%
± 20%	94.55%	83.33%
±25%	100%	96.67%
±30%	100%	100%

Table 6.3 Deviations of pressure drop correlations for staggered and in-line tube arrangements.

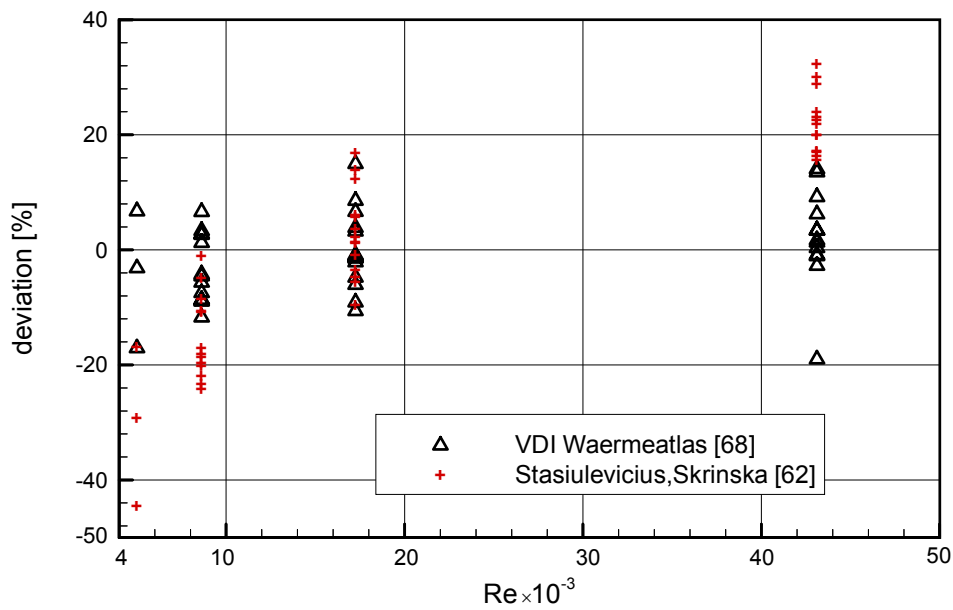
6.3 Data Comparison

The developments for the enhancement of heat transfer and pressure drop predictions of circular finned-tube banks have already been described in the literature review. Moreover, related correlations and their limitations are discussed in section 2.2.3. Most of the experimental investigations were completed for the optimisation of the finning geometry while a few attentions on the tube spacing effect and the bundle arrangement. Since the tabulated experimental data covering wide ranges of geometric variables and Reynolds numbers are not available for the analysis, it was necessary to read from respective figures regardless of the factual error. Moreover, as noted in the section 2.1 that no exact information was found in the published literature for the numerical simulation of circular finned-tube arrays. Therefore, comparisons can be made only between the present numerical results and the experimental ones. The results and comparisons are presented by the relative deviations and plotted as a function of Reynolds number.

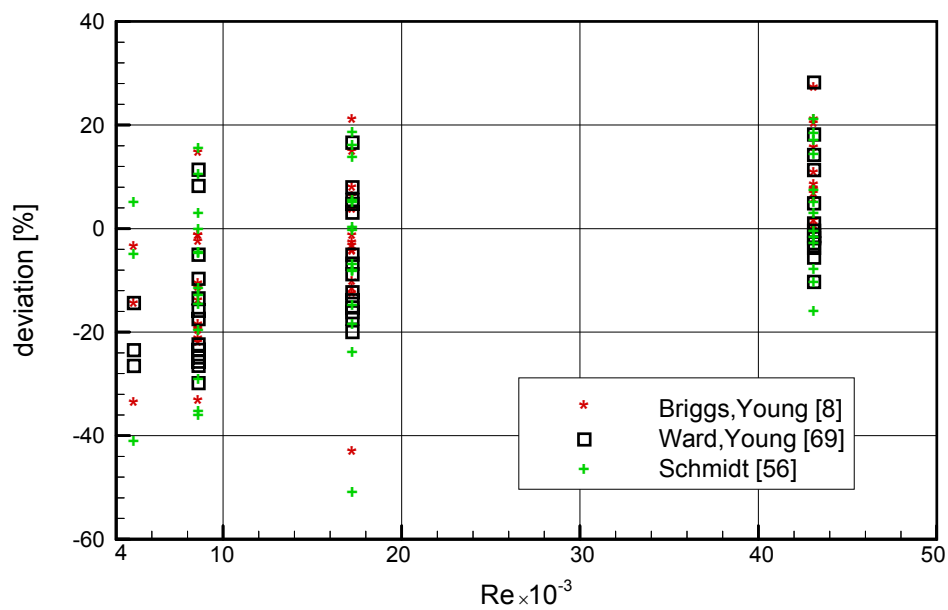
6.3.1 Comparison of Heat Transfer Results for Staggered Arrangement

Comparison of the numerical results with the correlations from the literature is shown in Figure 6.5 as the relative deviation. It is seen that a number of Nu numbers calculated by the correlations are greater than numerically calculated Nu numbers, even though some are found to be smaller. Generally, at low Re range, the numerical results are higher than the experimental data. At this point, it is appropriate to note that present numerical simulations were under the consideration of the turbulent modeling.

Figure 6.5(a) shows that the Stasiulevičius and Skrinška [62] equation yields smaller Nu numbers than the numerical results at $Re < 10^4$ since their correlation was based on higher Reynolds number in the range from 2×10^4 to 2×10^5 . On the other hand, at $Re = 4.3 \times 10^4$, Briggs and Young [8] and [62] predictions are about 28.7% and 26 % higher than the present results of bundle (s7) which is the largest fin spacing case ($s = 4$ mm). Their predictions are questionable that the boundary layer becomes thinner at high Re and therefore, the fin spacing effect may not be the decisive factor on heat transfer. For the bundles (s11) and (s14), numerical results are found to be lower than the results of [62]. It is reasonable to accept that the bundle (s11) having the smallest tube diameter (13.59 mm), which is outside of the applicable range of their tested geometries. However, for the latter bundle, it is expected that the heat transfer



(a)



(b)

Figure 6.5 Comparison of the numerical results with experiment based correlations,

$$\frac{Nu_{corr} - Nu_{nume}}{Nu_{corr}} \times 100\%.$$

performance of the larger tube spacing (for the case of bundle s14 with a largest transverse tube pitch computed) has a lower rate. They used a local modeling method, which overestimated the heat transfer coefficient that obtained from the total modeling by 11 % [37]. Moreover, Nir [46] reported that this method might lead to errors of more than 20 %. Comparison of the numerical results and VDI-Wärmeatlas correlation [68]

produces the best results in the total Reynolds number range with the maximum deviation of + 15 % and – 20 %. With regards to the Figure 6.5(b), the numerical result of Briggs and Young [8] deviates up to – 45 % partly due to the lack of the tube arrangement effect in their development.

At $Re = 1.7 \times 10^4$, Briggs and Young [8], and Schmidt [56] predictions for bundle (s8) registered about 45 % that is lower than numerical results. Nonetheless, the present results for the bundle (s8) is well accorded with those of Stasiulevičius and Skrinska [62], VDI-Wärmeatlas [68], and Ward and Young [69]. When comparing with the [69] equation, the deviation lies between + 29 % to – 30 %. However, no reference was termed in the [69] correlation to compensate for the fin pitch effect.

The relative deviations of heat transfer data obtained from experimental investigations and Equation (6.4) are shown in Figure 6.6. It is seen that all data of Briggs and Young [8], Kyuntysh et al. [34] and Stasiulevičius and Skrinska [62] are lie between ± 20 %. Most of Mirkovic [43]'s data are also within ± 20 %; however, data of the bundle with the largest tube diameter are deviated up to – 60 %.

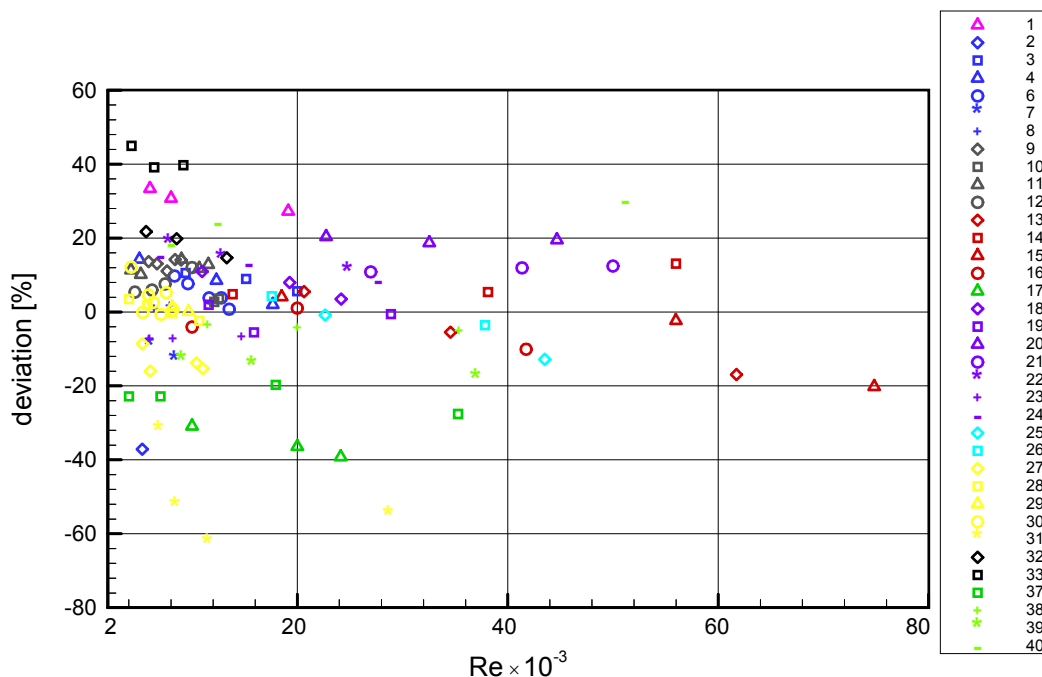


Figure 6.6 Comparison of the experimental data with Equation (6.4),

$$\frac{Nu_{Eq.6.4} - Nu_{exp}}{Nu_{Eq.6.4}} \times 100\% .$$

(1 – Kuntysch and Stenin [37], 2 to 8 – Ward and Young [69], 9 to 12 – Briggs and Young [8], 13 to 16 – Stasiulevičius and Skrinska [62], 17 – Hashizume [20], 18 to 24 – Kuntysch et al. [34], 25 to 26 – Yudin et al. [62], 27 to 31 – Mirkovic [43], 32 to 33 – Rabas et al. [47], 37 – Weierman [76], 38 to 40 – Brauer [6])

In Figure 6.7, the experimental data are compared with the VDI-Wärmeatlas correlation [68] in the similar manner as Figure 6.6. From Figure 6.7, it is seen that VDI-Wärmeatlas equation predicts well for the data of Briggs and Young, and Kyuntysh et al. with a deviation of + 20 %. It differs up to – 50 % for Stasiulevičius and Skrinska' data. However, all finned- tube bundles of Stasiulevičius and Skrinska are based on non-equilateral triangular pitch. Thus, it is reasonable to accept the above result since there is no correction term for non-equilateral triangular pitch in VDI-Wärmeatlas equation. Most of the Mirkovic data are deviated – 35 % except for the largest tube diameter bundle. For this bundle, VDI- Wärmeatlas equation prediction is the same as above Equation (6.4).

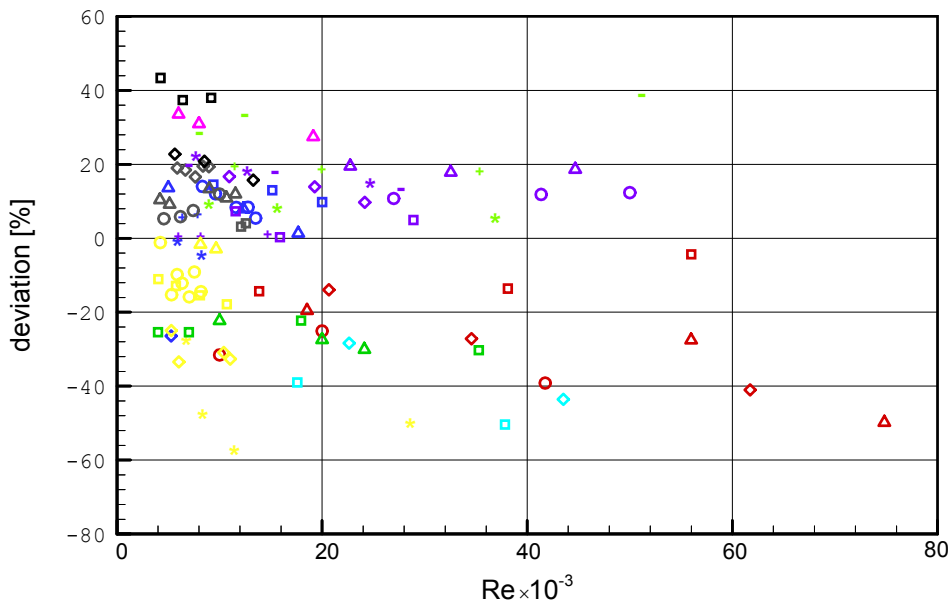


Figure 6.7 Comparison of the experimental data with VDI-Wärmeatlas equation,

$$\frac{Nu_{VDI} - Nu_{exp}}{Nu_{VDI}} \times 100\% .$$

(The legends shown in the Figure 6.7 are the same as Figure 6.6)

Figure 6.8 proved that Equation (6.4) is more accurate than the VDI-Wärmeatlas equation. If 80 % of experimental data are considered, the maximum deviation of Equation (6.4) is found to be $\pm 20\%$ and $\pm 30\%$ for the VDI-Wärmeatlas equation. In fact, if 90 % of the experimental data is taken into account for both cases, the maximum difference does not exceed $\pm 30.9\%$ for Equation (6.4), while the maximum deviation from the VDI-Wärmeatlas is equal to $\pm 38\%$.

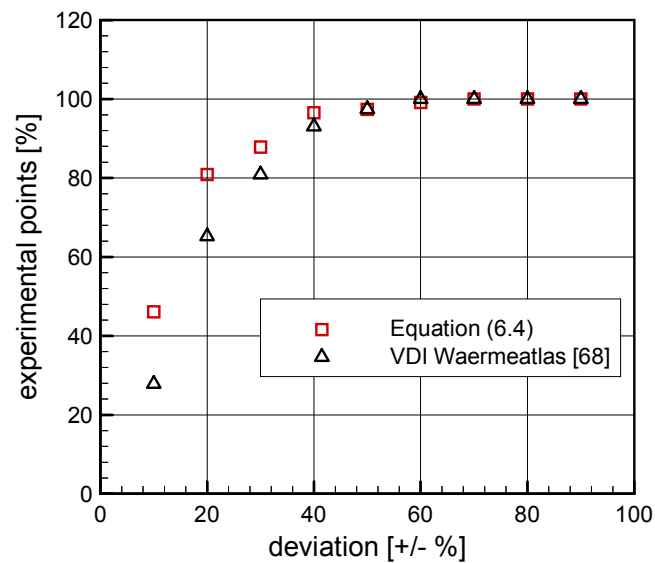


Figure 6.8 Comparison of Equation (6.4) and VDI correlation based on experimental data.

6.3.2 Comparison of Heat Transfer Results for In-line Arrangement

Figure 6.2 showed that the numerical results are slightly higher than the proposed correlation for the whole Reynolds range. This may be due to the fact that the incomplete set of Brauer's data [6] were reduced and encountered in this study, as a result of very few results for the in-line array were available. When comparing with others, Brauer's data proved to be relatively too small after being reduced. The comparison of the present correlation Equation (6.8) with the numerical and available experimental results is shown in Figure 6.9. It is noted that the Equation (6.8) only predicts about 20 % higher than the results of Brauer. Equation (6.8) is in good agreement with the data of Weierman [75] by within + 12 %. Most of data of Carnavos [48] lie within ± 30 %. If 90 % of points (numerical and experimental data points) are considered, the maximum deviation of Equation (6.8) is within 25 %.

The comparison of VDI-Wärmeatlas with the data described in the literature and the present numerical results are shown in Figures 6.10. The Figure 6.10 illustrates that the VDI-Wärmeatlas prediction is about 30 % higher than the Brauer, and Rabas and Huber [49] data, about 20 % higher than Kuntysch and Stenin [37], and about 25 % higher than Weierman [76]. Numerical results are in good agreement with VDI - Wärmeatlas equation in the low Reynolds region, $Re < 2 \times 10^4$; however, having an over prediction at high Reynolds number, $Re > 4 \times 10^4$. Due to the turbulent flow, the turbulence intensity becomes higher in the high Reynolds number range and enables a higher Nu number value.

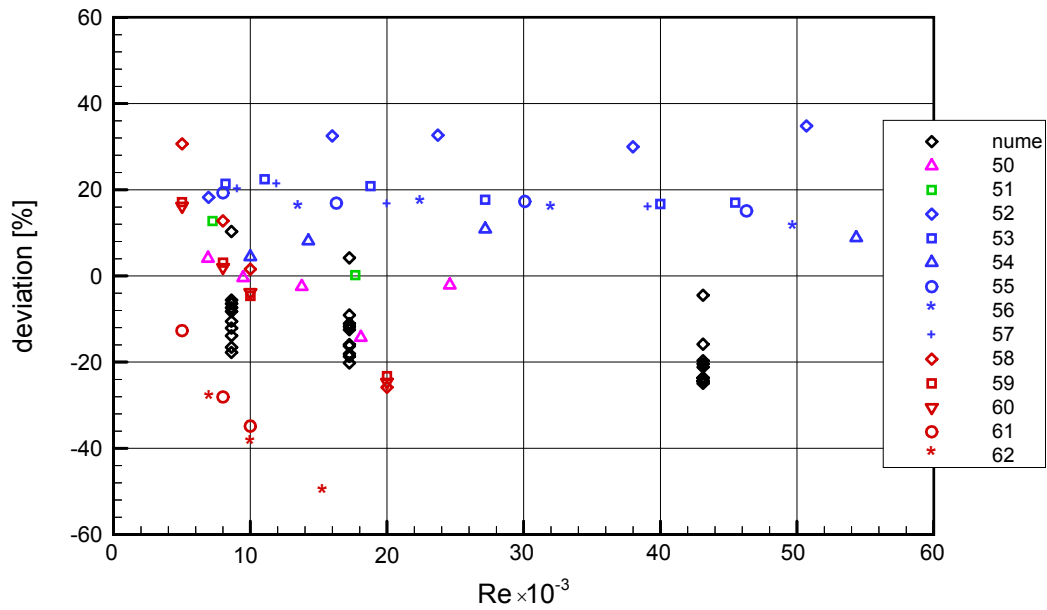


Figure 6.9 Comparison of numerical and experimental results with Equation (6.8),

$$\frac{Nu_{Eq.6.8} - Nu_{nume,exp}}{Nu_{Eq.6.8}} \times 100\%$$

(50 – Kuntysh, Stenin [37], 51 – Weierman [76], 52 to 57 – Brauer [6], 58 to 61 – Carnavos [49], 62 – Huber [49])

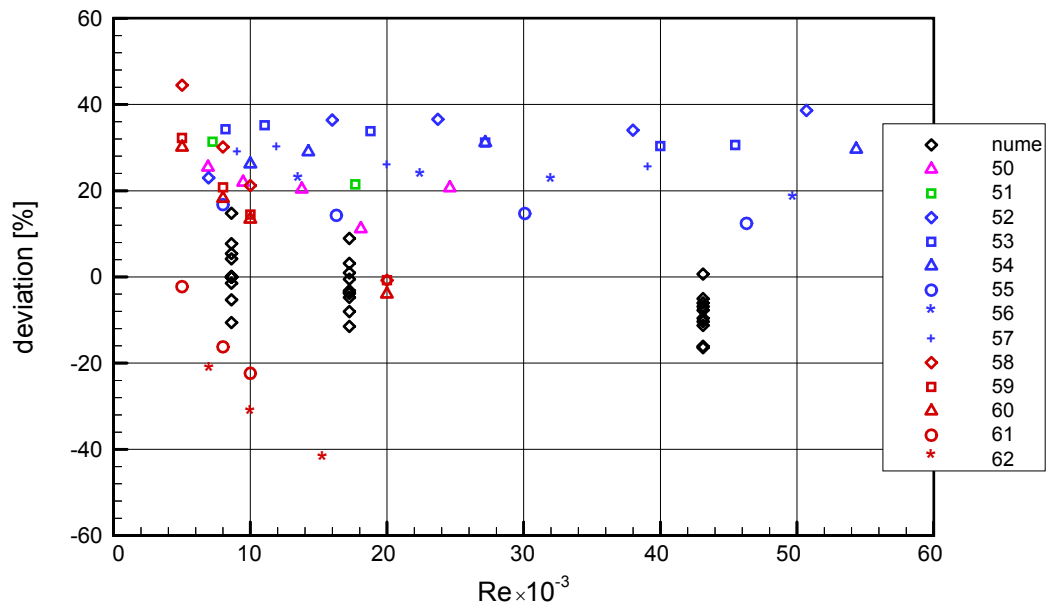


Figure 6.10 Comparison of numerical and experimental results with VDI equation,

$$\frac{Nu_{VDI} - Nu_{nume,exp}}{Nu_{VDI}} \times 100\%$$

6.3.3 Comparison of Pressure Drop Results

A few correlations were available despite some researchers conducted the tests for the pressure drop effect and unfortunately no correlations were developed. Therefore limited comparisons and discussions between these data and related correlations are reported here.

The numerically calculated Euler numbers compared with available experimental equations are shown in Figure 6.11(a). At $Re > 4 \times 10^4$, the numerical results are in good agreement with the Stasiulevičius and Skrinska [62] prediction, and in the low Re range, $Re < 10^4$, most of the numerical results deviated from the [62] equation by $\pm 20\%$. The Reynolds range for their work was $10^4 < Re < 10^5$ and the effects of the tube arrangement and fin geometry variables except for the fin thickness were reflected in their correlation.

When comparing Robinson and Briggs [50], and the numerical results, it is found that there is somewhat different at $Re < 2 \times 10^4$, due to the absence of the fin geometry variables such as fin height, fin thickness and fin spacing in their equation. It is noted that their correlation was very limited as $\frac{s}{h}$ varies only from 0.15 to 0.19. In the high Reynolds range, Robinson and Briggs equation is quite consistent with the numerical results and this trend continues beyond their tested Reynolds range. Their investigated Re range was $2 \times 10^3 < Re < 4 \times 10^4$ and it is seen that at high Reynolds number, the fin geometry variables effects are small. Further analysis of the Figure 6.11(a) provides that at $Re = 5000$, the prediction of pressure drop of Ward and Young [69] is up to 50% higher. For the rest of the Re range, most of the numerical results are satisfied within +30% to –20% with the [69] result.

Due to the different Reynolds definitions, a separate comparison was prepared for numerical results with Haaf [19] correlation in Figure 6.11(b). In Haaf equation (see appendix D), the average velocity in the bundle and the equivalent diameter were used as the reference dimensions in the Reynolds number. It is seen that the numerical results agree well with the Haaf correlation and most of numerical results are between $\pm 30\%$. It is observed from this figure that the maximum deviation from Haaf equation is the smallest fin height bundle (s1) at high Reynolds number.

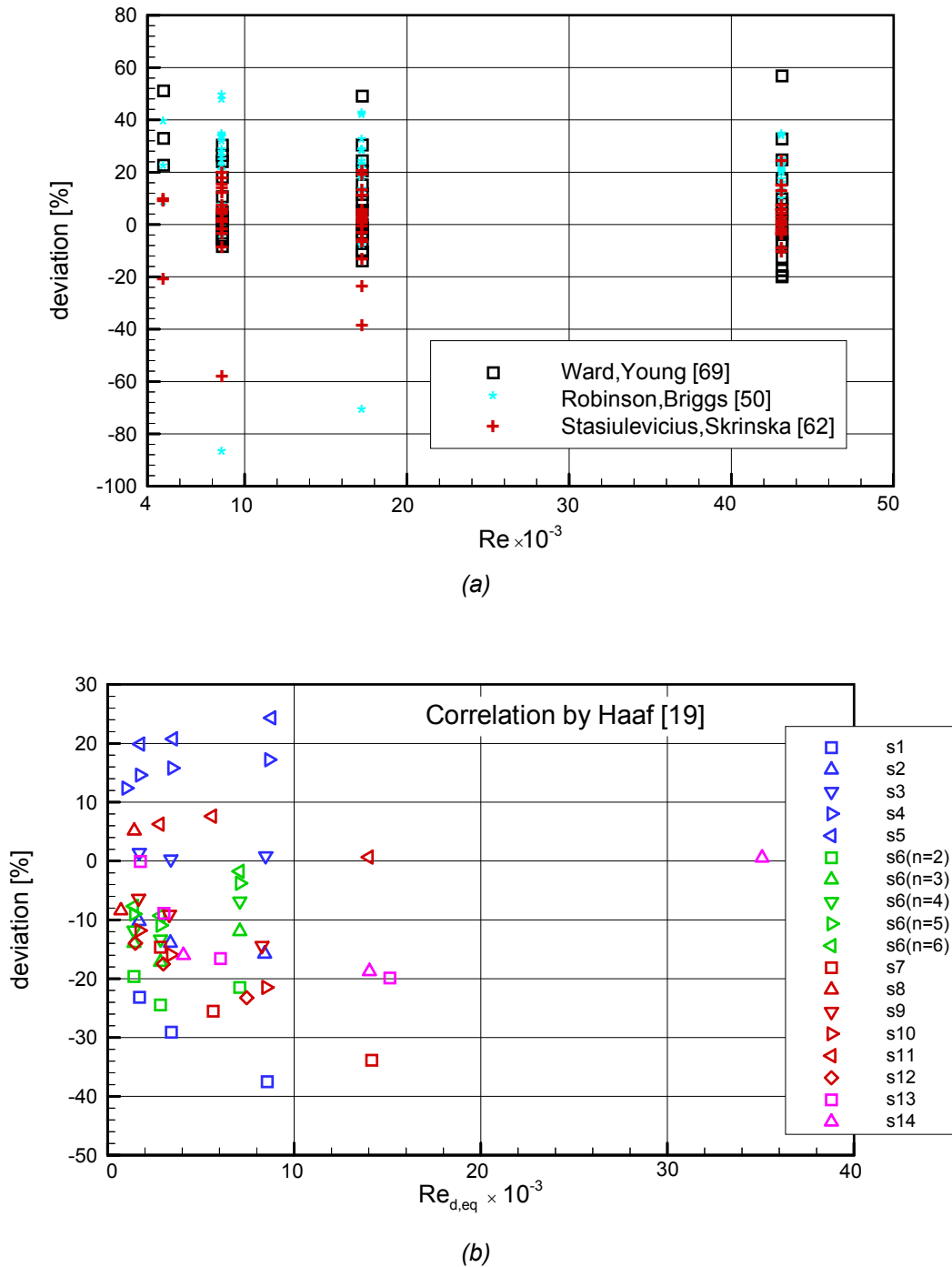


Figure 6.11 Comparison of the numerical results with experimental correlations,

$$\frac{Eu_{corr} - Eu_{nume}}{Eu_{corr}} \times 100\%.$$

For the in-line tube arrangement, a comparison of the experimental data with Equation (6.11) is also shown Figure 6.12. According to the Figure 6.12, most of data of Brauer [6] and Kyuntysh and Stenin data are within $\pm 20\%$ while Weierman [76] data are deviated up to -40% . It is appropriate to mention that Weierman's data are based on the segmental fins. For the entire range of the experimental data, Equation (6.11)

varied only between + 20 % and – 40 %. If 90 % of numerical and experimental points are considered, the maximum deviation was found to be within ± 26 %.

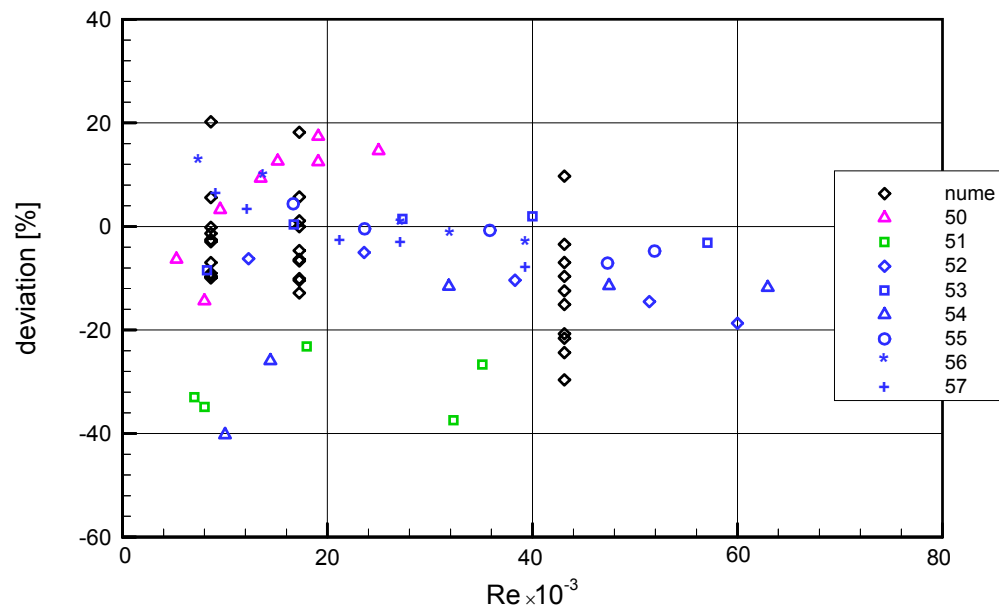


Figure 6.12 Comparison of numerical and experimental results with Equation (6.11),

$$\frac{Eu_{Eq.6.11} - Eu_{nume,exp}}{Eu_{Eq.6.11}} \times 100\% .$$

(50 – Kuntysh, Stenin [37], 51 – Weierman [76], 52 to 57 – Brauer [6])

7 Conclusions

The heat transfer and pressure drop performance on the air-side of circular finned-tube heat exchangers had been determined numerically. Using the present numerical investigation and published experimental data, improved heat transfer and pressure drop correlations (i.e., Equations 6.4, 6.6, 6.8, 6.10 and 6.11) for the air-cooled heat exchangers have been finally developed.

This study has been performed with 29 bundles having different finning geometries. 18 bundles containing tubes are placed on equilateral triangular arrangements and the rest also placed on in-line arrangement.

The present study has also concerned for the local flow and heat transfer characteristics and the influence of air flow distribution within the bundles. The numerical flow visualization results for the boundary layer developments and horseshoe vortex system between the fins, and local velocity and temperature distributions in the bundles are presented. The boundary layer developments and horseshoe vortices between the adjacent fins and tube surface of staggered tube arrangement are found to be strongly dependent on fin spacing and Reynolds number. The horseshoe vortices develop in all staggered rows; however, only for the first row in the in-line tube array. There may develop a horseshoe vortex system at the second row of in-line arrangement and subsequent rows, if the longitudinal pitch is long enough. However, within the tested geometric parameters range, no horseshoe vortex appeared upstream of deeper rows and instead of it, a reverse flow due to the wake of the preceding row is observed. Therefore, improved heat transfer coefficient is observed for the staggered arrangement.

The horseshoe vortex effect is more obvious in the largest fin spacing and at the high velocity. The flow visualization results suggest the extent of a new horseshoe vortex system for the deeper rows of the wider fin spacing of the staggered tube bundle (s7) at $Re = 4.3 \times 10^4$.

Temperature boundary layer developments between the fins are presented according to the different fin spacings. The temperature gradient decreases at the fin base and tube surface when two boundary layers are growing to touch each other. This will lead to a decreased convection heat transfer coefficient. The highest temperature gradient is revealed along the radial direction at ($\theta = 0^\circ$) for the first row of the both tube arrays. One interesting finding is that the temperature distributions over the fin surface and within the fins are rather identical.

The velocity distributions near the fin surface plane and on the mid-plane between the fins are quite different for the staggered array. The velocity on the mid-plane of both tube arrays is stronger than near the fin surface plane. The velocity results of the in-line array show that a strong bypass stream between the tubes is in accordance with fin tip-to-tip clearance. It is approved by the temperature distribution figures that a high temperature stream passes through the in-line bundle without mixing well.

The temperature distributions within the bundle significantly vary from the first to the third row. The temperature on the mid-plane is higher than near the fin surface plane. The fin tip temperature at the upstream fin surface is found to be higher due to the thin boundary layer.

Geometric parameters have been noted regardless of the situation in which either is favourably or adversely influenced on the heat transfer coefficient and the pressure drop for both tube arrays at different Reynolds numbers. Respective results were also presented for the fin efficiency and the heat transfer rate. The relevant qualitative findings on the finning geometry of this study are:

- Numerical results on the fin height effect for both tube arrays agrees well with the experimental data in that increasing the fin height provides decreased heat transfer coefficient and increased pressure drop of the circular finned-tube bundle.
- Since the fin spacing effect is depending principally on the boundary layer corresponding with the velocity of air, the influence of the fin spacing on the heat transfer coefficient is not significant when boundary layers between the fins are departing from each other for the staggered array. For the in-line array, the higher rate of heat transfer is observed at the wider spacing.

- Circular fins of rectangular profile with uniform cross section area are applied for the fin thickness effect. Changes of the fin thickness are remarkably insensitive to the heat transfer coefficient and pressure drop of the staggered tube bank. Therefore, the effect of fin thickness is proved to be insignificant.
- The tube outside diameter effect has more influence on the in-line array. The heat transfer coefficient and pressure drop for both arrays are inversely proportional to the tube diameter at a same Reynolds number when S_t/d_f is constant. The effect of tube diameter on the performance of different tube configurations is quite insensitive to the large Reynolds numbers.
- The heat transfer coefficient and pressure drop are decreased as the tube spacing increases for both tube arrangements. The effect of the transverse tube pitch has more influence on the in-line tube arrangement than those for the staggered tube arrangement. For the same transverse pitch, increasing the longitudinal pitch of the in-line array provides an increased pressure drop and no significant effect on the heat transfer coefficient.
- The maximum heat transfer coefficient occurs in the second row for the staggered arrangement and at the first row for the in-line arrangement, respectively. For both staggered and in-line arrangements, the heat transfer coefficient becomes stable downstream the fourth tube row and the pressure drop increases linearly as the bundle depth becomes deeper.
- The staggered array clearly yields a higher heat transfer coefficient, while the pressure drop of the staggered array is generally higher than that of the in-line arrangement. Attempts were made to validate which tube configuration is more constructive. The in-line array has a better performance than the staggered arrangement at low Reynolds number. Hopefully this study will leave further discussion in that direction.

The heat transfer correlations are presented in Equations (6.4) and (6.8) for the staggered and in-line bundles with $n \geq 4$ respectively. For the staggered array, 98% of the numerical results deviate by $\pm 15\%$ while $\pm 25\%$ for the in-line array. For the heat exchangers having $n < 4$, the Nu number can be calculated according to Equations (6.4) and (6.6). The numerical results corresponded with the established correlation

with $\pm 15\%$. The heat transfer correlations obtained by the numerical investigation are improved in comparison with VDI-Wärmeatlas [68]. The pressure drop correlations are presented in Equations (6.10) and (6.11), respectively. The numerical results deviate $\pm 15\%$ for the staggered tube array and the maximum deviation of the in-line tube array is $\pm 30\%$.

Attention was devoted to the convective heat transfer from the fins and tubes to the dry air and hence, further numerical research for the improvement of the circular finned-tube heat exchanger design with humid air is required. Finally, the hope may be expressed that the present correlations will contribute to calculate the heat transfer and pressure drop for circular finned-tube heat exchangers at $5.0 \times 10^3 \leq Re \leq 7.0 \times 10^4$.

REFERENCES

1. Ackerman, J. W., and Brunsvold, A. R., "Heat Transfer and Draft Loss Performance of Extended Surface Tube Banks," *ASME Journal of Heat Transfer*, Vol.92, pp.215-220, 1970.
2. Antuf'ev, V. M., and Gusev, E. K., "Intensification of Heat Transfer of Cross-Flow Finned Surfaces," *Teploenergetika*, Vol. 15, No. 7, pp. 31-34, 1968.
3. Baker, C.J., "The Laminar Horseshoe Vortex," *Journal of Fluid Mechanics*, Vol.95, pp.347-367, 1979.
4. Bastani, A., Fiebig, M., and Mitra, N. K., "Numerical Simulation of Flow Field in a Fin Tube Heat Exchanger," *ASME Journal of Fluid Engineering*, Vol. 101, pp. 91-96, 1990.
5. Brauer, H., "Wärme- und strömungstechnische Untersuchungen an quer angeströmten Rippenrohrbündeln, Teil1; Versuchsanlagen und Meßergebnisse bei höheren Drucken," *Chem.-Ing. Technik*, Vol. 33, No. 5, pp. 327-335, 1961.
6. Brauer, H., "Wärme- und strömungstechnische Untersuchungen an quer angeströmten Rippenrohrbündeln, Teil2; Einfluß der Rippen- und der Rohranordnung," *Chem.-Ing. Technik*, Vol. 33, No.6, pp. 431-438, 1961.
7. Brauer, H., "Compact Heat Exchangers," *Chemical Progress Engineering*, London. Vol. 45, No. 8, pp. 451-460, 1964.
8. Briggs, D. E., and Young, E. H., "Convection Heat Transfer and Pressure Drop of Air Flowing Across Triangular Pitch Banks of Finned Tubes," *Chemical Engineering Progress Symposium Series*, No. 41, Vol. 59, pp. 1-10, 1963.
9. Faghri, M., and Rao, N., "Numerical Computation of Flow and Heat Transfer in Finned and Unfinned Tube Banks," *International Journal of Heat Mass Transfer*, Vol. 30, No. 2, pp. 363-372, 1987.

10. Fiebig, M., Gorsche-Georgemann, A., Chen, Y., and Mitra, N. K., "Conjugate Heat Transfer of a Finned Tube Part A: Heat Transfer Behaviour and Occurrence of Heat Transfer Reversal," *Numerical Heat transfer, Part A*, Vol. 28, pp.133-146, 1995.
11. FLUENT Incorporated, *FLUENT 5 User's Guide*, Fluent Incorporated Lebanon, NH-USA, 1998.
12. Gambit Modeling, *User's Manual*, Fluent Incorporated Lebanon, NH-USA, 1998.
13. Gardner, K. A., "Efficiency of Extended Surface," *ASME Transactions*, Vol. 67, No. 8, pp. 621-631, 1945.
14. Gianolio, E., and Cuti, F., "Heat Transfer Coefficients and Pressure Drops for Air Coolers Under Induced and Forced Draft," *Heat Transfer Engineering*, Vol. 3, No. 1, pp. 38-48, 1981.
15. Glück, B., *Zustands- und Stoffwerte Wasser Dampf Luft- Verbrennungsrechnung*, Berlin : VEB Verlag für Bauwesen, 1986 (Bausteine der Heizungstechnik - Berechnung- software)
16. Goldstein, R. J., and Karni, J., "The Effect of a Wall Boundary Layer on Local Mass Transfer from a Cylinder in Cross Flow," *ASME Journal of Heat Transfer*, Vol. 106, pp. 260-270, 1984.
17. Goldstein, R. J., Karni, J., and Zhu, Y., "Effect of Boundary Conditions on Mass Transfer near the Base of a Cylinder in Cross Flow," *ASME Journal of Heat Transfer*, Vol. 112, pp. 501-504, 1990.
18. Gunter, A. Y., and Shaw, W. A., "A General Correlation of Friction Factors for Various Types of Surfaces in Cross Flow," *ASME Transactions*, Vol. 67, pp. 643-660, 1945.
19. Haaf, S., *Wärmeübertragung in Luftkühlern*, Handbuch der Kältechnik, Bd. 6, Teil B: *Wärmeaustauscher*, Berlin u.a. : Springer Verlag, pp. 435-491, 1988.
20. Hashizume, K., "Heat Transfer and Pressure Drop of Finned Tubes in Cross Flow," *Heat Transfer Engineering*, Vol. 3, No.2, pp. 15-20, 1981.

21. Hu, X., and Jacobi, A.M., "Local Heat Transfer Behaviour and its Impact on a Single-Row Annularly Finned Tube Heat Exchanger," *ASME Journal of Heat transfer*, Vol. 115, pp. 66-74, 1993.
22. Jacobi, A. M., and Shah, R. K., "Air-Side Flow and Heat Transfer in Compact Heat Exchangers: A discussion of Enhancement Mechanisms," *Heat Transfer Engineering*, Vol.19, no.4, pp.29-41, 1998.
23. Jameson, S. L., "Tube Spacing in Finned Tube Banks," *ASME Transactions*, Vol. 67, pp. 633-642, 1945.
24. Jang, J. Y., Wu, M. C., and Chang, W. J., "Numerical and Experimental Studies of Three Dimensional Plate-Fin and Tube Heat Exchangers," *International Journal of Heat Mass Transfer*, Vol. 39, No. 14, pp.3057-3066, 1996.
25. Jang, J. Y., Lei, J. T., and Liu, L. C., "The Thermal-Hydraulic Characteristics of Staggered Circular Finned-Tube Heat Exchangers under Dry and Dehumidifying Conditions," *International journal of Heat and Mass Transfer*, Vol.41, pp.3321-3337, 1998.
26. Jaw, S. Y., and Chen, C. J., *Present Status of $k-\varepsilon$ Turbulence Models and their Achievements*, Flow Modeling and Turbulence Measurements VI, Chen, Shih, Lienau & Kung (eds), Balkema Rotterdam. ISBN 90 5410 826 6,1996.
27. Jones, T. V., and Russell, C. M. B., "Heat Transfer Distribution on Annular Fins," *ASME Transactions*, No.78-HT-30, 1978.
28. Kaminski, S., and Groß, U., "Luftseitiger Wärmeübergang und Druckverlust in Lamellenrohr-wärmeübertragen," *KI Lust- und Kältetechnik*, Vol.1, pp.13-18, 2000.
29. Kaminski, S., "Numerische Simulation der luftseitigen Strömungs- und Wärmetransportvorgänge in Lamellenrohr-Wärmeübertragen," *Freiberger Forschungshefte, A 867 Energie*, 2002.
30. Kays, W. M., and London, A. L., *Compact Heat Exchangers*, McGraw-Hill, New York, 1998.
31. Kearney, S. P., "Local and Average Heat Transfer and Pressure Drop Characteristics of Annularly Finned Tube Heat Exchangers," M. S. thesis, University of Illinois at Urbana-Champaign, Urbana, IL, 1995.

32. Kearney, S. P., and Jacobi, A. M., "Local Convective Behavior and Fin Efficiency in Shallow Banks of Inline and Staggered, Annularly Finned Tubes," *ASME Journal of Heat Transfer*, Vol. 118, pp.317-326, 1996.
33. Konstantinidis, E., Castiglia, D., and Balabani, S., "On the Flow and Vortex Shedding Characteristics of an Inline Tube Bundle in Steady and Pulsating Crossflow," *Transactions of IchemE*, Vol.78, Part A, pp.1129-1138, 2000.
34. Kuntysh, V. B., Taryan, I. G., and Yokhvedov, F. M., "On the Effect of the Relative Depth of the Interfin Space on Heat Transfer from Bundles of Finned Tubes," *Heat Transfer- Soviet Research*, Vol. 6, No. 6, pp. 5-9, 1974.
35. Kuntysh, V. B., Piir, A. E., Kolobova, L. F., Mirmov, N. I., and Fedotova, L. M., "Correlation Equation for Aerodynamic Resistance of Tube Bundles in Air-Cooled Heat Exchangers," *Chemistry and Technology of fuels and Oils*, Vol.15, Nr.5-6, pp.341-344, 1979.
36. Kuntysh, V. B., Piir, A. E., Fedotova, L. M., Tal' ving, T. A., and Varma, K. A., "Characteristics of Tube Bundles for Air-Cooled Exchangers," *Chemistry and Technology of fuels and Oils*, Vol.16, Nr.5-6, pp.312-315, 1980.
37. Kuntysh, V. B., and Stenin, N. N., "Heat Transfer and Pressure Drop in Cross Flow Through Mixed Inline-Staggered Finned Tube Bundles," *Thermal Engineering*, Vol. 40, No. 2, pp. 126-129, 1993.
38. Lapin, A., and Schurig, W. I., "Heat Transfer Coefficients of Finned Exchangers," *Ind. Eng. Chem.*, Vol. 51, No. 8, pp. 941-944, 1959.
39. Launder, B. E., and Massey, T.H., " The Numerical Prediction of Viscous Flow and Heat Transfer in Tube Banks," *ASME Journal of Heat Transfer*, Vol.3, pp.565-571, 1978.
40. Lee, J. W. H., and Chen, G. Q., " A Numerical Study of Turbulent Line Puffs via the Renormalization Group (RNG) $k-\varepsilon$ Model," *International Journal for Numerical Methods in Fluids*, Vol. 26, pp.217-234, 1998.
41. Legkiy, V. M., Pavlenko, V. P., Makarov, A. S., and Zheludov, Y. S., "Investigation of Local Heat Transfer in a Tube with Annular Fins in Transverse Air-Flow," *Heat Transfer- Soviet Research*, Vol. 6, No. 6, pp.101-107, 1974.
42. Lymer, A., "Finned Tubes and their Performance Characteristics," *Nuclear Engineering*, Vol. 2, pp. 504-509, 1957.

43. Mirkovic, Z., *Heat Transfer and Flow Resistance Correlation for Helically Finned and Staggered Tube Banks in Cross Flow*, Heat Exchangers: Design and Theory Source Book, (edited by N. H. Afgan and E. U. Schlünder), Hemisphere, Washington, D. C, pp. 559-584, 1974.
44. Mitra, N. K., Bastani, A., and Fiebig, M., "Numerical Simulation of 3D Periodically Fully Developed Flow Between Fins of a Compact Fin-Tube Heat Exchanger," *Advances in Heat Exchanger Design, Radiation, and Combustion, ASME HTD - Vol. 182*, pp. 37-41, 1991.
45. Neal, S. B H. C., and Hitchcock, J. A., "A Study of the Heat Transfer Process in Banks of Finned Tube in Cross Flow, Using a Large Scale Model Technique," *Proceeding of the Third International Heat Transfer Conference*, Vol. 3, Chicago, IL, pp. 290-298, 1966.
46. Nir, A., "Heat Transfer and Friction Factor Correlations for Cross Flow Over Staggered Finned Tube Banks," *Heat Transfer Engineering*, Vol. 12, No. 1, pp. 43-58, 1991.
47. Rabas, T. J., Eckels, P. W., and Sabatino, R. A., "The Effect of Fin Density on the Heat Transfer and Pressure Drop Performance of Low-Finned Tube Banks," *Chemical Engineering Communications*, Vol. 10, No.1-3, pp. 127-147, 1981.
48. Rabas, T. J., and Taborek, J., "Survey of Turbulent Forced-Convection Heat Transfer and Pressure Drop Characteristics of Low-Finned Tube Banks in Cross Flow," *Heat Transfer Engineering*, Vol. 8, No. 2, pp. 49-62, 1987.
49. Rabas, T. J., and Huber, F. V., "Row Number Effects on the Heat Transfer Performance of Inline Finned Tube Banks," *Heat Transfer Engineering*, Vol. 10, No. 4, pp. 19-29, 1989.
50. Robinson, K. K., and Briggs, D. E., "Pressure Drop of Air Flowing Across Triangular Pitch Banks of Finned Tubes," *Chemical Engineering Progress Symposium Series*, No. 64, Vol. 62, pp. 177-184, 1965.
51. Romero-Méndez, R., Sen, M., Yang, K. T., and McClain, R., "Effect of Fin Spacing on Convection in a Plate Fin and Tube Heat Exchanger," *International Journal of Heat and Mass Transfer*, Vol. 43, pp.39-51, 2000.

52. Saboya, F. E. M., and Sparrow, E. M., "Local and Average Transfer Coefficients for One-Row Plate Fin and Tube Heat Exchanger Configuration," *ASME Journal of Heat Transfer*, Series C, Vol. 96, No.3, pp. 265-272, 1974.
53. Saboya, F. E. M., and Sparrow, E. M., "Effect of Tube Relocation on the Transfer Capabilities of a Fin and Tube Heat Exchanger," *ASME Journal of Heat Transfer*, Vol. 96, pp. 421-422, 1974.
54. Saboya, F. E. M., and Sparrow, E. M., "Transfer Characteristics of Two-Row Plate Fin and Tube Heat Exchanger Configurations," *International Journal of Heat Mass Transfer*, Vol. 19, pp. 41-49, 1976.
55. Schmidt, E.Th., "Der Wärmeübergang an Rippenrohre und die Berechnung von Rohrbundle-Wärmeaustauschern," *Kältetechnik*, Band 15, Heft 4, 1963.
56. Schmidt, E.Th., "Der Wärmeübergang an Rippenrohre und die Berechnung von Rohrbundle-Wärmeaustauschern," *Kältetechnik*, Band 15, Heft 12, 1963.
57. Sharatchandra, M. C., and Rhode, D. L., "Turbulent Flow and Heat Transfer in Staggered Tube Banks With Displaced Tube Rows," *Numerical Heat transfer, Part A*, Vol. 31, pp.611-627, 1997.
58. Sheu, T. W. H., and Tsai, S. F., "A Comparison Study on Fin Surface in Finned-Tube Heat Exchangers," *International Journal of Numerical Methods for Heat & Fluid flow*, Vol. 9, No.1, pp.92-106, 1999.
59. Sparrow, E. M., and Samie, F., "Heat Transfer and Pressure Drop Results for One and Two-row Arrays of Finned Tubes," *International Journal of Heat Mass Transfer*, Vol. 28, No. 12, pp. 2247-2259, 1985.
60. Sparrow, E. M., and Chastain, S. R., "Effect of Angle of Attack on the Heat Transfer Coefficient for an Annular Fin," *International Journal of Heat Mass Transfer*, Vol. 29, pp.1185-1191, 1986.
61. Stasiulevičius, J., and Survila, V.J., "Heat transfer and Hydraulic Drag of Banks of Finned Tubes at High Reynolds Numbers," *5th International Heat Transfer Conference*, Tokyo, 1974.
62. Stasiulevičius, J., and Skrinska, A., *Heat Transfer of Finned Tube Bundles in Crossflow*, Hemisphere Publishing, ISBN 3-540-18211-x, 1988.

63. Sung, H. J., Yang, J. S., and Park, T. S., "Local Convective Mass Transfer on Circular Cylinder with Transverse Annular Fins in Cross Flow," *International Journal of Heat Mass Transfer*, Vol. 39, No. 5, pp. 1093-1101, 1996.
64. Torikoshi, K., and Xi, G. N., Nakazawa, Y., and Asano, H., "Flow and Heat Transfer Performance of a Plate-fin and Tube Heat Exchanger (1st report: Effect of fin pitch)," *ASME Heat Transfer Division*, Vol. 4, pp. 411-416, 1994.
65. Torikoshi, K., and Xi, G. N., "A Numerical Study of Flow and Thermal Fields in Finned Tube Heat Exchangers (Effect of the Tube Diameter)," *IMECE Proceedings of the ASME Heat Transfer Division*, HTD-Vol. 317-1, pp. 453-457, 1995.
66. Torikoshi, K., Xi, G. N., Kawabata, K., and Suzuki, K., "Numerical Analysis of Unsteady Flow and Heat Transfer Around Bodies by Making Use of a Compound Grid System," *ASME-JSME Thermal Engineering Conference*, Vol.4, pp. 381-388, 1995.
67. Tutar, M., and Holdo, A. E., "Computational Modelling of Flow around a Circular Cylinder in Sub-Critical Flow Regime with Various Turbulence Models," *International Journal for Numerical Methods in Fluids*, Vol.35, pp.763-784, 2001.
68. Verein Deutscher Ingenieure., *VDI-Wärmeatlas., Berechnungsblätter für den Wärmeübergang*, 8. Aufl. Berlin u.a., Springer, 1997.
69. Ward, D. J., and Young, E. H., "Heat Transfer and Pressure Drop of Air in Forced Convection Across Triangular Pitch Banks of Finned Tubes," *Chemical Engineering Progress Symposium Series*, Vol. 55, No. 29, pp.37-44, 1959.
70. Watel, B., Harmand, S., and Desmet, B., "Influence of Flow Velocity and Fin Spacing on the Forced Convective Heat Transfer from an Annular-Finned Tube," *JSME international Journal*, series B, Vol. 42, No. 1, pp. 56-64, 1999.
71. Watel, B., Harmand, S., and Desmet, B., "Experimental Study of Convective Heat Transfer from a Rotating Finned Tube in Transverse Air Flow," *Experiments in Fluids*, Vol. 29, No. 1, pp. 79-90, 2000.
72. Webb, R. L., "Air-Side Heat Transfer in Finned Tube Heat Exchanger," *Heat Transfer Engineering*, Vol. 1, No. 3, pp. 33-49, 1980.

73. Webb, R. L., *Externally Finned Tubes, Principles of Enhanced Heat Transfer*, John Wiley and Sons, Inc, pp. 125-159, 1994.
74. Weierman, C., "Correlations Ease the Selection of Finned Tubes," *Oil and Gas Journal*, Vol. 74, pp. 94-100, 1976.
75. Weierman, C., "Pressure Drop Data for Heavy-Duty Finned Tubes," *Chemical Engineering Progress*, pp. 69-72, 1977.
76. Weierman, C., Taborek, J., and Marner, W. J., "Comparison of Inline and Staggered Banks of Tubes with Segmented Fins," *AIChE Symp, Ser.*, Vol. 74, No. 174, pp. 39-46, 1978.
77. Weyrauch, E., " Der Einfluß der Rohranordnung auf den Wärmeübergang und Druckverlust bei Querstrom von Gasen durch Rippenrohrbündel," *Kältetechnik*, Band 21, Heft 3, 1969.
78. Wong, P. W., "Mass and Heat Transfer from Circular Finned Cylinders," *J. Inst. Heat. Vent. Eng.*, pp.1-23, April 1966.
79. Xi, G.N, and Torikoshi, K., "Computation and Visualization of Flow and Heat Transfer in Finned Tube Heat Exchangers," *International Symposium on Heat Transfer*, Tsinghua University, Beijing China,(7.10 – 11.10), pp. 632-637, 1996.
80. Yudin, V F., Tokhtarova, L. S. Lokshin, V., and Tulin, S. N., "Correlation of Experimental Data on Convective Heat Transfer in Cross Flow Over Bundles with Transverse Spiral and Circumferential Fins," *Trudy TsKTI*, No. 82, 1968.
81. Zhukauskas, A. A., "Investigation of Heat Transfer in Different Arrangements of Heat Exchanger Surfaces," *Teploenergetika*, Vol. 21, No. 5, pp. 40-46, 1974.
82. Zhukauskas, A., Stasiulevičius, J., and Skrinska, A., "Experimental Investigation of Efficiency of Heat Transfer of a Fin Tube with Spiral Fin in Cross Flow," *Third International Heat Transfer Conference*, Chicago, Vol. 3, pp. 299-305, 1966.
83. Zozulya, N. V., Vorob'yev, Y. P., and Khavin, A. A., "Effect of Flow Turbulization on Heat Transfer in a Finned Tube Bundle," *Heat Transfer Soviet Research*, Vol. 5, No. 1, pp. 154-156, 1973.

List of Figures

Figure	Page
1.1 Cross-flow circular finned-tube heat exchanger	1
2.1 Arrangements of tubes in bundles, (a) In-line arrangement, (b) Staggered arrangement	4
2.2 Schematic of general flow pattern over a second row of the staggered arrangement tube bundle [45].....	8
4.1 Cross-section of a circular fin tube	31
4.2 Computational domains, (a) In-line arrangement, (b) Staggered arrangement, (c) Top view	33
4.3 Grid generation (a) near tube, (b) at z - direction of the domain	35
4.4 Grid generation (a) Staggered arrangement, (b) In-line arrangement	35
5.1 Velocity distributions between the fins of first row of staggered arrangement at $Re = 8.6 \times 10^3$	45
5.2 Schematic flow patterns of horseshoe vortices around a circular cylinder between annular fins [63]	47
5.3 Flow pattern for the fourth row of bundle (s7) at $Re = 4.3 \times 10^4$	48
5.4 Velocity distributions between the fins of first row of in-line arrangement at $Re = 8.6 \times 10^3$	50
5.5 Temperature distributions between the fins for staggered arrangement at $Re = 8.6 \times 10^3$ (a) first row and (b) fourth row	52
5.6 Variations of local Nu number along the tube surface of bundle (s7) at $(\theta = 0^\circ)$ for $Re = 4.3 \times 10^4$	54
5.7 Temperature distributions between the fins for in-line arrangement at $Re = 8.6 \times 10^3$ (a) first row and (b) fourth row	55
5.8 Temperature contours for staggered arrangement at (a) over fin surface and (b) within fin of bundle (s3) at $Re = 4.3 \times 10^4$	57
5.9 Temperature contours for in-line arrangement at (a) over fin surface and (b) within fin of bundle (i2) at $Re = 4.3 \times 10^4$	58
5.10 Velocity distributions for bundle s6 ($n = 3$) at $Re = 8.6 \times 10^3$	60
5.11 Velocity distributions for bundle i4 ($n = 3$) at $Re = 8.6 \times 10^3$	61

5.12	Boundary layer separation point of first row of bundle (s3) at $Re = 1.7 \times 10^4$	63
5.13	Temperature distributions for bundle s6 ($n = 3$) at $Re = 8.6 \times 10^3$	64
5.14	Temperature distributions for bundle i4 ($n = 3$) at $Re = 8.6 \times 10^3$	65
5.15	Effect of fin height on the heat transfer rate for staggered and in-line tube bundles	67
5.16	Effect of fin height on the fin efficiency for staggered and in-line bundles	68
5.17	Effect of fin height on the heat transfer coefficient for staggered and in-line bundles.....	68
5.18	Effect of fin height on the pressure drop for staggered and in-line bundles.....	69
5.19	Performance parameter of the fin height effect for staggered and in-line bundles.....	70
5.20	Effect of fin spacing on the heat transfer rate for staggered and in-line bundles.....	71
5.21	Effect of the fin spacing on the fin efficiency for staggered and in-line bundles.....	72
5.22	Effect of fin spacing on heat transfer coefficient for staggered and in-line bundles.....	72
5.23	Effect of fin spacing on the pressure drop for staggered and in-line bundles	74
5.24	Performance parameter of the fin spacing effect for staggered and in-line bundles.....	74
5.25	Effect of fin thickness on the heat transfer rate for staggered bundle	75
5.26	Effect of fin thickness on the fin efficiency for staggered bundle	76
5.27	Effect of fin thickness on the heat transfer coefficient for staggered bundle	76
5.28	Effect of fin thickness on the pressure drop for staggered bundle	77
5.29	Performance parameter of the fin thickness effect for staggered bundle.....	78
5.30	Effect of tube outside diameter on the heat transfer rate for staggered and in-line bundles.....	78
5.31	Effect of tube outside diameter on the fin efficiency for staggered and in-line bundles.....	79
5.32	Effect of tube outside diameter on the heat transfer coefficient for staggered and in-line bundles	80
5.33	Effect of tube outside diameter on the pressure drop for staggered and in-line bundles.....	80
5.34	Performance parameter of the tube outside diameter effect for staggered and in-line bundles.....	81
5.35	Effect of tube spacing on the heat transfer rate for staggered and in-line bundles.....	82

5.36	Effect of the tube spacing on the fin efficiency for staggered and in-line bundles	83
5.37	Effect of the tube spacing on the heat transfer coefficient for staggered and in-line bundles	84
5.38	Effect of the tube spacing on the pressure drop for staggered and in-line bundles	85
5.39	Performance parameter of tube spacing effect for staggered and in-line bundles	86
5.40	Row-to-row effect on the heat transfer rate for staggered (above) and in-line (below) bundles at $Re = 4.3 \times 10^4$	87
5.41	Row-to-row effect on the fin efficiency for staggered (above) and in-line (below) bundles at $Re = 4.3 \times 10^4$	88
5.42	Row-to-row effect on the heat transfer coefficient for staggered (above) and in-line (below) bundles at $Re = 4.3 \times 10^4$	90
5.43	Effect of the number of rows effect on the heat transfer rate for staggered and in-line bundles	91
5.44	Effect of number of rows on the fin efficiency for staggered and in-line bundles	92
5.45	Effect of the number of rows on the heat transfer coefficient for staggered and in-line bundles	92
5.46	Effect of number of rows on the pressure drop for staggered and in-line bundles	93
5.47	Performance parameter of the rows effect for staggered and in-line bundles	94
6.1	Comparison of the numerical results with Equations (6.4 and 6.6).....	100
6.2	Comparison of the numerical results with Equation. (6.8).....	102
6.3	Comparison of the numerical results with Equation (6.10).....	103
6.4	Comparison of the numerical results with Equation (6.11).....	104
6.5	Comparison of the numerical results with experiment based correlations.....	106
6.6	Comparison of the experimental data with Equation (6.4)	107
6.7	Comparison of the experimental data with VDI equation	108
6.8	Comparison of Equation (6.4) and VDI correlation based on experimental data	109
6.9	Comparison of numerical and experimental results with Equation (6.8).....	110
6.10	Comparison of numerical and experimental results with VDI equation.....	110
6.11	Comparison of the numerical results with experimental correlations.....	112
6.12	Comparison of numerical and experimental results with Equation (6.11).....	113
B.1	Velocity distributions between the fins of first row of staggered arrangement at $Re = 4.3 \times 10^4$	134
B.2	Velocity distributions between the fins of second row of staggered arrangement at $Re = 4.3 \times 10^4$	135

B.3(a) Horseshoe Vortex near fin-tube junction at second row of bundle (s11) for $Re = 8.6 \times 10^3$	136
B.3(b) Flow pattern near fin-tube junction at first row of bundle (s8) for $Re = 8.6 \times 10^3$	136
B.4 Velocity distributions between the fins of first row of in-line arrangement at $Re = 4.3 \times 10^4$	137
B.5 Velocity distributions between the fins of second row of in-line arrangement at $Re = 4.3 \times 10^4$	138
B.6 Temperature distributions between the fins for staggered arrangement at $Re = 4.3 \times 10^4$ (a) first row and (b) fourth row.	139
B.7 Temperature distributions between fins for in-line arrangement at $Re = 4.3 \times 10^4$ (a) first row and (b) fourth row.	140

List of Tables

Table	Page
4.1 Dimensions of bundles used in numerical investigation	32
6.1 Deviations of heat transfer correlations for staggered arrangement....	101
6.2 Deviations of heat transfer correlations for in-line arrangement	102
6.3 Deviations of pressure drop correlations for staggered and in-line arrangements	104
C.1 Dimensions of finned - tube heat exchangers	141
D.1 Correlations for heat transfer of circular finned - tube heat exchangers.....	144
D.2 Correlations for heat transfer of circular finned - tube heat exchangers.....	145
D.3 Correlations for heat transfer of circular finned - tube heat exchangers.....	146
D.4 Correlations for pressure drop of circular finned - tube heat exchangers.....	147
D.5 Correlations for pressure drop of circular finned - tube heat exchangers.....	148
D.6 Correlations for pressure drop of circular finned - tube heat exchangers.....	149
E.1 Numerical results for bundle depth, $n = 2$	150
E.2 Numerical results for bundle depth, $n = 3$	150
E.3 Numerical results for bundle depth, $n = 4$	151
E.4 Numerical results for bundle depth, $n = 4$	152
E.5 Numerical results for bundle depth, $n = 5$	153
E.6 Numerical results for bundle depth, $n = 6$	153

APPENDIX

Appendix A - The Physical Properties of Air and Aluminium

The following temperature dependents, physical properties of air, specific heat, thermal conductivity and dynamic viscosity are set in FLUENT as Glück [14].

$$\phi = A + BT + CT^2 + DT^3$$

ϕ	A	B	C	D
c_p [kJ/kgK]	1.034754×10^0	-2.412242×10^{-4}	5.427329×10^{-7}	$-1.521916 \times 10^{-10}$
K [W/mK]	1.017381×10^{-3}	1.010288×10^{-4}	-6.930598×10^{-8}	5.292884×10^{-11}
μ [kg/sm]	4.148720×10^{-6}	4.914210×10^{-8}	$-5.994825 \times 10^{-12}$	$-3.382035 \times 10^{-15}$

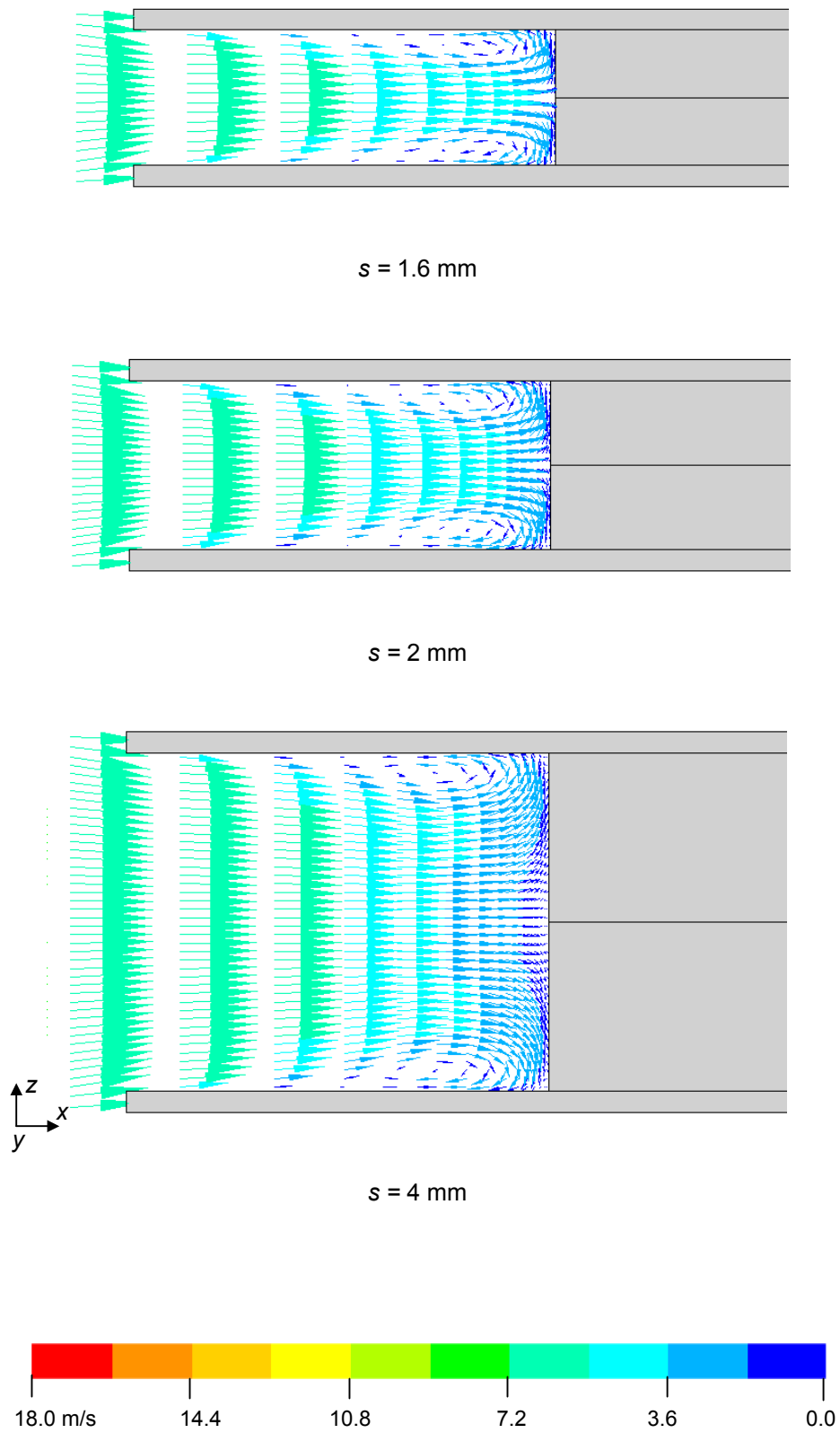
Molecular weight is 28.96 kg/kmol.

Properties of Aluminium:

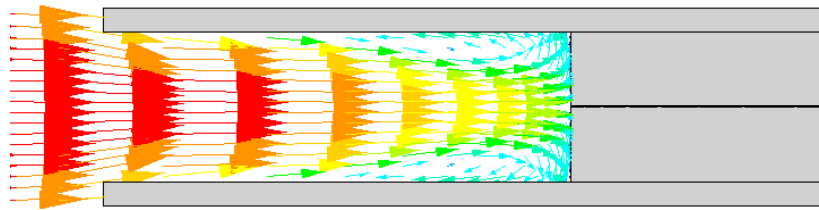
For the fins and tubes, the following properties are set constant as:

- Density $\rho = 2700 \text{ kg/m}^3$
- Specific Heat $c_p = 0.879 \times 10^3 \text{ J/kgK}$
- Thermal Conductivity $k = 229 \text{ W/mK}$

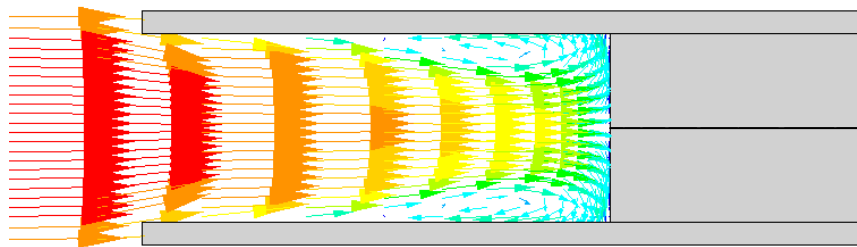
Appendix B – Further Figures



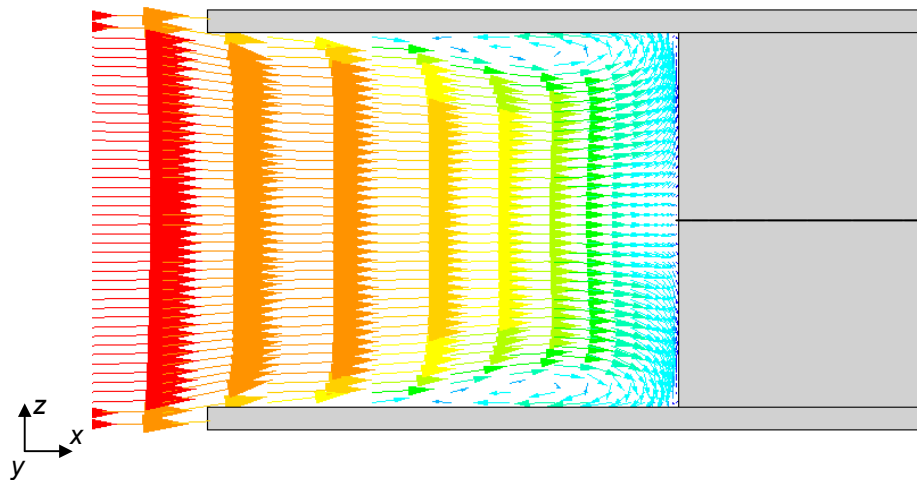
Appendix B.1 Velocity distributions between the fins of first row of staggered arrangement at $Re = 4.3 \times 10^4$.



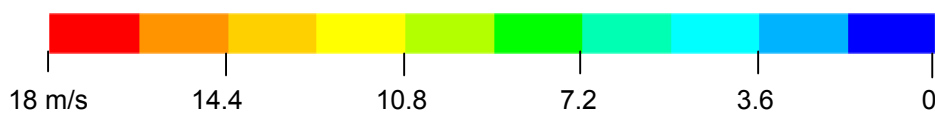
$s = 1.6 \text{ mm}$



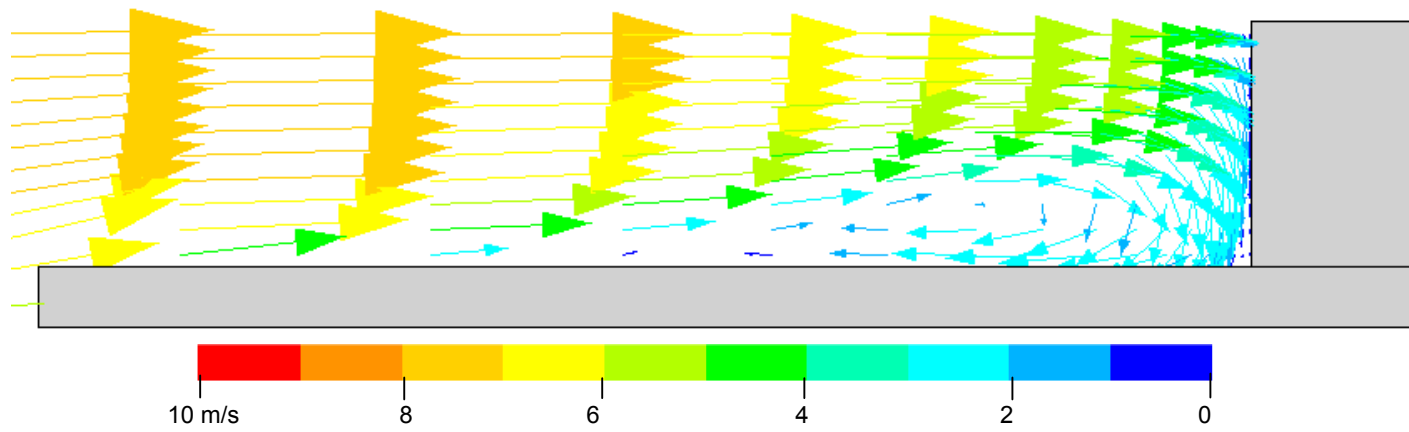
$s = 2 \text{ mm}$



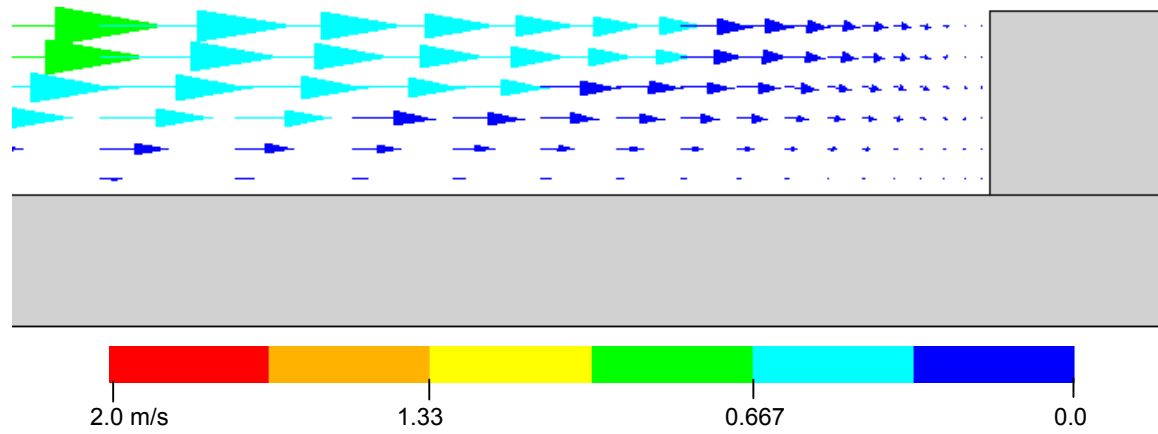
$s = 4 \text{ mm}$



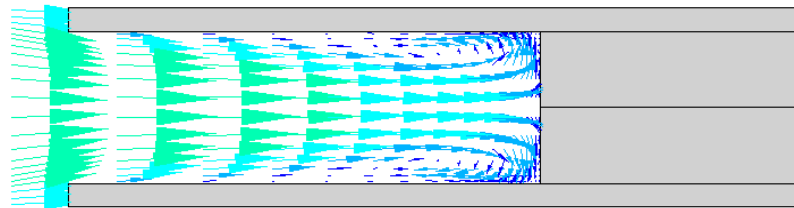
Appendix B.2 Velocity distributions between fins of second row of staggered arrangement at $Re = 4.3 \times 10^4$.



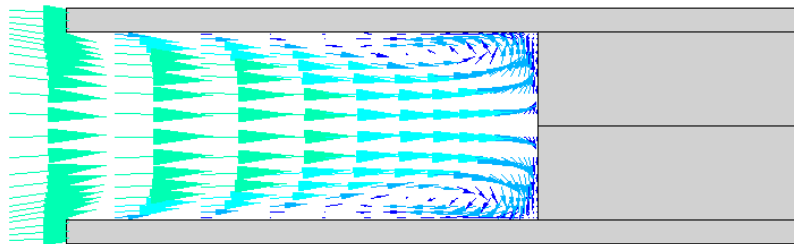
Appendix B.3 (a) *Horseshoe Vortex near fin-tube junction at second row of bundle (s11) for $Re = 8.6 \times 10^3$.*



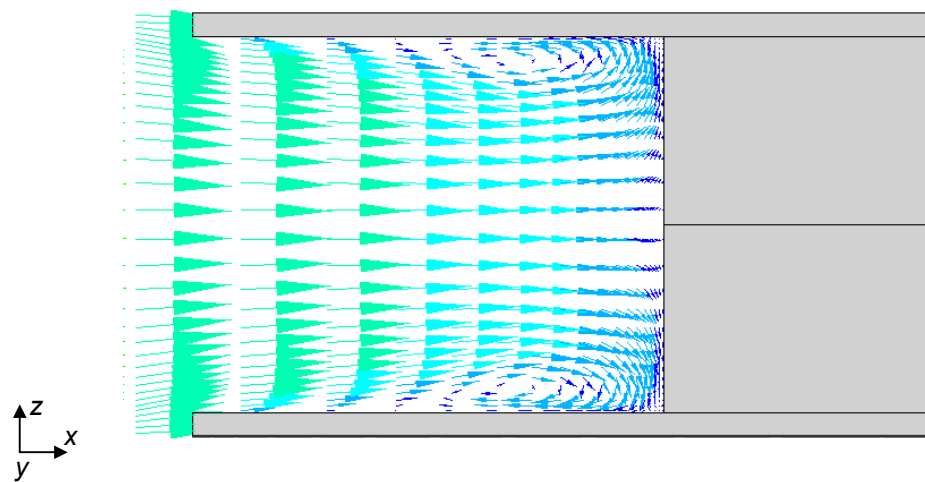
Appendix B.3 (b) *Flow pattern near fin-tube junction at first row of bundle (s8) for $Re = 8.6 \times 10^3$.*



$s = 1.6 \text{ mm}$



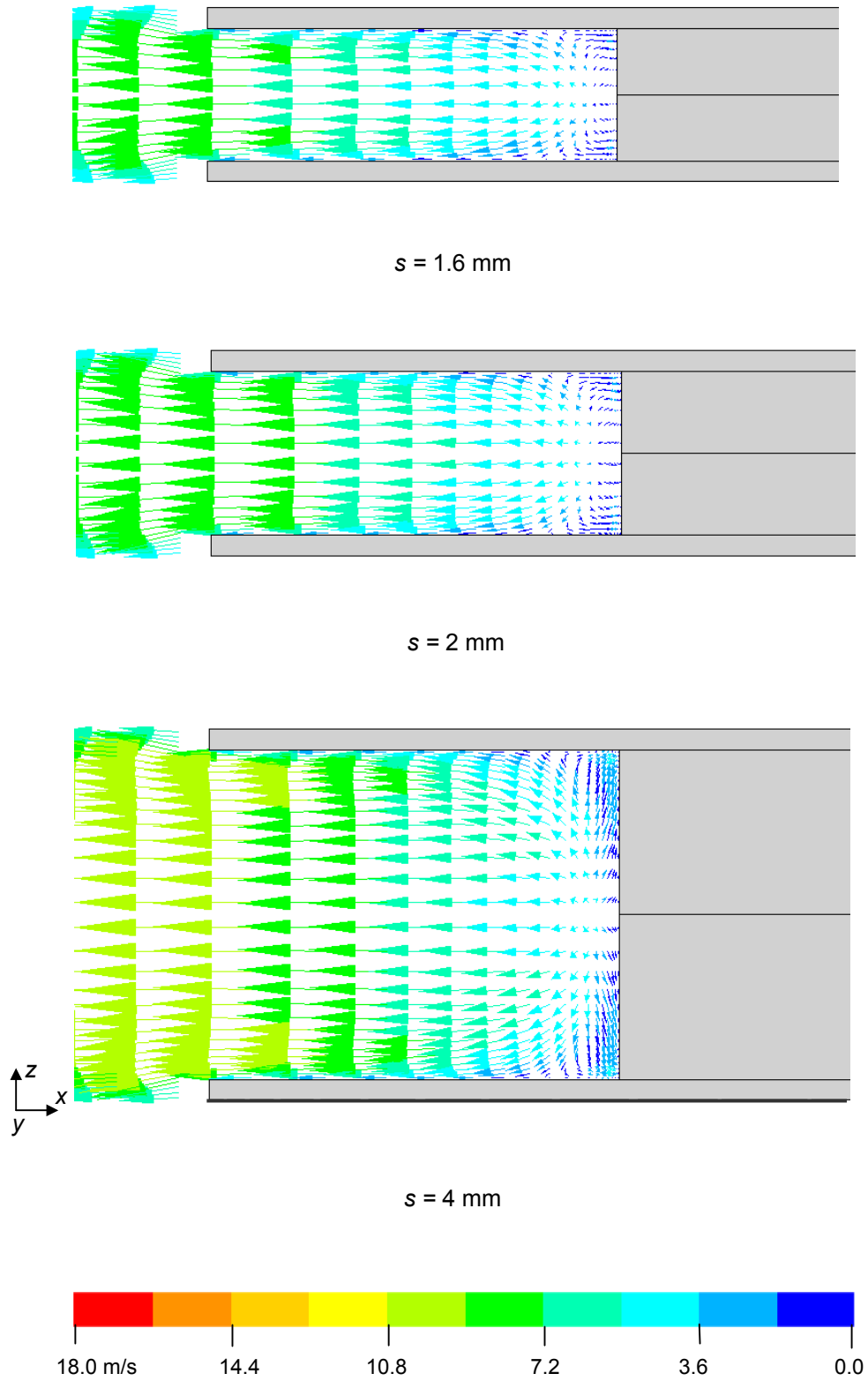
$s = 2 \text{ mm}$



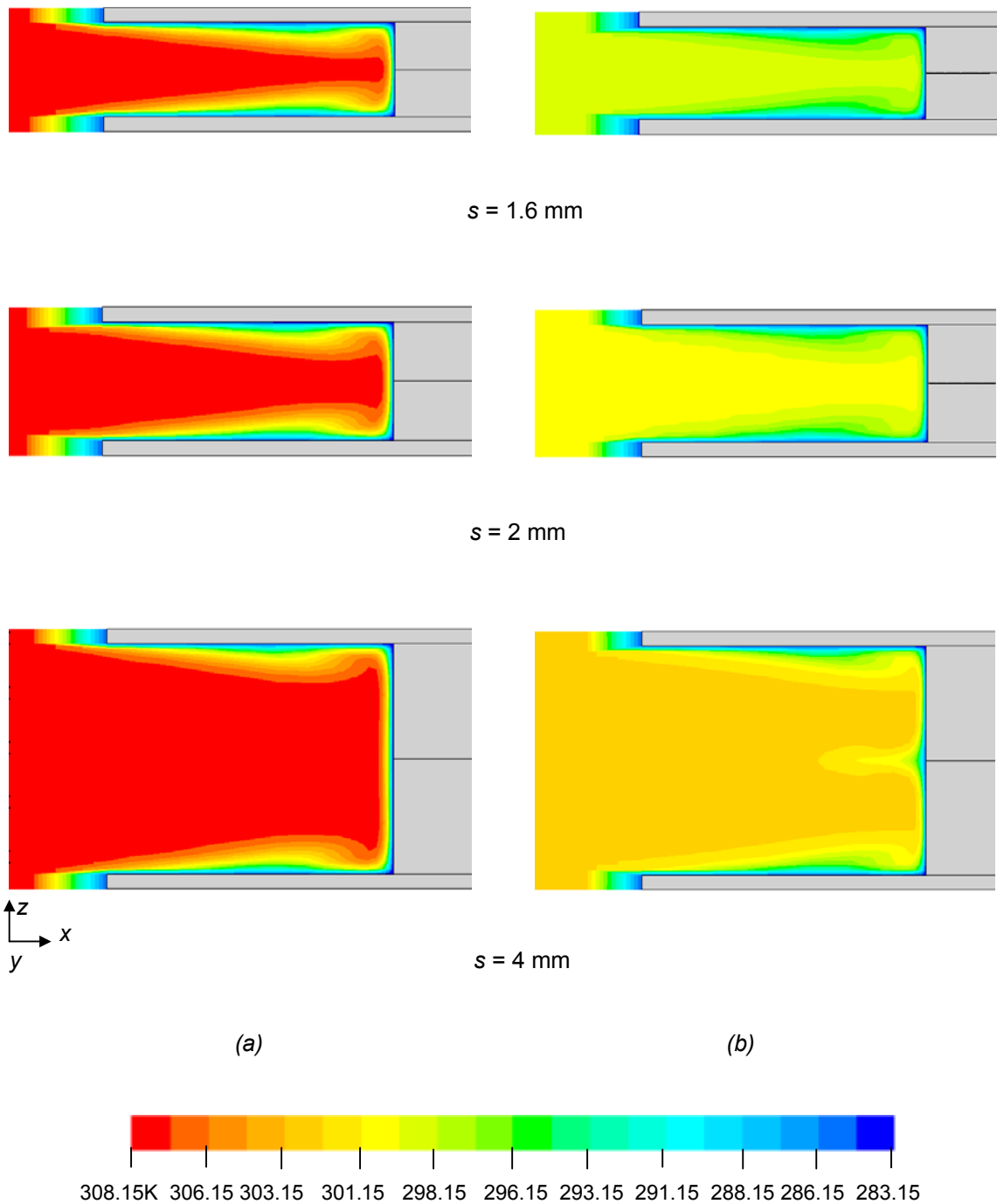
$s = 4 \text{ mm}$



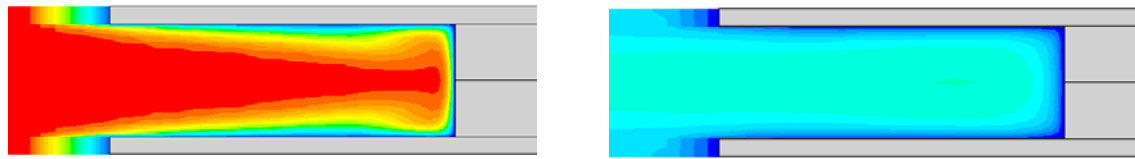
Appendix B.4 Velocity distributions between the fins of first row of in-line arrangement at $Re = 4.3 \times 10^4$.



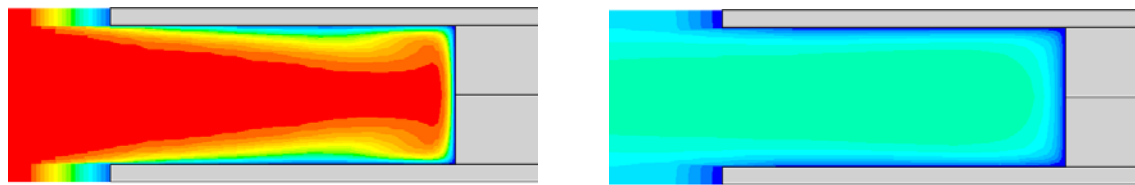
Appendix B.5 Velocity distributions between the fins of second row of in-line arrangement at $Re = 4.3 \times 10^4$.



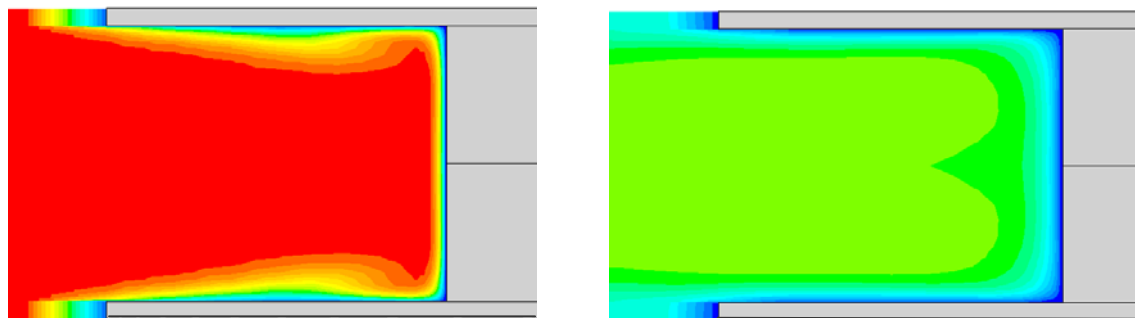
Appendix B.6 Temperature distributions between the fins for staggered arrangement at $Re = 4.3 \times 10^4$ (a) first row and (b) fourth row.



$s = 1.6 \text{ mm}$



$s = 2 \text{ mm}$

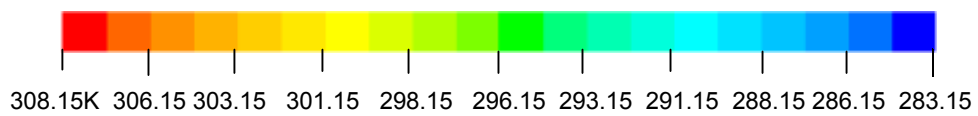


$\begin{matrix} \uparrow z \\ \rightarrow x \\ y \end{matrix}$

$s = 4 \text{ mm}$

(a)

(b)



Appendix B.7 Temperature distributions between the fins for in-line arrangement at $Re = 4.3 \times 10^4$ (a) first row and (b) fourth row.

Appendix C – Dimensions of Finned-Tube Heat Exchangers from Literature

Table C.1 Dimensions of Finned-Tube Heat Exchangers from Literature.

No.	Author	Arrangement	d	d_f	δ	s	S_t	S_l	n
1	Kuntysh [37]	Staggered	25.85	55.85	0.75	1.810	70	60.60	4
2	Ward & Young [69]	Staggered	11.125	22.73	0.56	2.960	26.99	23.37	6
3	Ward & Young	Staggered	28.96	49.78	0.56	4.390	55.56	48.12	4
4	Ward & Young	Staggered	28.52	49.73	0.53	1.920	55.56	48.12	4
5	Ward & Young	Staggered	29.13	58.50	0.43	2.745	61.91	53.62	8
6	Ward & Young	Staggered	15.875	18.72	0.41	0.89	23.81	20.62	6
7	Ward & Young	Staggered	13.87	19.36	0.43	1.810	23.81	20.62	6
8	Ward & Young	Staggered	14.070	22.71	0.46	1.8	26.99	23.37	6
9	Briggs & Young [8]	Staggered	13.95	22.56	1.06	2.115	27.43	23.76	6
10	Briggs & Young	Staggered	23.60	49.94	0.52	2.07	57.15	49.49	6
11	Briggs & Young	Staggered	24.13	57.28	0.55	2.08	62.33	53.98	6
12	Briggs & Young	Staggered	26.19	50.67	0.33	2.185	55.7	48.24	6
13	Stasiulevičius [62]	Staggered	32	50	1.50	4.50	70.4	41.60	7
14	Stasiulevičius	Staggered	23	31	1.50	2.50	61.4	33.60	7
15	Stasiulevičius	Staggered	32	59	1.50	2.50	76	46.60	7
16	Stasiulevičius	Staggered	23	43	1.50	5.00	93	45.60	7
17	Hashizume [20]	Staggered	19.50	42	0.40	2.60	46	42	5
18	Kuntysh [34]	Staggered	12.60	27	0.50	2.50	33.75	29.16	5
19	Kuntysh	Staggered	17	25	0.50	2	31.25	27	5
20	Kuntysh	Staggered	24.90	44.50	0.60	2.80	48.06	40.05	5
21	Kuntysh	Staggered	25.40	42	0.80	2.70	47.88	39.90	5
22	Kuntysh	Staggered	23	43	0.50	3	44.72	39.13	5
23	Kuntysh	Staggered	12	23	0.50	2.50	28.75	24.84	5
24	Kuntysh	Staggered	13	29	0.60	2.40	36.25	31.32	5
25	Yudin [62]	Staggered	23	43	1	4	64.86	34.50	
26	Yudin	Staggered	23	43	1	4	69	27.60	

Table C.1 (Continued) *Dimensions of Finned-Tube Heat Exchangers from Literature.*

No.	Author	Arrangement	d	d_f	δ	s	S_t	S_l	n
27	Mirkovic [43]	Staggered	25.40	44.45	1.27	2.96	100	60	8
28	Mirkovic	Staggered	25.40	44.45	1.27	2.96	100	70	8
29	Mirkovic	Staggered	25.40	44.45	1.27	2.96	109	80	8
30	Mirkovic	Staggered	25.40	44.45	1.27	2.96	120	70	8
31	Mirkovic	Staggered	38.10	57.25	1.27	2.96	100	80	8
32	Rabas [47]	Staggered	31.75	38.74	0.356	2.21	42.86	37.11	8
33	Rabas	Staggered	31.75	38.74	0.356	1.05	42.86	37.11	8
34	Rabas	Staggered	31.75	38.74	0.356	2.21	42.86	50.80	3
35	Rabas	Staggered	31.78	38.74	0.356	0.664	42.86	50.80	3
36	Weierman[76]	Staggered	50.80	102.36	1.22	3.06	114.30	99.06	4
37	Brauer [6]	Staggered	28	32	1.50	4	50.50	50.50	4
38	Brauer	Staggered	28	38	1.50	4	50.50	50.50	4
39	Brauer	Staggered	28	58	1.50	4	59	59	4
40	Robinson [50]	Staggered	18.64	39.65	0.47	1.85	48.997	48.997	6
41	Robinson	Staggered	18.64	39.65	0.47	1.85	85.725	85.725	6
42	Robinson	Staggered	40.89	69.85	0.457	2.76	114.046	114.046	6
43	Robinson	Staggered	40.89	69.85	0.457	2.76	76.02	76,0222	6
44	Robinson	Staggered	26.59	51.16	0.40	2.34	52.705	52.705	6
45	Robinson	Staggered	26.59	51.16	0.40	2.34	85.725	85.725	6
46	Robinson	Staggered	26.59	51.16	0.40	2.34	68.58	107.696	6
47	Robinson	Staggered	26.59	51.16	0.40	2.34	68.58	52.832	6
48	Weyrauch[77]	Staggered	13.90	27.70	0.30	2.20	28.50	24.70	4
49	Weyrauch	Staggered	17.90	37.84	0.35	2.40	38.50	33	4
50	Kuntysh [37]	In-line	25.85	55.85	0.75	1.810	70	60.60	4
51	Weierman[76]	In-line	50.80	102.36	1.22	3.06	114.30	114.30	7
52	Brauer [6]	In-line	28	38	1.50	2	50.50	50.50	4
53	Brauer	In-line	28	48	1.50	2	54.50	54.50	4
54	Brauer	In-line	28	58	1.50	2	59	59	4
55	Brauer	In-line	28	38	1.50	4	53.50	53.50	4
56	Brauer	In-line	28	48	1.50	4	54.90	54.90	4
57	Brauer	In-line	28	53	1.50	4	57	57	4
58	Carnavos[49]	In-line	9.525	19.05	0.203	0.64	30.17	23.83	10
59	Carnavos	In-line	9.525	19.05	0.203	0.64	27	23.83	10
60	Carnavos	In-line	9.525	19.05	0.203	0.64	23.83	23.83	10
61	Carnavos	In-line	4.775	9.525	0.203	0.64	13.51	11.91	10
62	Huber [49]	In-line	33.4	62.36	3.378	5.10	76.20	76.2	7

**Appendix D – Heat Transfer and Pressure Drop
Correlations for Circular
Finned - Tube Heat Exchangers
from Literature**

Author	Correlation	Remark
Briggs and Young [8]	$Nu = 0.134 Re^{0.681} Pr^{1/3} \left(\frac{s}{h_f}\right)^{0.2} \left(\frac{s}{\delta}\right)^{0.1134}$	For staggered tube arrangement, $1.1 \times 10^3 \leq Re \leq 1.8 \times 10^4$ $13.49 \text{ mm} \leq d \leq 40.89 \text{ mm}$ $4.31 \text{ mm} \leq h_f \leq 16.58 \text{ mm}$ $1.82 \text{ mm} \leq s \leq 2.76 \text{ mm}$ $0.33 \text{ mm} \leq \delta \leq 2.02 \text{ mm}$ $27.43 \text{ mm} \leq S_t \leq 110 \text{ mm}$ $23.76 \text{ mm} \leq S_l \leq 96.13 \text{ mm}$ $n \geq 4$ Standard deviation 5.1 %
Gianolio and Cuti [14]	$Nu = 0.287 Re^{0.7} Pr^{0.33} \left(\frac{s}{h_f}\right)^{0.37} \left(\frac{s}{\delta}\right)^{-0.25} \left(\frac{n}{6}\right)^{-0.136}$	For staggered tube arrangement and force draft, $5 \times 10^3 \leq Re \leq 2 \times 10^4$ $25.4 \text{ mm} \leq d \leq 38.1 \text{ mm}$ $15.15 \text{ mm} \leq h_f \leq 16.4 \text{ mm}$ $1.9 \text{ mm} \leq s \leq 2.37 \text{ mm}$ $0.41 \text{ mm} \leq \delta \leq 0.52 \text{ mm}$ $1 < n < 6$ 90 % of data within ± 8 %
Gianolio and Cuti [14]	$Nu = 0.271 Re^{0.685} Pr^{0.33} \left(\frac{A}{A_t}\right)^{-0.311} \left(\frac{n}{6}\right)^{-0.138}$	For staggered tube arrangement and forced draft, $5 \times 10^3 \leq Re \leq 2 \times 10^4$ $25.4 \text{ mm} \leq d \leq 38.1 \text{ mm}$ $15.15 \text{ mm} \leq h_f \leq 16.4 \text{ mm}$ $1.9 \text{ mm} \leq s \leq 2.37 \text{ mm}$ $0.41 \text{ mm} \leq \delta \leq 0.52 \text{ mm}$ $1 < n < 6$ 90 % of data within ± 6.5 %

Table D.1 Correlations for heat transfer of circular finned-tube heat exchangers.

Author	Correlation	Remark
Nir [46]	$St Pr^{2/3} = 1.745 Re_{dh}^{-0.4} \left(\frac{A'}{A_{ff}} \right)^{-2/3} R_b^{-0.4} K_{zh}$	For staggered tube arrangement, $300 \leq Re_{dh} \leq 1 \times 10^4$ $10 \leq A' / A_{ff} \leq 60$ $1 \leq R_b \leq 3$ $R_b =$ Ratio of free flow area in frontal space near tube to free flow area of tube $n \geq 1$ Deviation $\pm 10\%$
Rabas et al. [47]	$j = 0.292 Re^n \left(\frac{s}{d_f} \right)^{1.115} \left(\frac{s}{h_f} \right)^{0.26} \left(\frac{\delta}{s} \right)^{0.666} \left(\frac{d_f}{d} \right)^{0.473} \left(\frac{d_f}{\delta} \right)^{0.7717}$ $n = -0.415 + 0.0346 \ln(d_f/s)$	For staggered tube arrangement, $1 \times 10^3 \leq Re \leq 2.5 \times 10^4$ $15.87 \text{ mm} \leq d \leq 31.75 \text{ mm}$ $6.35 \text{ mm} < h_f$ $0.63 \text{ mm} \leq s \leq 2.188 \text{ mm}$ $0.305 \text{ mm} \leq \delta \leq 0.356 \text{ mm}$ $23.81 \text{ mm} \leq S_t \leq 42.86 \text{ mm}$ $20.62 \text{ mm} \leq S_l \leq 50.8 \text{ mm}$ $n \geq 6$ Deviation -20% to $+30\%$
Schmidt [56]	$Nu = C Re^{0.625} Pr^{1/3} \left(\frac{A}{A_t} \right)^{-0.375}$ <p>For staggered: $C = 0.45$</p> <p>For in-line: $C = 0.3$</p>	$1 \times 10^3 \leq Re \leq 4 \times 10^4$ $5 < A/A_t < 12$ $n \geq 3$ Maximum deviation $\pm 25\%$

Table D.2 Correlations for heat transfer of circular finned-tube heat exchangers.

Author	Correlation	Remark
Stasiulevičius and Skrinska [62]	$Nu = C \left(\frac{S_t}{S_l} \right)^{0.2} \left(\frac{S_f}{d} \right)^{0.18} \left(\frac{h_f}{d} \right)^{-0.14} Re^m$ <p>For $2 \times 10^4 \leq Re \leq 2 \times 10^5$: $C = 0.044$, $m = 0.8$ For $2 \times 10^5 \leq Re \leq 1.3 \times 10^6$: $C = 0.0067$, $m = 0.95$</p>	For staggered tube arrangement, $23 \text{ mm} \leq d \leq 32 \text{ mm}$ $4 \text{ mm} \leq h_f \leq 13.5 \text{ mm}$ $2.5 \text{ mm} \leq s \leq 6.5 \text{ mm}$ $61.4 \text{ mm} \leq S_t \leq 95 \text{ mm}$ $33.6 \text{ mm} \leq S_l \leq 49.2 \text{ mm}$ $n = 7$ Deviation $\pm 14 \%$
VDI-Wärmeatlas [68]	$Nu = C Re^{0.6} Pr^{1/3} \left(\frac{A}{A_t} \right)^{-0.15}$ <p>For $n \geq 4$ For staggered: $C = 0.38$ For in-line: $C = 0.22$</p> <p>For staggered, $n = 2$: $C = 0.33$ For staggered, $n = 3$: $C = 0.36$ For in-line, $n = 1$ to 3: $C = 0.2$</p>	$1 \times 10^3 \leq Re \leq 1 \times 10^5$ $5 \leq A/A_t \leq 30$ Maximum deviation $\pm 25 \%$
Ward and Young [69]	$Nu = 0.364 Re^{0.68} Pr^{1/3} \left(\frac{d_f}{d} \right)^{0.45} \left(\frac{\delta}{d_f} \right)^{0.3}$	For staggered tube arrangement, $1 \times 10^3 \leq Re \leq 2.8 \times 10^4$ $11.13 \text{ mm} \leq d \leq 29.13 \text{ mm}$ $1.42 \text{ mm} \leq h_f \leq 14.69 \text{ mm}$ $0.89 \text{ mm} \leq s \leq 4.39 \text{ mm}$ $0.41 \text{ mm} \leq \delta \leq 0.56 \text{ mm}$ $23.81 \text{ mm} \leq S_t \leq 61.91 \text{ mm}$ $20.62 \text{ mm} \leq S_l \leq 53.62 \text{ mm}$ $n \geq 3$ Maximum deviation $\pm 20 \%$

Table D.3 Correlations for heat transfer of circular finned-tube heat exchangers.

Author	Correlation	Remark
Gianolio and Cuti [14]	$Eu = 138.3 Re^{-0.478} \left(\frac{S_t}{d} \right)^{-1.454}$	For staggered tube arrangement and force draft, $5 \times 10^3 \leq Re \leq 2 \times 10^4$ $25.4 \text{ mm} \leq d \leq 38.1 \text{ mm}$ $15.15 \text{ mm} \leq h_f \leq 16.4 \text{ mm}$ $1.9 \text{ mm} \leq s \leq 2.37 \text{ mm}$ $0.41 \text{ mm} \leq \delta \leq 0.52 \text{ mm}$ $1 < n < 6$ 90 % of data within – 16 % to + 20 %
Gianolio and Cuti [14]	$Eu = 32.72 Re^{-0.412} \left(\frac{S_t}{d} \right)^{-1.54} \left(\frac{A}{A_t} \right)^{0.3}$	For staggered tube arrangement and forced draft, $5 \times 10^3 \leq Re \leq 2 \times 10^4$ $25.4 \text{ mm} \leq d \leq 38.1 \text{ mm}$ $15.15 \text{ mm} \leq h_f \leq 16.4 \text{ mm}$ $1.9 \text{ mm} \leq s \leq 2.37 \text{ mm}$ $0.41 \text{ mm} \leq \delta \leq 0.52 \text{ mm}$ $1 < n < 6$ 90 % of data within –14 % to +18 %
Haaf [19]	$Eu_m = C Re_{d,eq}^{-0.25} \left(\frac{S_l}{d_{eq}} \right)^{0.4} .n$ For staggered: $C = 4.25$ For in-line: $C = 2.5$	$2 \times 10^2 < Re_{d,eq} < 1 \times 10^4$ Maximum deviation $\pm 50 \%$

Table D.4 Correlations for pressure drop of circular finned-tube heat exchangers.

Author	Correlation	Remark
Jameson [23]	$Eu = 3.064 Re_{d,eq}^{-0.25} .n$	For staggered tube arrangement, $500 < Re_{d, eq} < 1 \times 10^4$ $15.88 \text{ mm} \leq d \leq 25.4 \text{ mm}$ $6.3 \text{ mm} \leq h_f \leq 9.36 \text{ mm}$ $2.5 \text{ mm} \leq s \leq 3.375 \text{ mm}$ $0.254 \text{ mm} \leq \delta \leq 0.305 \text{ mm}$ $31.293 \text{ mm} \leq S_t \leq 78.207 \text{ mm}$
Nir [46]	$Eu = 1.5 Re^{-0.25} \left(\frac{A'}{A_{ff}} \right)^{0.2} K_{z,p} .n$	For staggered tube arrangement, $300 \leq Re_{dth} \leq 1 \times 10^4$ $8.5 \leq A' / A_{ff} \leq 60$ $n \geq 1$ Deviation $\pm 10 \%$
Rabas et al. [47]	$Eu = 7.61 Re^{-0.2336} \left(\frac{s}{d_f} \right)^{0.2512} \left(\frac{h_f}{s} \right)^{0.7593} \left(\frac{d}{d_f} \right)^{0.7292} \left(\frac{d}{S_f} \right)^{0.7085} \left(\frac{S_t}{S_l} \right)^{0.3791} .n$	For staggered tube arrangement, $1 \times 10^3 \leq Re \leq 2.5 \times 10^4$ $15.87 \text{ mm} \leq d \leq 31.75 \text{ mm}$ $6.35 \text{ mm} < h_f$ $0.63 \text{ mm} \leq s \leq 2.188 \text{ mm}$ $0.305 \text{ mm} \leq \delta \leq 0.356 \text{ mm}$ $23.81 \text{ mm} \leq S_t \leq 42.86 \text{ mm}$ $20.62 \text{ mm} \leq S_l \leq 50.8 \text{ mm}$ $n \geq 6$ Deviation – 19 % to + 27 %

Table D.5 Correlations for pressure drop of circular finned-tube heat exchangers.

Author	Correlation	Remark
Robinson and Briggs [50]	$Eu = 18.93 Re^{-0.316} \left(\frac{S_t}{d}\right)^{-0.927} \left(\frac{S_t}{S_d}\right)^{0.515} .n$	For staggered tube arrangement, $2 \times 10^3 \leq Re \leq 5 \times 10^4$ $18.64 \text{ mm} \leq d \leq 40.89 \text{ mm}$ $10.5 \text{ mm} \leq h_f \leq 14.94 \text{ mm}$ $1.85 \text{ mm} \leq s \leq 2.76 \text{ mm}$ $0.4 \text{ mm} \leq \delta \leq 0.6 \text{ mm}$ $42.85 \text{ mm} \leq S_t \leq 114.3 \text{ mm}$ $42.85 \text{ mm} \leq S_l \leq 114.3 \text{ mm}$ $n \geq 4$ Standard deviation 7.8 %
Stasiulevičius and Skrinska [62]	$Eu = \frac{C \left(1 - \frac{S_f}{d}\right)^{1.8} Re^m .n}{\left(\frac{S_t}{d}\right)^{0.55} \left(\frac{S_l}{d}\right)^{0.5} \left(1 - \frac{h_f}{d}\right)^{1.4}}$ <p>For $1 \times 10^4 \leq Re \leq 1 \times 10^5$: C = 6.55, m = -0.25 For $1 \times 10^5 \leq Re \leq 1 \times 10^6$: C = 0.37, m = 0</p>	For staggered tube arrangement, $23 \text{ mm} \leq d \leq 32 \text{ mm}$ $4 \text{ mm} \leq h_f \leq 13.5 \text{ mm}$ $2.5 \text{ mm} \leq s \leq 6.5 \text{ mm}$ $61.4 \text{ mm} \leq S_t \leq 95 \text{ mm}$ $33.6 \text{ mm} \leq S_l \leq 49.2 \text{ mm}$ $n = 7$ Maximum deviation $\pm 20 \%$
Ward and Young [69]	$Eu = 0.256 Re^{-0.264} \left(\frac{\delta}{d_f}\right)^{-0.377} \left(\frac{s}{d}\right)^{-0.396} \left(\frac{S_l}{d}\right).n$	For staggered tube arrangement, $1 \times 10^3 \leq Re \leq 2.8 \times 10^4$ $11.13 \text{ mm} \leq d \leq 29.13 \text{ mm}$ $1.42 \text{ mm} \leq h_f \leq 14.69 \text{ mm}$ $0.89 \text{ mm} \leq s \leq 4.39 \text{ mm}$ $0.41 \text{ mm} \leq \delta \leq 0.56 \text{ mm}$ $23.81 \text{ mm} \leq S_t \leq 61.91 \text{ mm}$ $20.62 \text{ mm} \leq S_l \leq 53.62 \text{ mm}$ $n \geq 6$

Table D.6 Correlations for pressure drop of circular finned-tube heat exchangers.

Appendix E - Numerical Results

The following results correspond to the calculated finned-tube geometries that are displayed in Table 4.1.

Table E.1 Numerical results for bundle depth, $n = 2$.

	T_{out} [K]	\dot{Q} [W]	η	h [W/m ² K]	Re	Nu	Δp [Pa]	Eu
s6 (n=2)	295.302	-2.474	0.988	64.680	8600	59.220	38.369	1.071
s6 (n=2)	297.890	-3.950	0.983	95.161	17000	87.129	134.271	0.937
s6 (n=2)	300.725	-7.113	0.972	159.563	43000	146.094	651.455	0.727

Table E.2 Numerical results for bundle depth, $n = 3$.

	T_{out} [K]	\dot{Q} [W]	η	h [W/m ² K]	Re	Nu	Δp [Pa]	Eu
s6 (n=3)	291.371	-3.238	0.988	66.646	8600	61.021	54.824	1.531
s6 (n=3)	294.177	-5.385	0.982	98.451	17000	90.141	189.635	1.323
s6 (n=3)	297.703	-10.062	0.971	164.337	43000	150.466	900.390	1.005
i4 (n=3)	296.495	-2.249	0.995	27.984	8600	25.622	33.421	0.933
i4 (n=3)	298.398	-3.756	0.992	44.245	17000	40.510	115.551	0.806
i4 (n=3)	300.501	-7.262	0.985	80.940	43000	74.108	669.203	0.747

Table E.3 Numerical results for bundle depth, $n = 4$.

	T_{out}	\dot{Q}	η	h	Re	Nu	Δp	Eu
	[K]	[W]		[W/m ² K]			[Pa]	
s4	286.726	-4.897	0.960	48.952	5000	44.820	27.753	2.304
s13	291.731	-3.280	0.991	48.253	5000	44.180	3.197	1.662
s14	298.535	-3.761	0.992	42.857	5000	39.240	3.197	1.622
s1	291.261	-2.901	0.996	68.601	8600	62.810	57.321	1.600
s2	290.178	-4.229	0.988	67.614	8600	61.907	64.201	1.792
s3	289.692	-5.521	0.976	65.096	8600	59.601	67.524	1.885
s4	288.936	-7.492	0.949	63.009	8600	57.690	70.221	1.960
s5	288.944	-8.796	0.928	61.121	8600	55.962	72.620	2.027
s6 (n=4)	288.625	-3.764	0.988	68.194	8600	62.438	71.716	2.002
s7	295.302	-4.578	0.988	64.909	8600	59.430	49.290	1.376
s8	284.638	-3.677	0.959	50.907	8600	46.610	140.389	3.918
s9	290.102	-4.096	0.980	67.551	8600	61.850	61.850	1.798
s10	290.320	-4.279	0.990	67.765	8600	62.045	63.936	1.785
s11	293.848	-5.112	0.978	109.494	8600	56.768	163.730	1.465
s12	289.448	-3.985	0.990	58.341	8600	62.319	49.241	1.871
s13	294.630	-4.811	0.989	62.701	8600	57.409	56.524	1.578
s1	294.012	-4.863	0.994	101.905	17000	93.304	202.086	1.410
s2	293.045	-7.116	0.982	99.406	17000	91.015	223.161	1.557
s3	292.688	-9.252	0.965	94.560	17000	86.579	229.650	1.602
s4	292.365	-12.432	0.930	89.177	17000	81.650	232.875	1.625
s5	292.356	-14.468	0.902	85.772	17000	78.532	241.560	1.686
s6 (n=4)	291.346	-6.485	0.982	100.778	17000	92.272	244.511	1.706
s7	297.802	-9.293	0.983	96.333	17000	88.202	181.537	1.267
s8	285.613	-7.091	0.931	87.637	17000	80.240	413.185	2.883
s9	292.963	-6.874	0.971	99.231	17000	90.855	222.211	1.551
s10	293.127	-7.189	0.985	99.626	17000	91.217	222.937	1.556
s11	296.711	-8.189	0.968	159.405	17000	82.644	542.773	1.214
s12	292.152	-6.794	0.985	86.358	17000	92.247	170.759	1.622
s13	297.105	-7.871	0.983	94.517	17000	86.539	203.570	1.420
s14	301.712	-7.961	0.985	83.626	17000	76.568	174.626	1.219
s1	297.472	-9.198	0.990	171.100	43000	156.658	1070.040	1.195
s2	296.641	-13.582	0.970	167.469	43000	153.333	1127.152	1.258
s3	296.382	-17.628	0.943	159.647	43000	146.171	1135.400	1.268
s4	296.463	-23.093	0.891	147.184	43000	134.761	1137.803	1.270
s5	296.533	-26.651	0.849	142.243	43000	130.237	1146.259	1.280
s6 (n=4)	295.140	-12.579	0.970	168.145	43000	153.952	1145.935	1.279
s7	300.503	-17.135	0.971	165.772	43000	151.779	962.220	1.074
s8	288.844	-15.119	0.893	143.208	43000	131.121	1661.686	1.855
s9	296.649	-13.033	0.952	166.482	43000	152.430	1157.986	1.293
s10	296.622	-13.811	0.975	168.084	43000	153.896	1161.374	1.297
s11	300.119	-14.305	0.950	255.868	43000	132.656	2901.381	1.039
s12	295.698	-13.263	0.974	148.065	43000	158.162	890.170	1.353
s13	299.878	-14.632	0.971	163.397	43000	149.605	1040.340	1.161
s14	303.174	-14.497	0.974	148.320	43000	135.801	726.977	0.812
s1	299.211	-12.494	0.987	221.042	70000	202.385	2556.280	1.083
s3	298.276	-23.908	0.927	206.820	70000	189.363	2563.079	1.086
s7	301.768	-22.882	0.962	214.825	70000	196.693	2469.828	1.046

Table E.4 Numerical results for bundle depth, $n = 4$.

	T_{out} [K]	\dot{Q} [W]	η	h [W/m ² K]	Re	Nu	Δp [Pa]	Eu
i1	295.457	-2.985	0.993	37.581	8600	34.409	38.558	1.076
i2	295.064	-3.911	0.987	35.622	8600	32.616	39.780	1.110
i3	294.575	-5.345	0.972	33.590	8600	30.755	39.933	1.115
i4 (n=4)	294.524	-2.629	0.994	35.206	8600	32.234	41.144	1.148
i5	298.709	-4.248	0.992	42.388	8600	38.810	29.500	0.823
i6	297.370	-3.844	0.985	72.121	8600	37.391	102.197	0.915
i7	295.218	-2.748	0.995	30.555	8600	32.638	32.638	1.240
i8	299.707	-2.912	0.994	32.016	8600	29.314	29.236	0.816
i9	295.333	-3.012	0.993	38.099	8600	34.883	39.154	1.093
i1	297.498	-5.009	0.989	59.078	17000	54.091	135.000	0.942
i2	297.165	-6.564	0.979	55.991	17000	51.265	135.262	0.944
i3	296.820	-8.918	0.957	52.510	17000	48.078	136.050	0.949
i4 (n=4)	296.542	-4.477	0.990	55.975	17000	51.250	133.930	0.935
i5	300.494	-6.926	0.988	65.908	17000	60.345	107.889	0.753
i6	299.426	-6.206	0.978	110.190	17000	57.129	361.518	0.809
i7	297.199	-4.656	0.991	48.502	17000	51.810	51.810	0.492
i8	301.023	-4.872	0.991	51.844	17000	47.468	104.442	0.729
i9	297.422	-5.044	0.989	59.634	17000	54.601	136.937	0.956
i1	299.739	-9.792	0.981	108.868	43000	99.679	696.770	0.778
i2	299.548	-12.731	0.962	102.637	43000	93.974	703.740	0.786
i3	299.520	-16.855	0.926	94.231	43000	86.278	711.996	0.795
i4 (n=4)	298.899	-8.884	0.981	103.957	43000	95.182	782.151	0.873
i5	302.144	-13.396	0.978	123.063	43000	112.676	641.331	0.716
i6	301.447	-11.653	0.961	198.895	43000	103.118	2092.145	0.749
i7	299.487	-9.198	0.984	89.973	43000	96.109	96.109	0.146
i8	302.471	-9.487	0.982	97.982	43000	89.712	601.119	0.671
i9	299.686	-9.855	0.980	109.746	43000	100.483	764.971	0.854

Table E.5 Numerical results for bundle depth, $n = 5$.

	T_{out} [K]	\dot{Q} [W]	η	h [W/m ² K]	Re	Nu	Δp [Pa]	Eu
s6 (n=5)	286.806	-4.110	0.988	69.004	8600	63.180	87.403	2.440
s6 (n=5)	289.248	-7.294	0.982	102.005	17000	93.395	299.164	2.088
s6 (n=5)	293.069	-14.625	0.970	169.759	43000	155.430	1391.268	1.553
i4 (n=5)	292.826	-2.954	0.994	33.906	8600	31.044	47.545	1.327
i4 (n=5)	294.922	-5.095	0.990	53.933	17000	49.380	150.868	1.053
i4 (n=5)	297.357	-10.332	0.982	101.353	43000	92.798	866.267	0.967

Table E.6 Numerical results for bundle depth, $n = 6$.

	T_{out} [K]	\dot{Q} [W]	η	h [W/m ² K]	Re	Nu	Δp [Pa]	Eu
s6 (n=6)	285.605	-4.344	0.987	69.463	8600	63.600	103.634	2.893
s6 (n=6)	287.695	-7.900	0.982	102.814	17000	94.136	353.724	2.468
s6 (n=6)	291.350	-16.351	0.970	171.250	43000	156.796	1637.153	1.828

Lebenslauf

Name: Mi Sandar Mon
Geburtsdatum: 20. 06. 1967
Geburtsort: Yangon, Myanmar
Familienstand: verheiratet

Schulbildung

1972 – 1974: Grundschule in Mawlamyaing, Myanmar
1975 – 1982: Oberschule in Yangon, Myanmar

Hochschulstudium

12/1983 – 11/1992: Maschinenbau
Yangon Institute of Technology, Abschluß: B.E
07/1993 – 09/1996: Maschinenbau
Yangon Institute of Technology, Abschluß: M.E
09/1998 – 05/2003: Stipendiat im Graduiertenkolleg
Technische Universität Bergakademie Freiberg

Berufliche Tätigkeit

06/1994 – 03/1997: Instructor am Yangon Institute of Technology,
Fakultät für Maschinenbau
03/1997 – 08/2002: Assistant Lecturer
an der Yangon Technological University,
Fakultät für Maschinenbau
seit 09/2002: Lecturer an der Yangon Technological University,
Fakultät für Maschinenbau